11-6-2019

An Investigation of High-Speed Consolidation and Repair of Carbon Fiber - Epoxy Composites Through Ultrasonic Welding

David A. Hoskins
Louisiana State University and Agricultural and Mechanical College

AN INVESTIGATION OF HIGH-SPEED CONSOLIDATION AND REPAIR OF CARBON FIBER - EPOXY COMPOSITES THROUGH ULTRASONIC WELDING

A Thesis

Submitted to the Graduate Faculty of the
Louisiana State University and
Agricultural and Mechanical College
in partial fulfillment of the
requirements for the degree of
Master of Science in Mechanical Engineering

in

The Department of Mechanical Engineering

by
David Hoskins
B.S. Materials Engineering, Iowa State University, 2017
December 2019

ACKNOWLEDGEMENTS

I would first like to thank my faculty advisor Dr. Genevieve Palardy for her relentless support, invaluable guidance, and insightful discussions throughout my graduate studies. Her expertise as a researcher and instructor has helped me become a better communicator, a more innovative researcher, and an effective engineer. I would also like to thank Dr. Guoqiang Li and Dr. John Pojman for agreeing to serve on my advisory committee.

I thank the Louisiana Space Consortium and the Louisiana Board of Regents for sponsoring this research. I would like to acknowledge Dr. Mark McElroy and Dr. Daniel Kim from the NASA Johnson Space Center and Dr. Susan Danley from the NASA Kennedy Space Center for their collaboration in this project offering valuable input. I would also like to thank all the members of my research group: Steven Williams, Harry Frederick, Armaghan Naderi, and Wencai Li for their support and assistance.

Finally, I give my deepest gratitude to my family for their unyielding support and inspiration from which I have drawn the strength and perseverance to overcome many challenges. Thank you for being there every step of the way.

TABLE OF CONTENTS

LIST OF TABLES

LIST OF FIGURES

ABSTRACT

Adhesive repair of carbon fiber composite structures is commonly done on damaged structures to extend the service life. This method requires careful preparation of the damaged surface with intricate steps to ensure good bonding between the repair patch and the parent structure by means of an adhesive film. As with many forms of composite manufacturing, it is required to perform vacuum bagging, debulking, and a heated cure depending on the resin. All these steps make the repair process costly and time consuming.

In this present work, an alternative method of repair is investigated which explores the experimental feasibility of using ultrasonic vibrations as a substitute to the vacuum bagging and debulking steps. This would ultimately reduce the manufacturing time, labor, and cost. Ultrasonic welding parameters were explored (time, travel, force, and amplitude) with two welding modes to optimize the consolidation process. Welded specimens were then post-cured in the oven following the recommended cure cycle from the manufacturer. Temperature measurements were obtained during the welding process and cure kinetics and viscosity behavior were predicted using semi-empirical models developed for Cycom 5320. Interlaminar shear strength was compared for welded and vacuum bagged samples. Repair of composite structures was simulated by applying flat repair patches over an open-hole and testing in uniaxial tension. The strength recovery was compared for welded and vacuum bagged repair samples.

CHAPTER 1.
INTRODUCTION

1.1. Motivation and Purpose

In recent years, fiber reinforced composites have become frequently used in the aerospace industry where high strength and low weight are crucial. Compared to metals, composite materials offer more beneficial features such as better resistance to fatigue damage, increased stiffness and strength, and corrosion resistance [1, 2]. While composite materials may possess better characteristics, they are generally more expensive and require careful manufacturing procedures to achieve the desired quality. Considering the economic factors related to composite manufacturing, the increase in demand – ranging from primary structural components through recreational goods – has enabled the composite industry to develop faster methods of manufacturing while maintaining similar quality to well established methods (such as autoclave manufacturing). While faster manufacturing methods have been successfully incorporated in the aerospace industry (i.e. resin transfer molding, compression molding, and filament finding), improvements can be made by further reducing the manufacturing time and ultimately lowering the cost of composite materials [1].

The expense associated with composite materials is not limited to the manufacturing process. While composite materials have exceptional properties, this makes them candidates for the most severe conditions where damage may occur. Depending on the extent of damage of primary structures, replacing the entire component is one option, however, this may be time consuming and costly. Structural repair can be performed on damaged structures to extend the service life, which, is a more cost-effective approach compared to complete replacement [2].

There are multiple methods of repair for composite materials either through mechanical fastening or adhesive bonding techniques. Structural repair manuals rely on bolted repair (i.e doubler repair) which can provide restoration of structural strength. However, these are mainly used on thick composite parts leaving uneven surfaces, and creating stress concentrations around the bolts [2-4]. Conversely, bonded repair (i.e. scarf repair) can offer higher strength and stiffness recovery, reduction of stress concentrations, weight saving, and flush surfaces [2, 3]. In theory, bonded scarf repair can produce the most efficient joints for bonded repair, however, the repair process can be intricate and expensive [2].

Bonded repair of carbon fiber (CF) / epoxy is usually done manually introducing inconsistencies in the repair quality caused by human error. In fact, many aspects of bonded repair make it challenging to produce reliable and consistent outcomes [2]. Repair requires several steps to complete: (1) removal of damaged plies, (2) scarf of the parent structure, (3) surface preparation, (4) adhesive application and patch consolidation, (5) post-repair inspection, and (6) refinishing. Multiple defects can be faced during the repair process, such as voids and debonding, wrinkles in the patches, and variations in the bondline thickness [3]. Furthermore, patch consolidation is usually carried out by vacuum bagging, followed by curing with an autoclave, oven, or heated blanket. Altogether, this process is time-consuming and can be costly.

One promising method for high-speed consolidation of fiber reinforced composites is ultrasonic consolidation. In the literature, application of ultrasonic welding (USW) on thermoplastic composites has been shown to consolidate plies removing trapped air and increasing the temperature to allow resin to flow [5, 6]. Ultrasonic welding has very fast cycle times (<5.0 s) with comparable mechanical properties to traditional manufacturing methods [6, 7]. While ultrasonic welding is primarily used with thermoplastics, its limited use with thermoset resins has

indicated good consolidation of plies, and heat generation that would potentially allow partial curing of the resin [8-10].

In this manuscript, an alternative method of repair for carbon fiber / epoxy composites, which could potentially eliminate the vacuum bagging process, is investigated using ultrasonic welding. It would ultimately reduce the manufacturing time, labor, and cost of composites repair. First, the feasibility of using ultrasonic welding to consolidate repair patches was experimentally assessed. Once a range of possible welding parameters was identified, temperature measurements were obtained during the welding process to characterize the heat generation. Temperature measurements were used to predict the behavior of the resin during the welding process using semi-empirical models for cure kinetics and viscosity. Next, the void content for welded samples was measured and compared to vacuum bagged samples. With an understanding of the effects of various welding parameters, short beam shear samples and open-hole repaired specimens were manufactured by ultrasonic welding and traditional vacuum bagging. Adhesive repair of open-hole samples was done using soft-patch and hard-patch repair techniques. The strength recovery was then compared for repair samples manufactured by vacuum bagging and ultrasonic welding.

1.2. Research Objectives

The primary research objective of this manuscript is to investigate the feasibility of ultrasonic welding as a high-speed method to repair carbon fiber / epoxy composites. This process would greatly simplify structural repair and bonding by eliminating the vacuum bagging step, and promoting time, cost, and weight reduction. Within this scope, several sub-objectives were investigated:

1. Effect of ultrasonic welding parameters (force, time, travel, amplitude) on expected patch quality. Assess damage to fiber weave and characterize the quality by measuring void content.
2. Surface temperature profiles and through-thickness temperature measurements for carbon fiber / epoxy samples during the welding process.
3. Characterize welded specimens regarding cure kinetics (degree-of-cure) and viscosity. Establish a relationship with ultrasonic parameters and temperature measurements.
4. Perform short beam shear tests to characterize and compare the interlaminar shear strength of welded specimens and vacuum bagged specimens. Test the effects of using an adhesive film for short beam samples.
5. Apply flat repair patches using ultrasonic welding on open-hole specimens and test under uniaxial tension. Measure the strength recovery to validate ultrasonic welding as a repair technique.

1.3. Chapter Summary

The present study is organized in the following way: Chapter 1 will introduce the scope of this study and the objectives. Chapter 2 will cover the literature review on topics within the scope of this research project. Chapter 3 explains the methods employed to investigate the research objectives. Chapter 4 presents the results of this study highlighting the effects of welding parameters on the quality of the samples, temperature measurements obtained during ultrasonic welding, and predictions of the changes to the degree-of-cure and viscosity. Mechanical characterization of welded samples was investigated using short beam shear testing to evaluate the interlaminar shear strength. Lastly, adhesive repair of composite structures was simulated by applying flat repair patches on open-hole tensile specimens. The strength recovery was measured

and compared to vacuum bagged repair methods. Chapter 5 provides a conclusion to the topics discussed in this study as well as potential areas for future work.

CHAPTER 2.
LITERATURE REVIEW

This chapter will review the references that are related to the scope of this thesis. First, the constituent materials will be reviewed, followed by a summary on cure kinetic models developed for epoxy resins. Common out-of-autoclave (OOA) manufacturing methods for thermoset polymers will be explained. Next, relevant work on ultrasonic welding will be reviewed with a focus on carbon fiber composites. Previous work on temperature measurements during ultrasonic welding will be reviewed followed by microstructural analysis of carbon fiber composites. Lastly, bonding and repair methods for composite materials will be covered.

2.1. Fiber-Reinforced Thermoset Composites

Fiber-reinforced thermoset composites, also described as polymer matrix composites, are commonly used in the aerospace industry. These materials are composed of two dissimilar materials referred to as the matrix (i.e. epoxy) and the reinforcement (i.e. carbon fibers) which have distinct properties. Combining these two materials yields a composite material with superior properties compared to their independent constituents [1, 11].

The properties of composite materials can be modified for the desired application based on fiber orientation and architecture, fiber volume fraction, and the various options for fibers and resins. There are many types of fiber architectures classified into two groups: unidirectional ply and fabric ply [1]. For unidirectional plies, the fibers are all aligned in a single direction [11]. For fabric plies, fibers are woven in different patterns summarized in Figure 2.1. It should be noted that other common weaves are 5- and 8-harness satin.

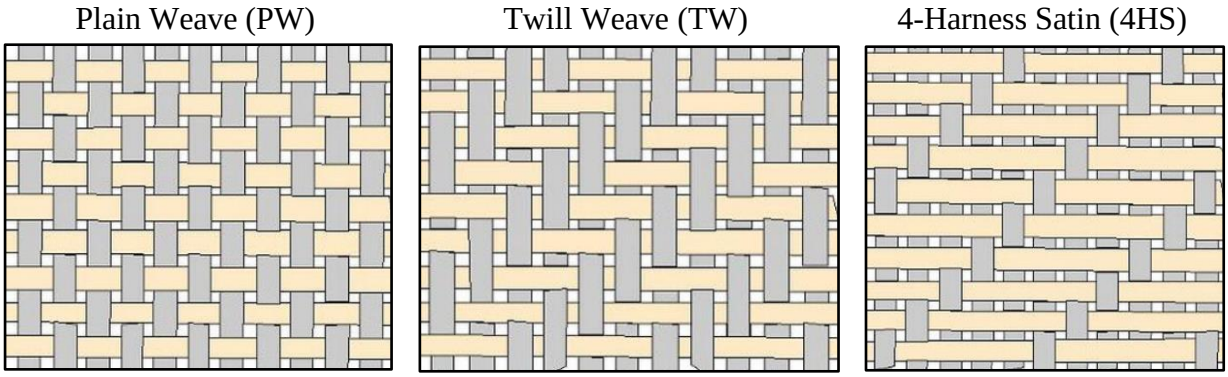

Figure 2.1. Summary of common weave patterns for fabric plies [12].

Fibers are the major load bearing constituent in composite materials [1, 11]. Applying a load along the fibers (longitudinal loading) and perpendicular to the fibers (transverse loading) will result in different mechanical performance. As represented in Figure 2.2, loading in the transverse direction (Axis 2, T) will primary load the matrix and not the fibers. For this reason, combined with the vast possibility of fiber orientations, composite materials can be anisotropic or orthotropic.

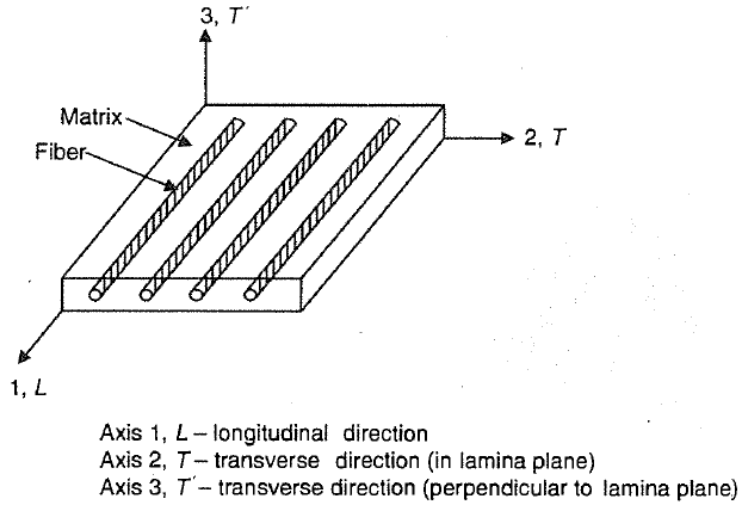

Figure 2.2. Representation of unidirectional composite material [11].

Carbon fiber can be sold as a dry fabric (also referred to as dry fibers) and as pre-impregnated (prepreg) fibers that are already mixed with catalyzed, but uncured resin as shown in

Figure 2.3 [11, 13]. Fiber and resin systems are manufactured by companies such as Cytec Solvay Group, Hexcel, Toray and many others. Common types of thermosetting resin are listed in Table 2.1. However, epoxy resins are usually preferred in the aerospace industry due to their superior properties regarding adhesion, moisture resistance, and chemical resistance [11].

Figure 2.3. Schematic of constituent of a prepreg [13].

Table 2.1. Properties of common thermoset resins [11].

Property, units	Epoxy	Polyester	Vinyl Esters	Polyimides	Phenolics
Density, g/cm^3	1.2-1.3	1.1-1.4	1.12-1.32	1.46	1.30
Tensile strength, MPa	55-120	34.5-103.5	73-81	120	50-55
Tensile Modulus, GPa	2.75-4.10	2-4.4	3.0-3.5	3.5-4.5	2.7-4.1
Thermal Expansion, $10^{-6}/°C$	45-65	55-100	53	90	45-110
Water absorption in 24 hr, %	0.08-0.15	0.15-0.6	–	0.3	0.1-0.2

2.2. Out-of-Autoclave Manufacturing Methods

Manufacturing of carbon fiber / epoxy can be done using an autoclave (pressurized oven) or out-of-autoclave (OOA). For autoclave manufacturing, the part is vacuum bagged, then placed in a pressurized oven where additional pressure can be applied during the cure cycle of the resin [11]. Alternatively, out-of-autoclave manufacturing only requires vacuum bagging without the need of applying additional pressure. It is crucial to suppress porosity during manufacturing that can emerge from trapped air between plies, or cure-generated volatiles [13]. Applying vacuum to the part will facilitate evacuation of entrapped air found between the plies.

The primary difference between these two manufacturing methods is the resin properties. Autoclave resins are designed for higher pressure manufacturing where any remaining voids (those

not removed by vacuum pressure) are collapsed by the additional pressure applied in the oven. However, for out-of-autoclave resins, the resin is designed to remain viscous during the early stages of the cure cycle allowing dry regions to act as air evacuation paths [13].

2.2.1. Hand Layup and Vacuum Bagging

Hand layup is a common and relatively simple method for manufacturing of composites [11]. This process can be used to manufacture composites of various sizes ranging from small parts to boat hulls. The manufacturing process is relatively simple where plies of prepreg or dry fibers with resin (wet layup) are stacked until the desired thickness is reached. Prepregs are usually preferred for their ease of use and better control of material properties [1]. Following the ply layup, the laminate can be consolidated through vacuum bagging – a process that encloses the laminate with bagging film and then pulled vacuum on. A schematic showing all the required materials is illustrated in Figure 2.4.

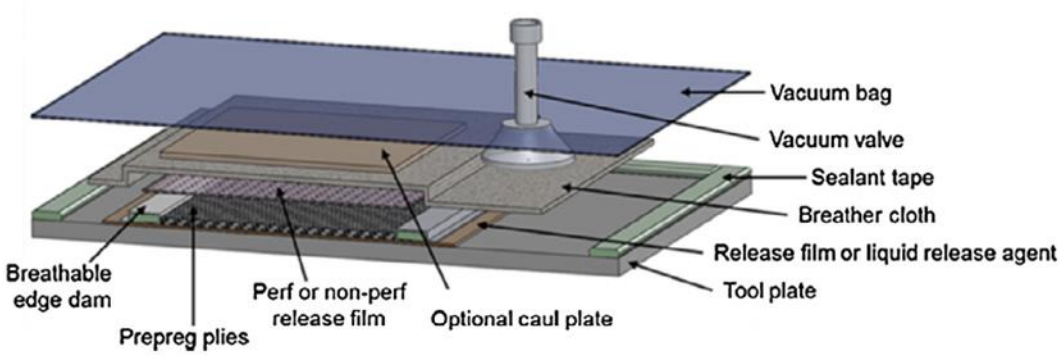

Figure 2.4. Schematic of vacuum bagging setup [13].

Curing the resin can be done at room temperature or at elevated temperatures which in general follows the cycle shown in Figure 2.5. Hand layup followed by vacuum bagging is a versatile process, however it is usually not meant for mass production as production volumes are low and size or complexity of the part can be limited [11].

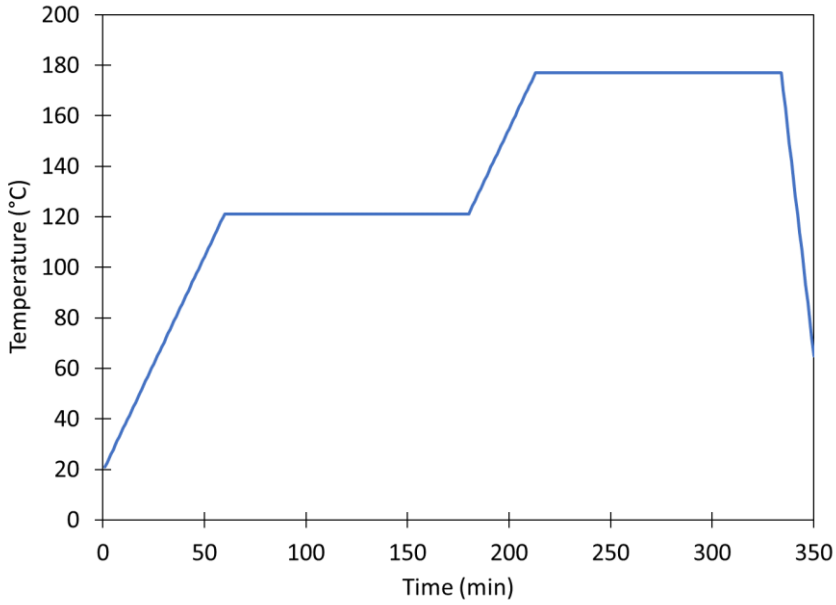

Figure 2.5. Typical cure cycle for Cycom 5320.

2.2.2. Liquid Composite Molding and Vacuum Assisted Resin Infusion

Liquid composite molding (LCM) is a process characterized by the injection of liquid resin into a dry fiber preform. This encompasses methods such as resin transfer molding (RTM). Vacuum assisted resin infusion does not inject resin into the part, instead, it uses vacuum pressure to pull resin through the mold such as vacuum assisted resin transfer molding (VARTM) [14]. There are many variations to each of these manufacturing methods.

2.2.2.1. Resin Transfer Molding (RTM)

RTM is a wet impregnation process where dry fibers are placed in a closed mold and liquid resin is injected into the mold cavity [11]. As the resin moves through the mold, it pushes air out and saturates fibers. Once the entire mold is full of resin and air has been pushed out, the mold inlets and outlets are sealed [11]. This process can been used in the aircraft industry [1]. High-pressure RTM (HP-RTM) is a more recent version of the process typically used for high production rates in the automotive industry [15].

2.2.2.2. Vacuum Assisted Resin Transfer Molding (VARTM)

This process is very similar to RTM except that vacuum is applied to pull resin through the part. [14] Vacuum bagging may be necessary to cause a pressure differential that will transfer the resin through the part [11].

2.2.3. Automated Fiber Placement and Automated Tape Layup

Automated fiber placement (AFP) is a computer-guided process where several small-width tows measuring less than or equal to 8 mm are automatically placed onto a mold or mandrel using a robotic arm or a gantry system. This method can be used to manufacture complicated geometries and, in the process, reduce material waste and manufacturing time by 70-85% [6]. Automated tape layup (ATL) is a similar process to AFP, however, it uses wider unidirectional prepreg tape. This allows for larger areas to be covered quickly but for simpler geometries [6].

2.3. Resin Cure Kinetics

Cure kinetic models have been developed to predict the degree-of-cure of the resin during the manufacturing cycle. These models have been modified over time to more adequately describe the curing process and microstructural transformations. Each model uses the Arrhenius temperature dependence, K of the following form [16-19]:

$$K = A\exp^{\left(\frac{-E_A}{RT}\right)} \qquad 2.1$$

where E_A is the activation energy of the resin, R is the ideal gas constant, T is the temperature and A is a constant. Eq. 2.2 to 2.4 show common cure kinetic models in terms of the cure rate $d\alpha/dt$ that have been developed for epoxy/amine thermoset resins such as:

- Diglycidyl ether of bisphenol A (DGEBA) and m-phenylene diamine (m-PDA) [16]
- Diglycidyl ether of bisphenol A (DGEBA) and diaminodiphenylmethane (DDM) [16]

- Tetraglycidyl 4,4'- diaminodiphenylmethane (TGDDM) and 4,4′-diaminodiphenylsulfone (DDS) [20, 21]

Nth Order [16] $$\frac{d\alpha}{dt} = K(1-\alpha)^n \quad (2.2)$$

Autocatalytic [16] $$\frac{d\alpha}{dt} = K\alpha^m(1-\alpha)^n \quad (2.3)$$

Kamal-Sourour [17] $$\frac{d\alpha}{dt} = (K_1 + K_2\alpha^m)(1-\alpha)^n \quad (2.4)$$

In Eq. 2.2 through 2.4, m and n are constants that depend on the resin. Epoxy/amine resins are modified for specific applications which results in some models being more accurate than others. Figure 2.6 compares several models and how effectively they predict the cure kinetics for thermoset resin Cycom 5320 [18].

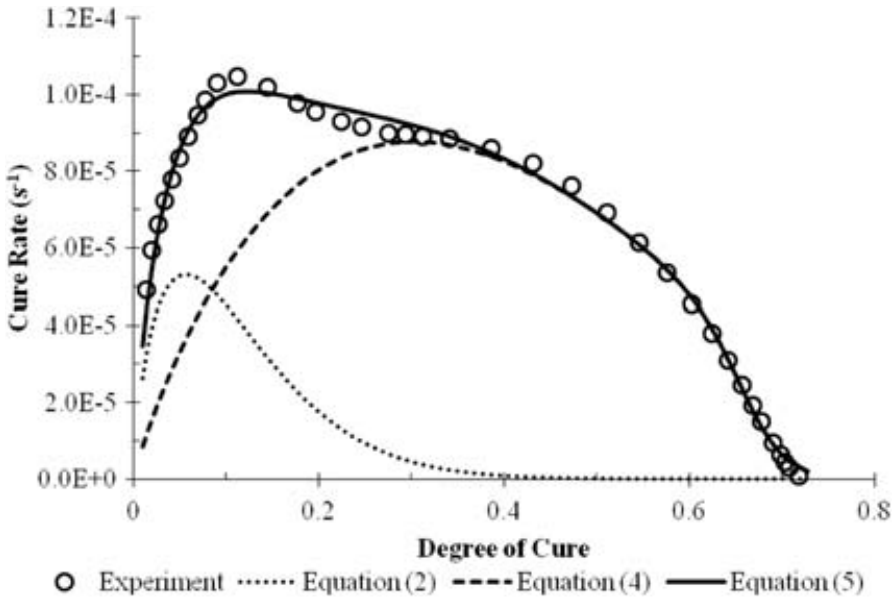

Figure 2.6. Measured and predicted cure rates for Cycom 5320 resin at 120 °C. Equations 2 corresponds with Eq. 2.3, Equations 4 and 5 are other cure kinetic models developed by Cole et al. [21], and Kratz et al. respectively. [18]

Polymers are susceptible to temperature changes. In the case of thermosetting polymers such as epoxy, the thermal history will have an effect on physical and mechanical properties of the manufactured part [22]. Process modeling can be used to verify a cure cycle to make sure it is suitable for the materials. Using the previously mentioned cure kinetic models, Kratz et al. developed cure kinetics, viscosity, and glass transition temperature models specifically for Cycom 5320 and MTM45-1 resins [18]. Thermal models were developed using differential scanning calorimetry (DSC) on small resin samples and then validated using thick composite laminates. The cure kinetics model for Cycom 5320 was mentioned to have excellent fit up to a temperature of 120 °C. Above this temperature, slight deviations from the experimental data were observed [18].

Viscosity is an important property of epoxy resins that determines the ability of resin to flow. The viscosity for epoxy resins decreases as the temperature is increased. The viscosity will remain low enough to flow until molecules cross-link and form a gel, at which point the viscosity will increase very quickly [18]. Predicting the behavior of the resin can offer valuable insight to the microstructural changes that are occurring. While numerous viscosity models have been developed, Castro and Macosko developed a model that uses the degree-of-cure (α), degree-of-cure at gelation (α_g or α_{gel}) and A and B which are constants as shown in Eq. 2.5 [23, 24]. This viscosity model has been modified by others to better predict different epoxy resins [18, 23, 24].

$$\eta = \eta_0 \left(\frac{\alpha_g}{\alpha - \alpha_g} \right)^{A+B\alpha} \tag{2.5}$$

The initial viscosity η_0 follows an Arrhenius temperature dependency:

$$\eta_0 = A_\eta \exp\left(\frac{E_\eta}{RT}\right) \tag{2.6}$$

where E_η is the viscosity activation energy, A_η is a constant, R is the ideal gas constant, and T is the temperature [18, 23, 24].

Kratz et al. tested a modified model (Eq. 3.3) by capturing experimental data using a 25 mm diameter parallel plate rheometer. Collected data was then fit to a semi-empirical model as shown in Figure 2.7. Difficulty in capturing the minimum viscosity at 130 °C in dynamic conditions was reported, however, the model effectively captures the viscosity evolution into the gelation stage of Cycom 5320. Using a cure temperature of 120 °C allowed for accurate description of the viscosity up to gelation [18].

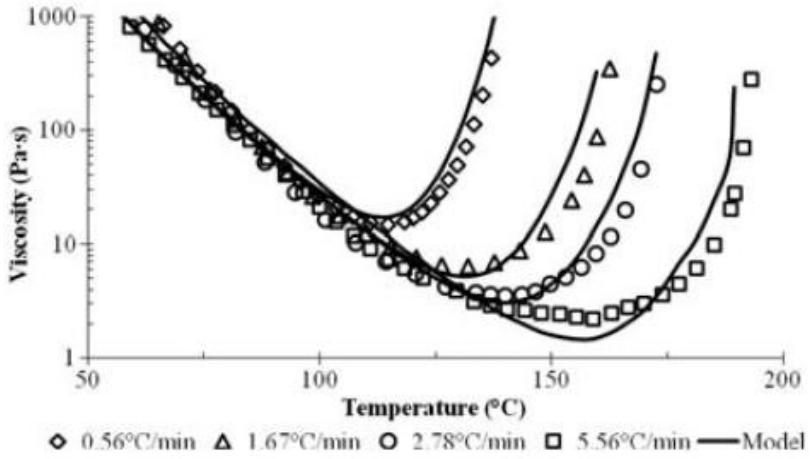

Figure 2.7. Measured and predicted dynamic viscosity for Cycom 5320 epoxy resin [18].

2.4. Ultrasonic-Assisted Consolidation

Ultrasonic welding (USW) is a fusion bonding method usually characterized as a friction welding process [25]. This process is typically used for joining thermoplastics (unreinforced and reinforced): it has a very short weld time (<5 s), does not require any foreign materials at the interface, is automatable, and can even join dissimilar materials [26, 27]. During the USW process, high-frequency (10 kHz – 70 kHz) and low amplitude (10 μm – 120 μm) vibrations are applied to the parts [27]. Most welders have the ability to control the applied force and amplitude of vibrations. Furthermore, additional parameters can be controlled depending on the welder such as stop conditions that control the duration of vibrations. The sonotrode, also referred to as the horn

illustrated in Figure 2.8 comes into contact with the part to be welded and can be manufactured into various shapes and sizes.

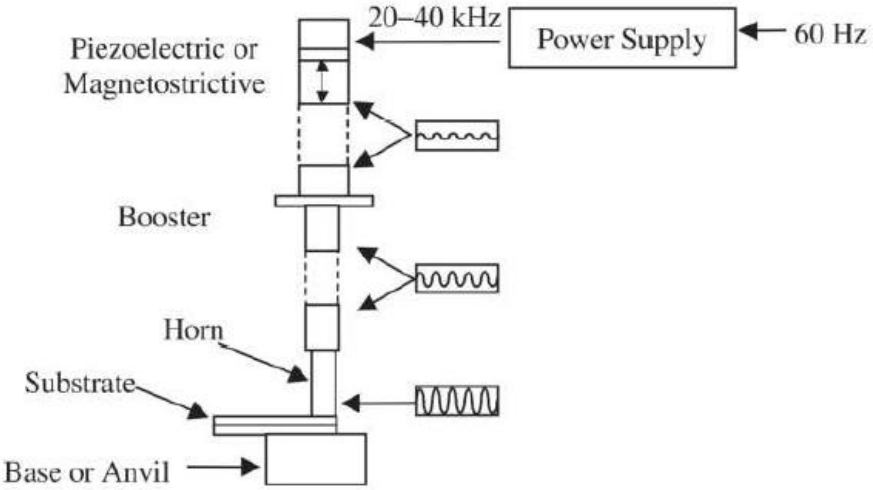

Figure 2.8. Components of a common ultrasonic welder [25].

USW of composites, for the most part, has been performed on thermoplastic composites [5, 6, 25-31]. Other applications of USW are consolidation of thermoplastic prepregs and debulking of thermoset prepregs for filament winding, automated tape layup, and automated fiber placement. Rizzolo et al. investigated ultrasonic consolidation (UC) of carbon fiber (CF) / polyethylene terephthalate (PET) prepreg tape indicating that it was an effective method [6]. The welding setup used for this investigation is shown in Figure 2.9.

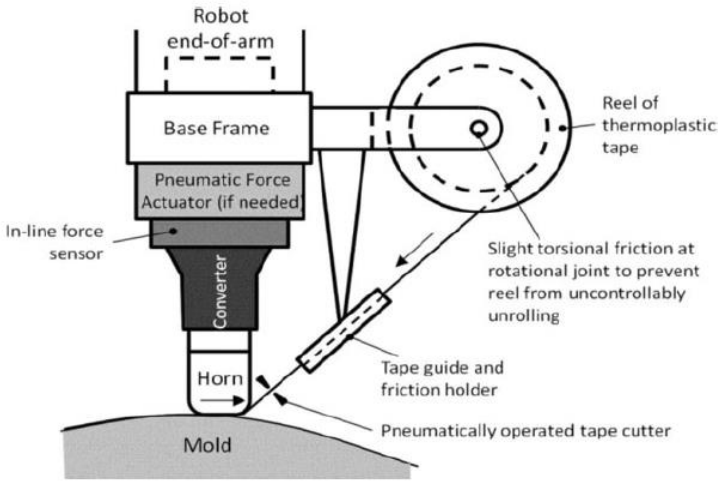

Figure 2.9. Ultrasonic consolidation (UC) during ATL using carbon fiber / polyethylene terephthalate [6].

Lionetto et al. investigated the simultaneous deposition and consolidation of commingled glass fiber (GF) / polypropylene (PP) rovings though ultrasonic welding for filament winding – a process that would impregnate the glass fibers and consolidate plies in a single process, depicted in Figure 2.10 (a) [5]. The results indicated that consolidation of the matrix and the fibers was achieved with mechanical properties comparable to compression molding – a common manufacturing method for thermoplastics [5]. Roylance et al. investigated ultrasonic tape lamination (UTL) for carbon fiber / epoxy prepregs – a process where ultrasonic vibrations were applied during filament winding shown in Figure 2.10 (b) – indicating that consolidation was produced, however, advances on degree-of-cure for the resin were low [8]. Justo et al. investigated heat generation and distribution for ultrasonic consolidation in ATL using a thermomechanical model for viscous heating [32]. In a second publication, the authors implemented a model for viscous heating and temperature distribution during the compaction of composite materials [33].

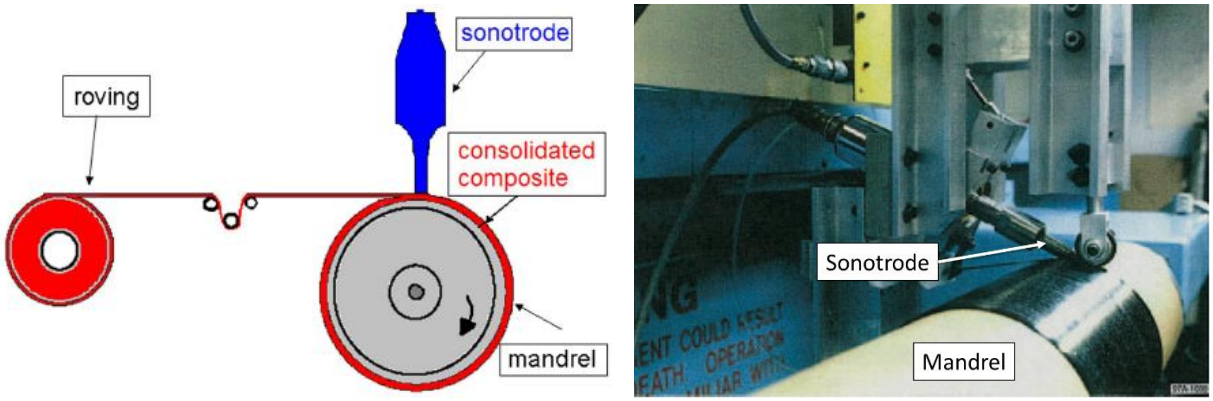

(a) (b)

Figure 2.10. Ultrasonic welding during filament winding for (a) glass fiber / polypropylene filament rovings by Lionetto et al. [5] and, (b) for UTL at 30° for carbon fiber / epoxy prepregs by Roylance et al. modified from [8].

Grewell et al. developed a continuous, automated closed-loop system using ultrasonic vibrations for debulking of composite laminates [9]. Their method of ultrasonic processing of thermoset composite laminates was patented by Textron Innovations as a method of debulking [34]. The system controlled the temperature of the laminate by adjusting the vibration amplitude and the scan speed. The study investigated multiple parameters that influenced the final thickness of the welded laminates such as force, travel speed, amplitude, and horn angle. It was found that increasing the force and amplitude promoted better debulking. Higher travel rates reduced the heat generation which caused a reduction in the squeeze flow, and horn angle did not significantly affect the thickness. The authors also noted that increasing the number of plies required a slower travel speeds to maintain the same temperature [9].

2.4.1. Heat Generation and Temperature Monitoring during Ultrasonic Processing

Thermosetting polymers, such as epoxy, exhibit viscoelastic properties when subjected to strains. During USW, the high-speed vibrations create sinusoidal strains that generate heat through viscoelastic heating. An equation was derived to model viscoelastic heat dissipation over time, $\dot{Q}_{avg}$, as shown in Eq. 2.7, where ω is the vibration frequency, ε_0 is the amplitude of vibrations,

and E" is the resin's loss modulus [26, 28]. The loss modulus depends on multiple parameters such as epoxy out-time, temperature, thermal history, and degree-of-cure, making it difficult to accurately predict heat dissipation [22].

$$\dot{Q}_{avg} = \frac{\omega \varepsilon_0^2 E''}{2} \tag{2.7}$$

While heat generation and temperature monitoring for USW of thermoplastic polymers has been investigated by several researchers [29-31, 35-40], the scarcity of literature on USW of thermosetting polymers limits the understanding of this process. Roylance et al. performed modeling of the ultrasonic welding process for thermosets [8]. The results are listed below:

- Previous work has been performed on the UTL process testing the effects of pressure and amplitude. Increasing pressure resulted in no observable effects for heat generation, suggesting that viscoelastic heating is dominant over frictional heating [8]. These results are also in agreement with Tolunay et al. who experimentally investigated the heating and bonding mechanism of USW on polystyrene (PS) [28].
- USW of IM7 / Hexcel 8552 worked best as a method of consolidation rather than a method of curing the resin. However, with the appropriate welding parameters and resin, consolidation and cure could be possible [8]. It is important to note that the Hexcel 8552 resin is meant for autoclave manufacturing, not out-of-autoclave [13].
- USW induces rapid localized heating with a temperature field developed by finite element analysis (FEA) as shown in Figure 2.11.

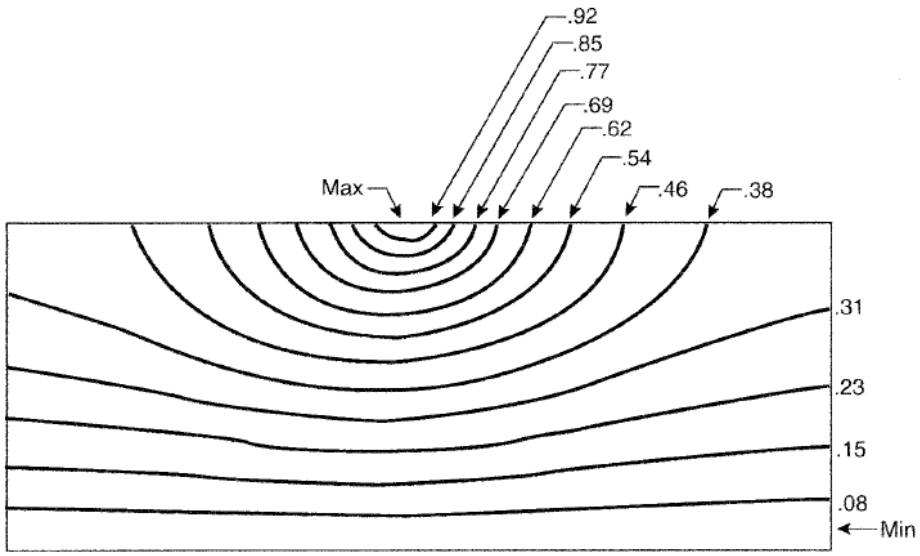

Figure 2.11. Temperature field from displacement of sonotrode at a 30° angle from the horizontal [8].

Grewell et al. also investigated the heating effects on thermoset composites and reported that increasing the number of plies resulted in a decrease in surface temperature illustrated in Figure 2.12 [9]. Capturing the temperature of the welded materials during the welding process is challenging for several reasons: (1) introducing thermocouples is intrusive and they may act as energy directors [29] and (2) ultrasonic vibrations interact with the thermocouple leads raising the possibility of erroneous measurements [27].

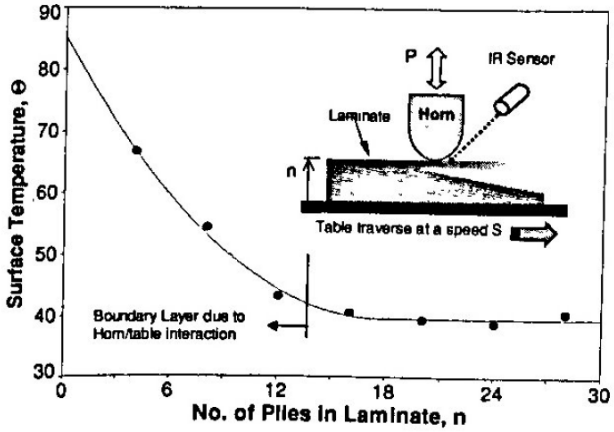

Figure 2.12. Maximum surface temperature as a function of number of plies in the laminate [9].

Temperature measurements after the vibrations have stopped are more reliable as outside factors will not affect the thermocouples. Temperature monitoring has been performed by numerous authors to investigate thermal gradients, heating rate and dissipation [5, 6, 28, 30, 33, 41, 42]. Due to the difficult nature of capturing physical measurements, models have been developed to predict the complex nature of the heating process [5, 6, 8, 26, 29, 32, 33, 42]. For instance, Lionetto et al. compared experimental and simulated temperatures and reported good agreement illustrated in Figure 2.13 (a). Justo modeled ultrasonic consolidation of automated tape layup (ATL) and compared modeled and experimental temperature measurements indicating reasonably good agreement shown in Figure 2.13 (b) [33, 42].

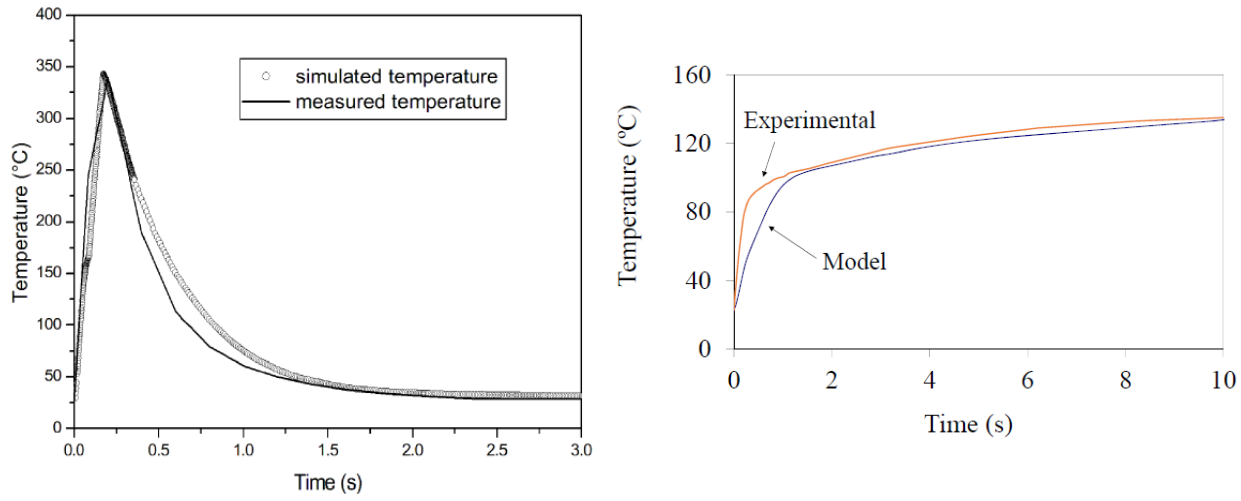

(a) (b)

Figure 2.13. (a) Numerical modeling and experimental temperature measurements with active sonotrode for 0.2 s for glass roving's and polypropylene filaments [5]. (b) Comparison of experimental and numerical temperature measurements during ultrasonic consolidation of a composite laminate [42].

2.5. Process-Induced Defects in Composite Materials

This section will address some of the common defects encountered during the manufacturing process of thermoset composites. A brief discussion will follow on processing conditions that could affect the quality of composite materials. The effect of porosity on

composites will then be explained showing the detrimental effect it has on mechanical performance.

2.5.1. Microstructural Consideration and the Consolidation Process

Composite materials go through microstructural transformations during the curing process, those being gelation (liquid to gel) and vitrification (gel to glass) illustrated in Figure 2.14. Once the gelation stage has been reached, the microstructure will no longer change meaning that any voids left in the laminate will be "locked" in place. For this reason, it is important to have the proper vacuum bagging setup and follow the appropriate curing cycle.

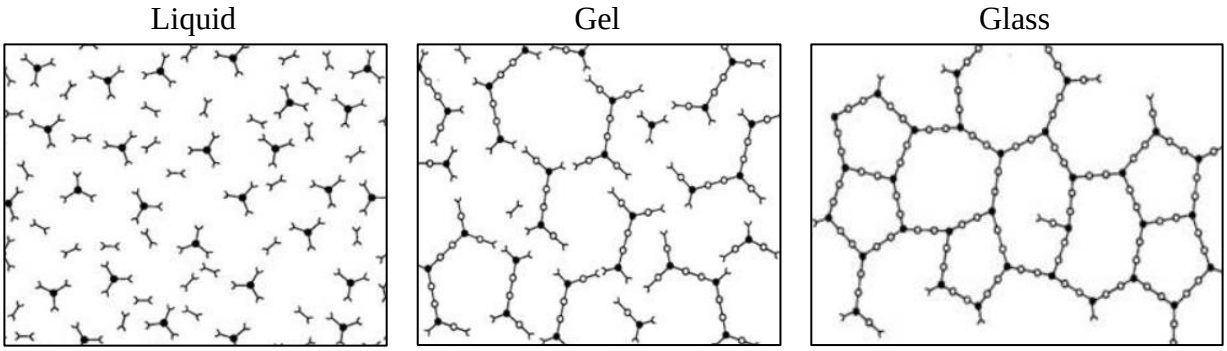

Figure 2.14. Microstructural transformations during cure of thermosets. (a) Low viscosity liquid composed of unreacted monomers and oligomers. (b) As resin and hardener react, the viscosity increases, and a cross-linked network of molecules is formed. (c) Thermoset has transitioned from gel phase to glassy phase (vitrified) and cross-linking continues to form a solid material [43].

Processing of composites can be divided into three steps:

1. Layup of plies;
2. Air evacuation and consolidation;
3. Heated cure.

The consolidation process for composites is shown in Figure 2.15. Initially, once the layup of plies is complete, the plies are unconsolidated with micro and macro voids trapped throughout the laminate. Next, the part is placed in a vacuum bag for the debulking step, which evacuates

entrapped air from within the plies. Finally, the heated cure will enable the resin to flow and impregnate the fiber, pushing any remaining air out [13].

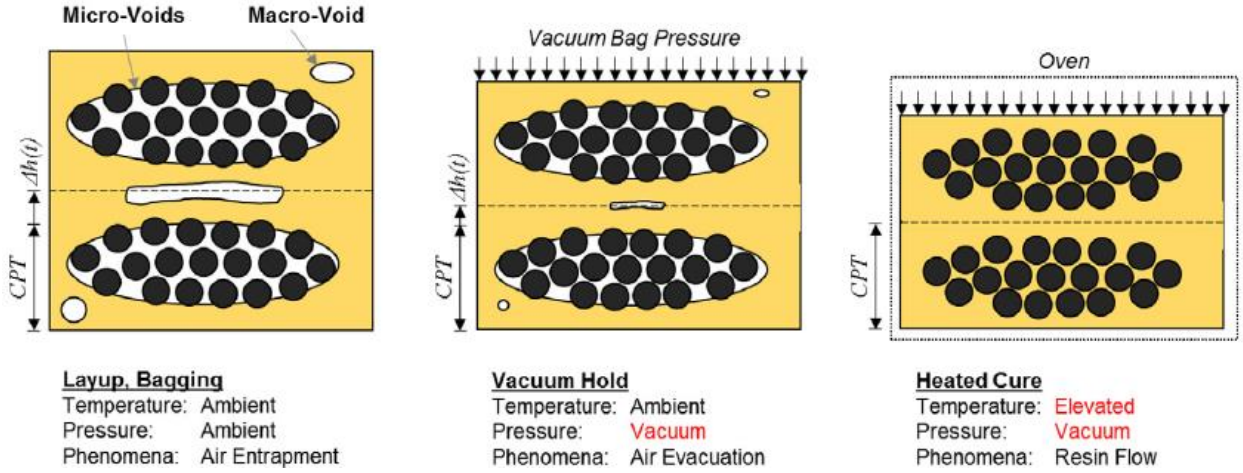

Figure 2.15. Schematic of out-of-autoclave prepreg consolidation of two plies. (a) Layup: circular fibers are surrounded by resin and voids. (b) Debulking: entrapped air is evacuated and plies consolidate. (c) Heated Cure: Resin flows filling in voids. Thickness is further decreased reaching the cure-ply thickness (CPT). Modified from [13].

Effects of processing conditions on the microstructure of carbon fiber/epoxy have been investigated where impregnation and evolution of porosity during processing stages were analyzed using micro-CT [19]. The effect of oven ramp rates was discussed indicating that high ramp rates may lead to high macro-void content. Alternatively, low ramp rates will cause slow infiltration causing the resin to reach gelation before the fiber tows are saturated with resin. The results clarified the principal resin flow phenomena, which are tow impregnation and macro-flow into inter-ply gaps [19].

The effect of deficient pressure at reduced ambient pressures during consolidation of out-of-autoclave laminates was investigated by Centea et al. The authors analyzed the effects of processing conditions on the thickness and porosity of the laminates. Deficient pressures will cause higher void contents therefore, air evacuation should be maximized by using proper vacuum bagging setups and allowing for room temperature vacuum hold times [44].

2.5.2. Effect of Porosity on Interlaminar Shear Strength

Woven fabrics are sensitive to porosity because they contain large interstitial spaces where air gets trapped during the layup [13]. Studies have been performed to understand the effect of voids on the interlaminar shear strength (ILSS) of composites. Mathematical expressions were developed to predict the ILSS based on cylindrical and spherical voids – two accepted void configurations in composites – show in Eq. 2.8 and Eq. 2.9. The $ILSS_r$ is the ratio of the ILSS with voids to the ILSS without voids, V_V is the void content, and V_{f_v} is the fiber volume fraction [20, 45, 46].

Cylindrical Voids

$$ILSS_r = \left[1 - \frac{4V_V}{3.14\left(1 - V_{f_v}\right)}\right]^{1/2} \quad (2.8)$$

Spherical Voids

$$ILSS_r = 1 - \frac{3.1416}{4}\left[\frac{6V_V}{3.1416\left(1 - V_{f_v}\right)}\right]^{2/3} \quad (2.9)$$

As shown in Table 2.2 and Figure 2.16, as void content increases, ILSS quickly decreases. In regard to Eq. 2.8 and 2.9, the best fit was reported using a power equation by means of the correlation coefficient (R^2) [45].

Table 2.2. Void content V_v, absorption coefficient α, and interlaminar shear strength (ILSS) for carbon fiber / epoxy laminates with a layup of $[(0/90)_{14}]$ [47].

Porosity level	Average void content, V_v (%)	Absorption coefficient α (db/mm)	ILSS (MPa)
Reference	0.55±0.03	0.11	82.2±3.0
EP-1	1.41±0.03	0.55	71.4±3.0
EP-2	1.90±0.02	0.88	67.8±1.7
EP-3	2.17±0.02	0.99	65.7±8.5
EP-4	2.18±0.02	1.22	63.5±3.7
EP-5	2.40±0.09	1.51	65.3±4.0
EP-6	4.01±0.02	1.82	59.5±3.5
EP-7	5.60±0.03	2.18	54.5±2.8

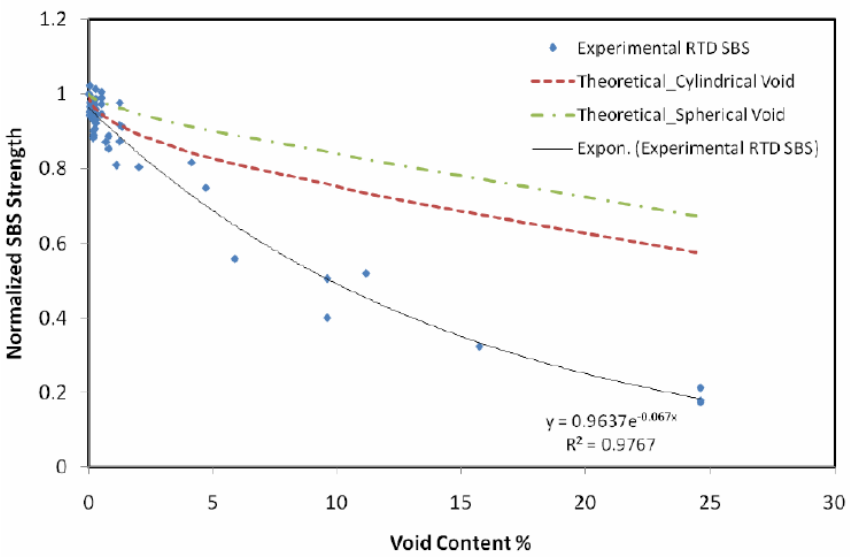

Figure 2.16. Comparison of experimental and theoretical short beam strength for UD carbon fiber / epoxy (IM7 / 977-2). The stacking sequence was $[(0/90_2/0)]_{4s}$ [20, 46].

Mahdavi investigated the effects of thermal cycling on carbon fiber / epoxy materials and reported that cross-ply specimens were more susceptible to microcracks at early stages of thermal cycling compared to unidirectional specimens. One cause for this phenomenon is the presence of higher void content in cross-ply specimens where cracks can initiate and propagate around voids [22]. Voids can act as stress concentrators causing cracks to emanate from them illustrated in Figure 2.17 [47].

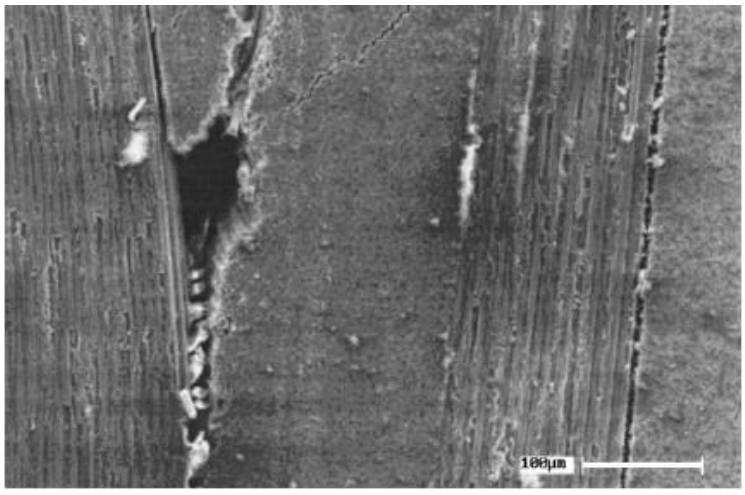

Figure 2.17. Carbon fiber / epoxy laminate with porosity after short beam testing [47].

2.6. Joining and Repair of Thermoset Composites

This section will discuss joining and repair methods for thermoset composites. First, two joining methods will be described: (1) adhesive bonding and (2) mechanical fastening. These will be compared showing common configuration used for joining. Next, two common methods of adhesive repair will be introduced: (1) hard-patch repair and (2) soft-patch repair. The advantages and challenges during the implementation of these repair methods will be discussed.

2.6.1. Joining Methods

There are two common methods of joining thermoset composite materials, those being mechanically fastened or adhesively bonded. Composite materials may also be joined to metals or other kinds of composite materials. The advantages of each method are listed in Table 2.3. Joining configurations will depend on the applications and loading conditions of the joined structure. Common configurations for adhesively bonded and mechanically fastened joints are illustrated in Figure 2.18 and Figure 2.19 respectively.

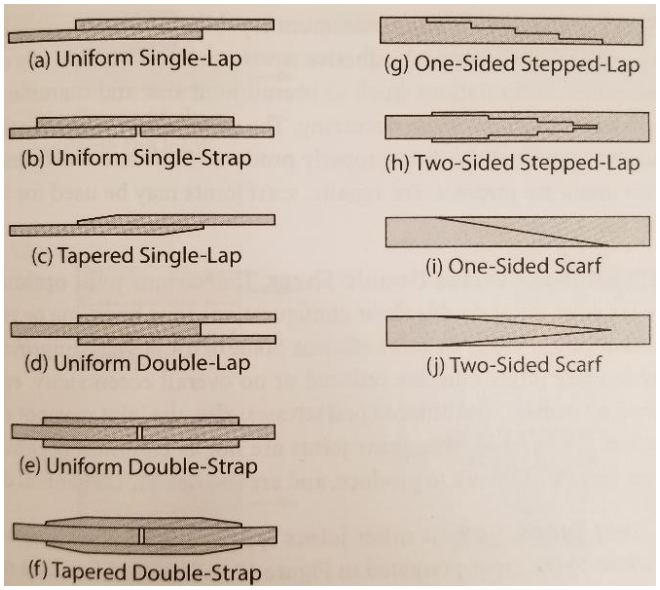

Figure 2.18. Common configurations for bonded joints used in in-plane loading [1].

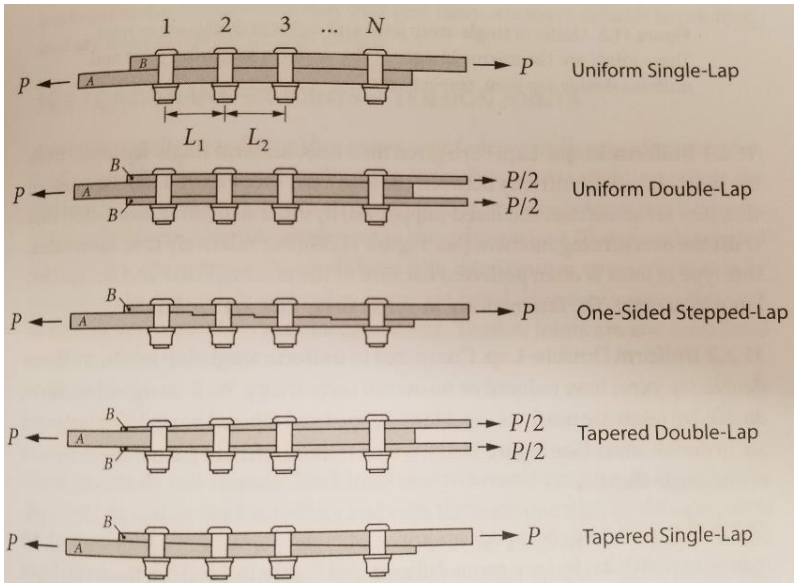

Figure 2.19. Configurations for fastened shear joints [1].

Table 2.3. Advantages of adhesive bonding and mechanical fastening [1].

Adhesive Bonding	Mechanical Fastening
• Better fatigue performance since there are fewer holes to act as stress concentrators. Eliminates the fastener fatigue failures. • Weight reduction as no fasteners are required with the potential to make certain structures such as aircraft more efficient. • The potential load capability is greater than for fastened joints (again, no holes meaning no reduction in net section area). • Aerodynamic and corrosion resistant.	• They are simpler to manufacture compared to bonded joints. • Can tolerate extreme temperature and moisture conditions. • Can be disassembled and replaced or repaired with more ease. • Fastened joints are usually better for thick parts as opposed to thin ones. • Even if a fastener is poorly processed, it has some capability of bearing or transferring a load due to redundant load paths (typically multiple fasteners are applied).

2.6.2. Repair Methods

Adhesive repair patches can be fabricated through different methods listed below [48]:

- Pre-cured patch (hard patch);
- Co-cured patch (soft patch);

A common configuration for adhesive repair is using the scarf configuration shown in Figure 2.20. Developing the appropriate repair methods will depend on the application of the repaired structures. This section will focus on the work that has been done regarding repair methods of carbon fiber composites using soft- and hard-patches on scarf and open hole repair.

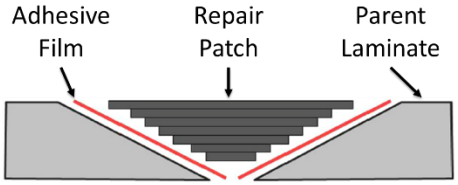

Figure 2.20. Schematic of scarf repair modified from [3].

2.6.2.1. Hard patch

The hard-patch repair method consists of pre-curing a patch and then bonding it using adhesive films to the damaged region. The fabrication of the hard patch can be done with either a mold or by machining the patch to the contour of the damaged region [2, 49]. The advantages to this method include controlled manufacturing conditions of the patch (typically done by vacuum bagging and oven cure) where material properties can more closely match those of the parent structure. In addition, the repair patch may have a superior surface finish (no wrinkles) with more control on moisture content reducing the introduction of porosity into the repair region [2]. However, challenges can still be faced leading to defects such as ply mismatch, porosity in the adhesive film, and warping of plies as shown in Figure 2.21 for a scarf joint [49].

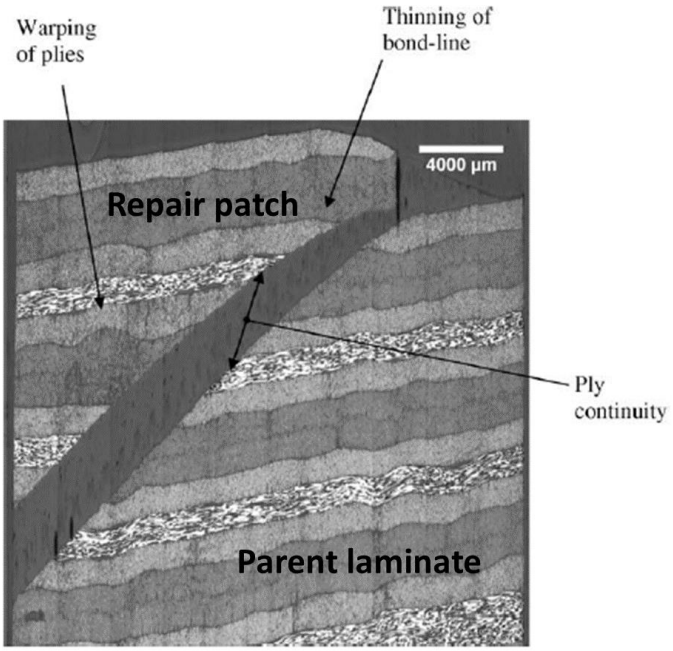

Figure 2.21. Cross-section of machined hard-patch on scarf repair, modified from [49].

2.6.2.2. Soft patch

The soft-patch repair method consists of in-situ repair by cutting prepregs or dry fibers to match the contour of the damaged region. Adhesive films are placed over the damaged region followed by the repair plies. These are then co-cured by vacuum bagging and application of a heated blanket (or other forms of heat, e.g. oven) [2, 3, 49]. For dry fibers, resin infusion can be used to impregnate the fibers and bond the patch to the parent structure.

The advantages to soft-patch repair is that it can be done in-situ with fewer manufacturing steps compared to hard-patch repair. Soft-patch repair can be less expensive, able to conform to complex damaged regions, and does not require a mold or extensive machining [2, 3]. Preau et al. investigated evacuation strategies for co-bonded scarf repairs and found that embossing – a texturing process for the adhesive film – resulted in lower void content and improved bondline quality, illustrated in Figure 2.22 [3].

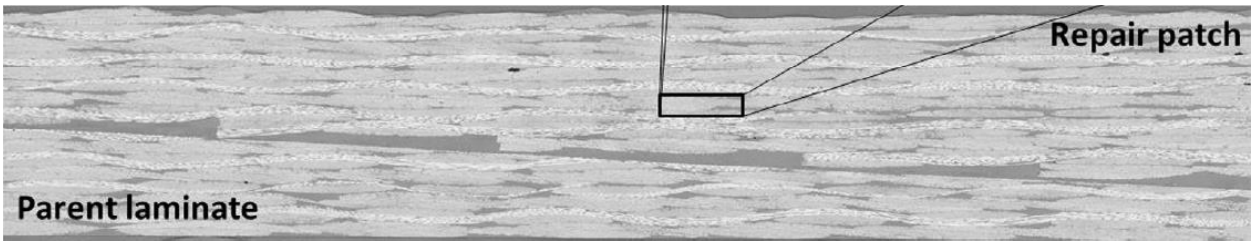

Figure 2.22. Optical microscopy of scarf repair with breathable adhesive [3].

2.6.3. Open Hole (Notched) Repair

Caminero et al. investigated repair of open-hole (notched) T700 / M21 carbon fiber / epoxy specimens using single- and double-sided hard-patch repairs, as shown in Figure 2.23. These were then analyzed for strength recovery where about 70% of the unnotched strength was recovered for the double-sided repair [50]. Other sources on repair of notched samples are scarce, however, there are numerous articles on estimating open-hole strength using finite-element models, digital image correlation (DIC), and experimental testing with different layup configurations [50-52].

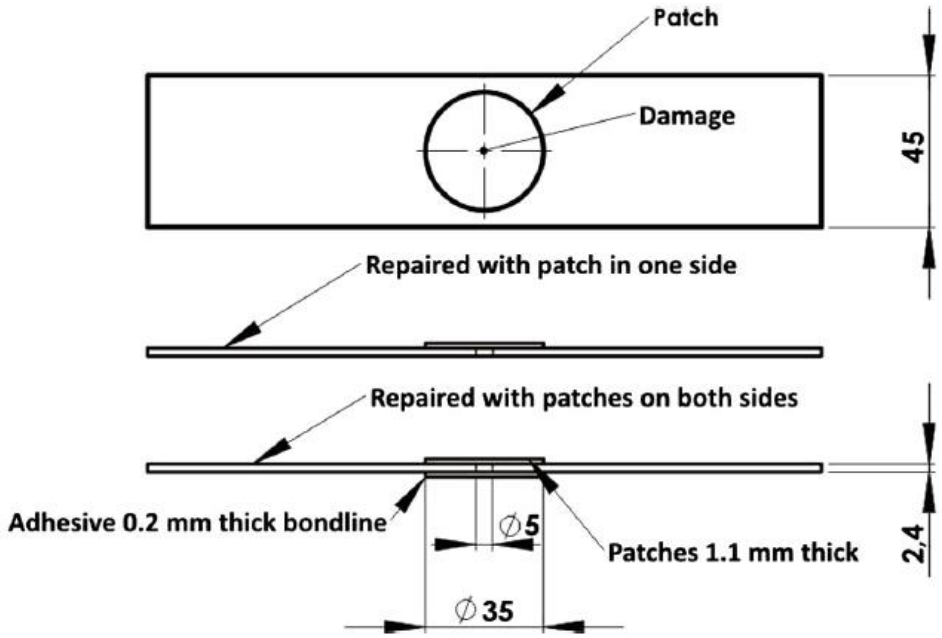

Figure 2.23. Geometry and configurations for single- and double-sided bonded patch repair [50].

2.7. Research Gap

Although ultrasonic welding is commonly used for thermoplastics, there is a lack of information about its effects on fiber reinforced thermoset composites. As seen from previous work done with USW, this method was reported to effectively consolidate plies. This was demonstrated in continuous applications such as filament winding and automated fiber placement. Following the literature review, three main knowledge gaps were identified:

1. There are no sources on how the consolidation quality and void content are affected by USW for thermoset composites. More work needs to be done to gain a better understanding on how to achieve the best quality, related to ultrasonic parameters (force, amplitude, sonotrode geometry) and material properties (fiber architecture, number of plies).
2. Experimental temperature measurements during USW are scarce for thermoset composites. The effect of temperature on degree-of-cure and resin flow is not well understood with the possibility of leading to property gradients caused by the application of ultrasonic vibrations.
3. Articles were not found regarding repair methods using USW. This field would need to be researched to find how effective USW is at consolidating and removing trapped air from repair patches. In addition, quantifying the strength recovery of repaired structures would be useful for comparison to other repair methods.

CHAPTER 3.
EXPERIMENTAL METHODOLOGY

This chapter will describe the experimental procedures used for each aspect of this project. The materials will first be introduced, followed by some common manufacturing methods. Next, ultrasonic welding will be explained focusing on the equipment's functions, weld modes, and relevant welding parameters. Afterwards, experimental setups for temperature measurements and models for characterization of cure kinetics and rheological behavior will be explained. Lastly, the procedures on repair techniques and mechanical tests will be covered.

3.1. Materials

Carbon fiber (CF) prepregs were used in this project for the convenience in handling and manufacturing. Using prepregs avoided the inconsistencies that may be cause from varying fiber volume fractions. Thus, prepregs may produce more consistent and better quality parts [13]. Three carbon fiber / epoxy prepregs and one adhesive film were used for this project summarized in Table 3.1.

Table 3.1. Summary of materials used in this project.

Fiber / Resin	Weave	Manufacturer	Fiber areal weight (g/m^2)	Fiber vol. fraction (%)	Cure ply thickness (mm)
AS4 / Newport 301	Twill Weave (TW)	Rock West Composites	200	55	0.30
IM7 / Cycom® 5320	Unidirectional (UD)	Cytec Solvay Group	145	59.9	0.14
T650 / Cycom® 5320	Plain Weave (PW)	Cytec Solvay Group	193	64	0.20
Adhesive Film: FM 300-2M	NA	Cytec Solvay Group	*293	NA	**0.25

* Nominal weight, ** Nominal thickness

From this list, AS4 / Newport 301 was a general purpose prepreg designed for autoclave or out-of-autoclave manufacturing. Alternatively, IM7 / Cycom 5320 and T650 / Cycom 5320 were aerospace grade prepreg designed for out-of-autoclave manufacturing. The weave patterns for each material are shown in Figure 3.1. To simplify the discussions regarding these materials, these prepregs may also be referred to by their weave pattern:

- Twill Weave – TW
- Unidirectional – UD
- Plain Weave – PW

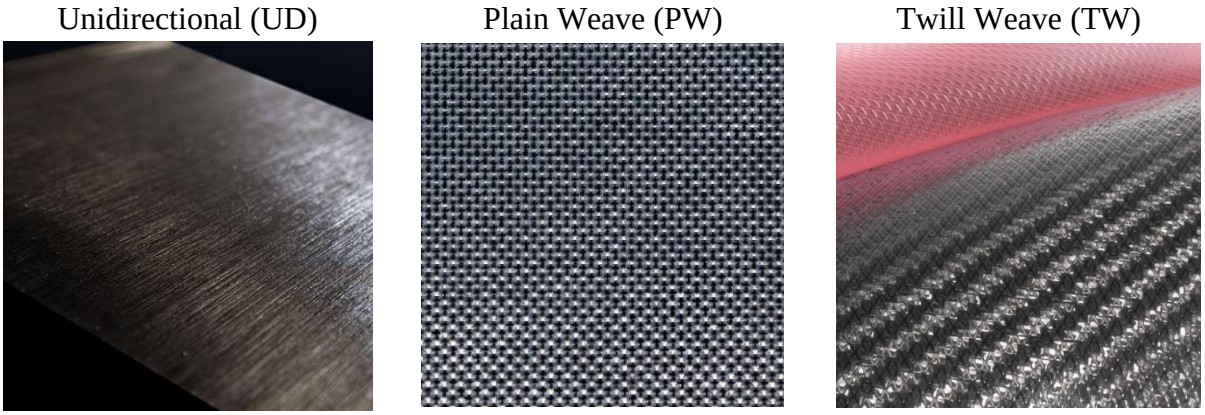

Figure 3.1. Images of carbon fiber weave pattern for materials used in this project. (a) Unidirectional (UD) prepreg [53], (b) plain weave (PW) prepreg [54], and (c) twill weave (TW) prepreg [55].

3.2. Manufacturing Methods

This section will describe manufacturing by hand layup and vacuum bagging. Vacuum bagging is commonly used due to its versatility and ability to create good quality parts with low porosity. In general, vacuum bagging is done by enclosing the part with bagging film and pulling vacuum. This allows air trapped between the prepreg plies to be evacuated. In addition, by pulling vacuum, 1.0 atm (101325 Pa) of pressure is applied on the laminate, consolidating the prepreg

plies. Vacuum bagging can be divided into three stages; (1) gathering materials and hand layup of the prepreg plies, (2) debulking, and (3) curing the resin.

3.2.1. Vacuum Bagging

A schematic of the vacuum bagging setup is illustrated in Figure 3.2. A steel plate – also referred to as the tool plate – was cleaned with acetone. Release film was then applied to the tool plate and secured with flash break tape. The prepreg plies were then applied over the film one at a time using a roller to push air out before applying the next ply. Once all the plies were positioned, release film was placed over the laminate. Two layers of bleeder/breather were placed over the release film followed by the bagging film. The bagging film was sealed to the tool plate using vacuum sealant tape.

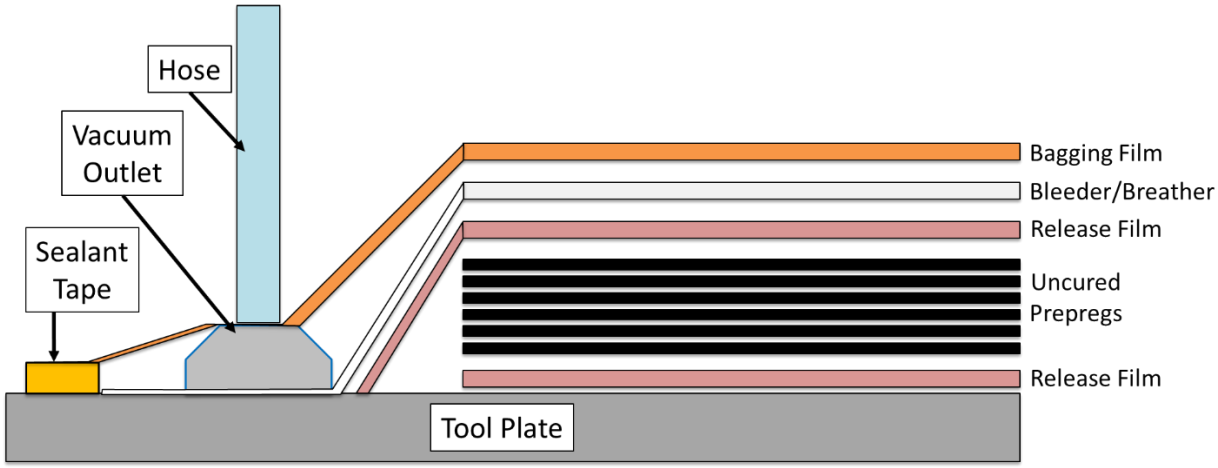

Figure 3.2. Vacuum bagging schematic.

Once the part was sealed inside the bag, the debulking process was initiated. Vacuum was applied to the bag making sure to find and eliminate air leaks. The vacuum pressure was observed until there was no air loss greater than 1.0 in-Hg (3386.4 Pa) over 10 minutes. For each prepreg, a room temperature debulking cycle of two hours was applied.

After the debulking process, the curing process was initiated by placing the laminates in an oven. The manufacturers' recommended cure cycle was used for the resin system of each prepreg

listed in Table 3.1. The vacuum bagging steps are summarized in Figure 3.3. After the curing cycle was complete, the laminates were cooled to room temperature at a maximum rate of 10°C/min.

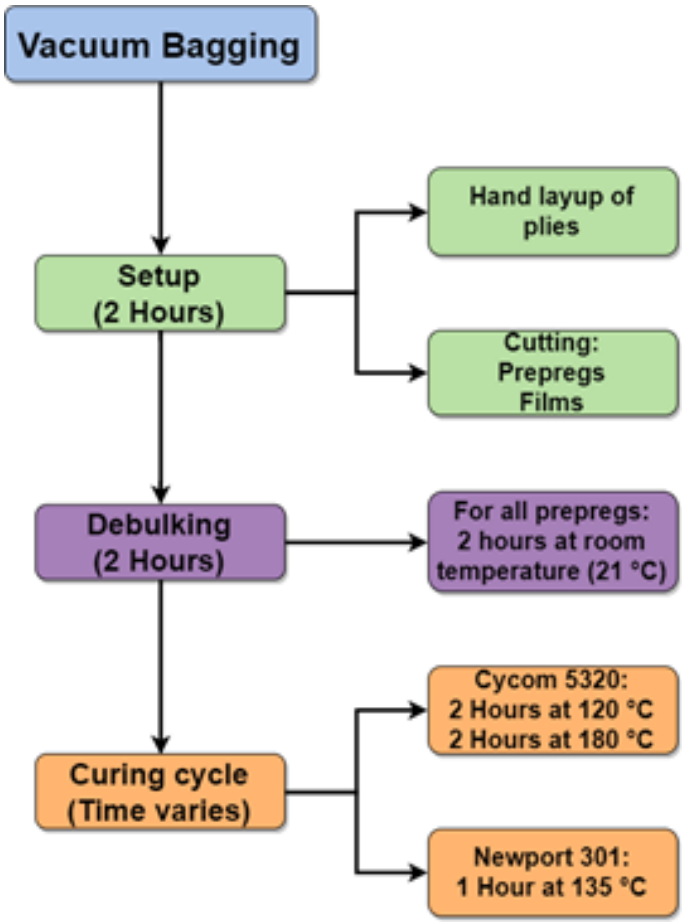

Figure 3.3. Summary of vacuum bagging steps and time duration.

3.3. Ultrasonic Welding

This section will begin by explaining how the ultrasonic welder works. The welding procedure will be shown explaining each step of the process. Next, the welding parameters will be defined showing the range of parameters investigated. Lastly, the welding set-up used to test the welding parameters will be explained.

3.3.1. Equipment and Process

The ultrasonic welder used in this project was the Rinco Dynamic 3000 with a frequency of 20 kHz and a force capacity of 3000 N, shown in Figure 3.5 (a). The press was controlled pneumatically and in conjunction with the ACU Control module generator. Multiple components control the oscillator system, those being the converter, booster and sonotrode (also called a "horn") shown in Figure 3.5 (b). The shape of the sonotrode was round and flat with a diameter of 40 mm as show in Figure 3.4.

Figure 3.4. Titanium sonotrode used for experiments measuring 40 mm in diameter.

Altogether, these components control the amplification of the vibrations through a series of ratios. In this case, the booster had a ratio of 1:1.5 and the sonotrode had a ratio of 1:3.85 [56]. Half the peak-to-peak amplitude ranged between 38.1 and 63.5 µm. The welding process consists of six steps that can be controlled by the user. Table 3.2 describes each step as shown in Figure 3.5 (c).

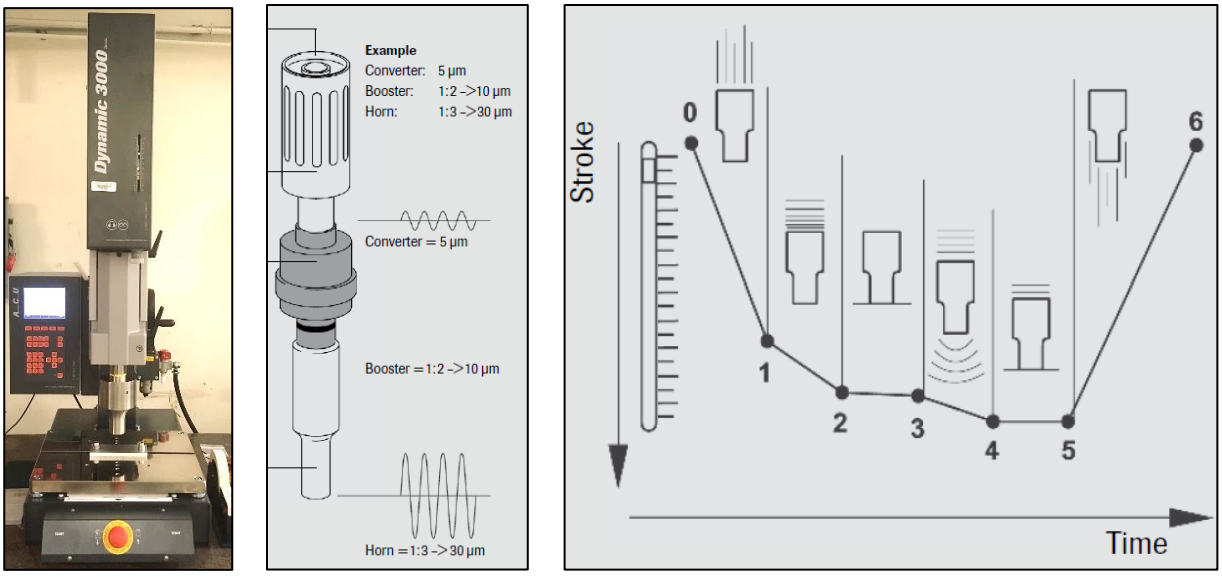

(a) (b) (c)

Figure 3.5. (a) Rinco Dynamic 3000 ultrasonic welder. (b) Oscillating system showing amplification of vibrations. (c) Schematic of welding process [56].

Table 3.2. Description of each step in the welding process as shown in Figure 3.5(c)

Step	Description
0 – 1	Pre stroke: Fast downward movement of the sonotrode
1 – 2	Braking: Reduction of speed until gentle stop
2 – 3	Force Build-up: Gradual build-up of force until programmed force is reached
3 – 4	Melting on: Vibrations are applied
4 – 5	Solidification: Vibrations stop yet sonotrode continues applying timed force
5 – 6	Return Stroke: Fast return of sonotrode to upper rest position

3.3.2. Definition of Welding Modes and Parameters

The ultrasonic welder has multiple welding modes and welding parameters. The two welding modes explored for this study were:

1. Weld by time: Vibrations stop once time (duration of weld) is met.
2. Weld by travel: Vibrations stop once travel (vertical displacement of the sonotrode) is met.

When using the weld by time mode, the user cannot control the travel, however, after the weld is complete, the welder will provide the travel reached. Likewise, when using the weld by travel mode, the user cannot control the duration of the weld, however, after the weld is complete, the welder will provide the weld time. Various parameters can be controlled at each stage of the welding process listed and described in Table 3.3.

Table 3.3. Description of ultrasonic welding parameters.

Parameter	**Description**
Time	Controls duration of weld (only in weld by time mode).
Travel	Controls vertical displacement of sonotrode (only in weld by travel mode).
Force	Force applied by the sonotrode to the weld specimen.
Force Buildup	The rate at which force will increase before the vibration phase.
Rise of Force	The rate at which force will increase during the vibration phase.
Amplitude	Half the peak-to-peak mechanical vibration of the sonotrode.
Solidification	Sonotrode will continue applying pressure to specimen after vibration phase. User decides solidification force and duration time.

An in-depth qualitative analysis was performed to understand the appropriate welding parameters for each prepreg used. A summary of the welding parameters investigated is shown in Table 3.4. In addition, the welder will monitor the travel, force, and power in real time. This allows for precise monitoring of the welding process.

Table 3.4. Summary of welding parameters examined

Welding Parameter	Settings
Force (N)	100, 300, 500
Time (s)	0.5, 1.0 – 5.0
Travel (%)	12.5 – 50.0
Amplitude (μm)	38.1 – 63.5
*Number of Plies	2 – 12

* Number of plies is not a welding parameter, however it is a parameter that is correlated to the resulting quality of welded specimens.

3.3.3. Testing Ultrasonic Welding Parameters

Ultrasonic welding parameters were tested by welding multiple plies of prepregs measuring 25.4 mm x 25.4 mm (1” x 1”) demonstrated in Figure 3.6. This setup allowed for a qualitative assessment of the effects of the welding parameters. Based on the results, the welding parameters were modified to optimize the quality of the weld. To compare the welder’s real time travel, the thickness of the samples was measured with a caliper before and after the weld.

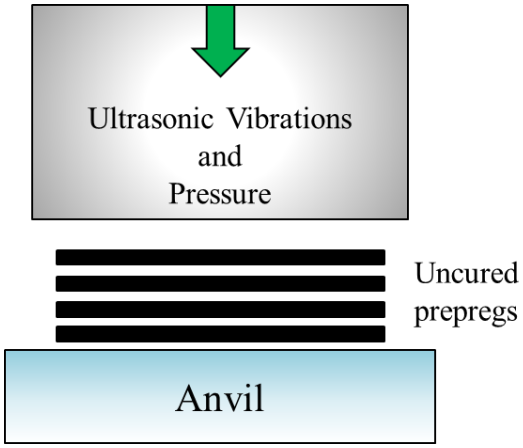

Figure 3.6. Welding setup used to test welding parameters.

3.4. Temperature Measurements

Temperatures were monitored using type-K thermocouples and a FLIR A325sc infrared (IR) camera. These instruments were positioned as shown in Figure 3.7 to obtain general temperature profiles during USW. This setup was used on 4 and 12 plies of UD prepreg. The laminates each had a symmetric (0/90) layup and measured 25.4 mm x 25.4 mm (1” x 1”). The welding parameters used for both laminates were a force of 100 N, amplitude of 38.1 μm, and travel of 25% the laminate thickness.

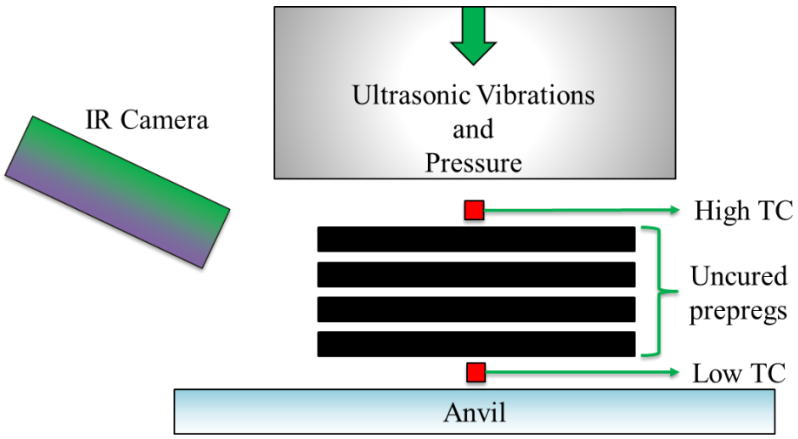

Figure 3.7. Temperature monitoring setup using thermocouples (TC) and IR camera. Low TC corresponds to thermocouple below laminate while High TC corresponds to the thermocouple above the laminate.

Further measurements were performed to find the through-the-thickness temperature profile. This was done as shown in Figure 3.8 using seven type-K thermocouples placed at the center of every other prepreg ply. Samples measured 25.4 mm x 25.4 mm (1" x 1") and were tested for a UD laminate consisting of 12 plies. Temperature measurements were captured using a DATAQ DI-2008 data acquisition system featuring 8 analogue input channels.

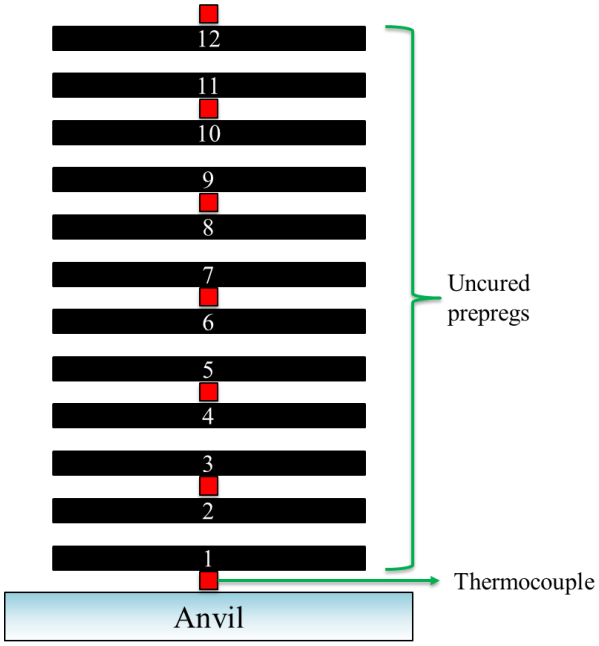

Figure 3.8. Schematic of thermocouple placement for through-the-thickness temperature monitoring during USW of a 12 ply, 25.4 mm x 25.4 mm laminate of UD prepreg.

3.5. Degree of Cure and Viscosity

For thermoset polymers, the degree-of-cure and viscosity are important parameters to consider during manufacturing procedures. Semi-empirical models for cure kinetics and viscosity of Cycom 5320 were previously developed using a DSC and parallel plate rheometer [18]. These models along with temperatures collected from the thermocouples and the IR camera were used to understand if USW allowed resin to cure and flow.

The cure kinetic models developed by Kratz et al. uses the Arrhenius temperature dependency (K) shown in Eq. 2.1. The model in terms of the cure rate, $d\alpha/dt$, is shown in Eq. 3.1 where α is the degree-of-cure, α_{c_0} is the critical degree-of-cure at absolute zero, α_{CT} is a factor that accounts for the increase in critical degree-of-cure with temperature, D is the diffusion constant, and m, n, and A are constants.

$$\frac{d\alpha}{dt} = K_1\alpha^{m_1}(1-\alpha)^{n_1} + \frac{K_2\alpha^{m_2}(1-\alpha)^{n_2}}{1+\exp^{(D(\alpha-(\alpha_{C0}+\alpha_{CT}T)))}} \tag{3.1}$$

Parameters for this model were found by method of least squares curve fitting, and in the case of the activation energy, this was found by measuring the slope of $\ln d\alpha/dt$ vs. $1/T$ for degrees-of-cure less than 0.1 [18]. The values obtained for the model can be found in Table 3.5.

Much like the cure kinetics model, a similar approach was used to develop the model for viscosity. In Eq. 3.2 the Arrhenius temperature dependency (η_i), consists of E_{η_i} the viscosity activation energy, R the ideal gas constant, T the absolute temperature, and A_{η_i} a constant.

$$\eta_i = A_{\eta i}\exp^{\left(\frac{E_{\eta i}}{RT}\right)},\ i = 1, 2 \tag{3.2}$$

The viscosity model shown in Eq. 3.3 accounts for viscosity in the gelation stage by including the exponential polynomial where A, B, and C are constants, α is the instantaneous

degree-of-cure using the predicted degree-of-cure from Eq. 3.1, α_{gel} the degree-of-cure at gelation, and η_i the Arrhenius temperature dependency.

$$\eta = \eta_1 + \eta_2 \left(\frac{\alpha_{gel}}{\alpha_{gel} - \alpha} \right)^{A+B\alpha+C\alpha^2} \quad 3.3$$

Table 3.5. Parameters for 5320 resin cure kinetics model modified from [18].

Parameter	Cycom 5320
$A_1(s^{-1})$	8.23×10^7
E_{A_1} (J/mol)	82,375
m_1	0.75
n_1	12.46
A_2 (s^{-1})	1.04×10^5
E_{A_2} (J/mol)	62,355
m_2	0.90
n_2	2.07
D	40.4
α_{c_0}	-1.12
α_{CT} (K^{-1})	4.53×10^{-3}

The constants for this model shown in Table 3.6 were found by calculating the weighted least squares curve fit, activation energy was found by taking the slope of the plot of ln μ vs. $1/T$, and degree-of-cure at gelation was found by averaging the degree-of-cure when $\tan(\delta) = 1$ in the dynamic and isothermal tests [18].

Table 3.6. Parameters for Cycom 5320 resin viscosity model [18].

Parameter	Cycom 5320
$A_{\mu_1}(Pa \cdot s)$	8.0×10^{-13}
E_{μ_1} (J/mol)	93,931
A_{μ_2} ($Pa \cdot s$)	2.9×10^{-11}
E_{μ_2}(J/mol)	83,400
α_{gel}	0.48
A	3.2
B	12.7
C	-29.6

3.6. Microstructural Analysis

Welding parameters were validated by performing image analysis of the microstructure for void content. Welded samples were prepared for microscopy by post-curing in the oven following the manufacturers' cure cycle and then trimming of the edges using a Pico 155 precision diamond saw (Pace Technologies). The samples were then mounted in low viscosity mounting epoxy in either 12.7- or 38.1-mm diameter pucks.

Once the epoxy cured, the samples were removed from the plastic molds to be ground and polished. The grinding steps were modified from ASTM E2015 – 04 using 180, 360, 600, 800, and 1200-grit SiC abrasive pads. The samples were cleaned in an ultrasonic bath before proceeding to the next grinding step. Once the grinding sequence was complete, samples were polished using 6- and 1-micron diamond polishing solutions.

Microstructures were then analyzed using a Meiji MT8100 optical microscope. Image analysis was performed using ImageJ developed by the National Institute of Health (NIH) to quantify and compare the void content for each welding parameter investigated. Void content was calculated by dividing the area of voids by the total cross-sectional area of the welded samples.

3.7. Mechanical Testing

Mechanical tests were conducted on ultrasonic welded samples to evaluate the effectiveness of welding procedures and then compared with vacuum bagged only (VBO) samples. This section will cover short beam testing and open-hole tensile testing for all three prepregs investigated.

3.7.1. Short Beam Shear Test

Short beam shear (SBS) tests were carried out in accordance to ASTM D2344. The configurations shown in Figure 3.9 (a) and (b) were used to test the interlaminar shear strength

(ILSS) of the prepreg-laminate and adhesive-laminate interface respectively. The vacuum bagged laminates measure 152.4 mm x 152.4 mm (6" x 6") with varying number of plies. As shown in Table 3.7, the laminates were manufactured using a symmetric layup to produce a balanced laminate to reduce any bending or twisting moments. It is important to note that the same laminates were used for the upper and lower laminates labeled in Figure 3.9.

Table 3.7. Laminate layup and number of plies for each material used in short beam testing.

Material	Number of Plies	Layup	Thickness (mm)	Void Content (%)
AS4 / Newport 301 (TW)	6	$[(0/90)_3]_s$	1.68 ± 0.03	1.85 ± 0.66
IM7 / Cycom 5320 (UD)	12	$[(0/90)_6]_s$	1.75 ± 0.02	0.64 ± 0.04
T650 / Cycom 5320 (PW)	8	$[(0/90)_4]_s$	1.69 ± 0.01	0.85 ± 0.28

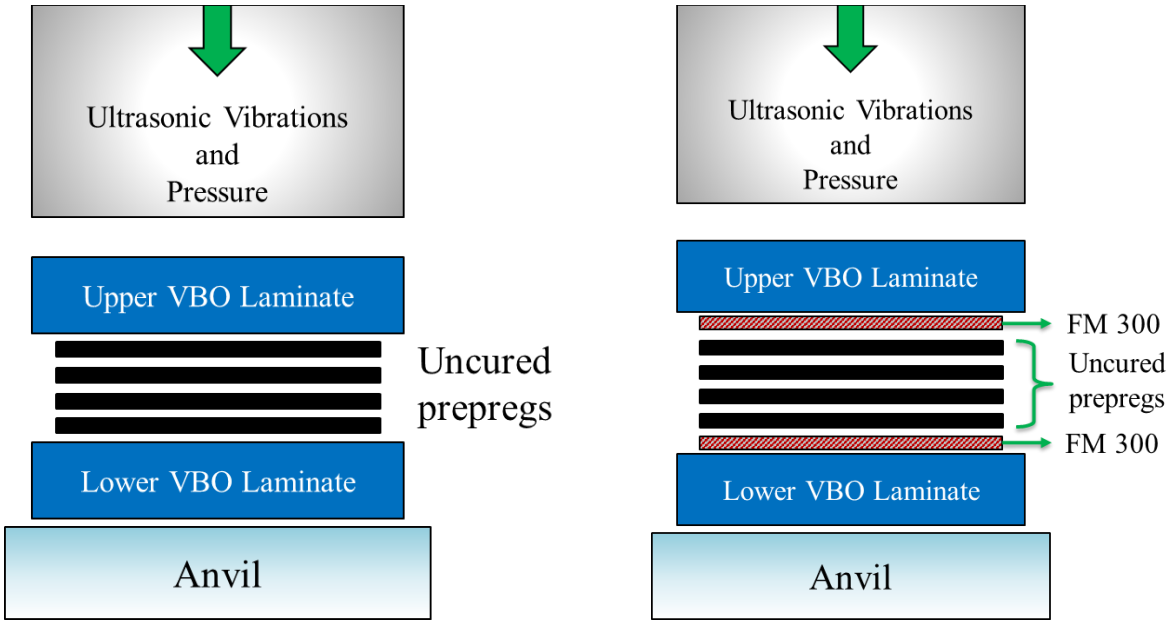

Figure 3.9. Welding setup for short beam shear samples: (a) without adhesive film and (b) with adhesive film (FM 300-2M).

All materials (laminates, prepreg, and adhesive film) measured 25 mm x 10 mm when they were welded or vacuum bagged and then sanded to size. For each material, five samples were tested per test condition. Additional details on the tested samples can be found in Table 3.8.

Table 3.8. Physical properties for short beam shear samples. The test conditions were abbreviated to USW for ultrasonic welded and VBO for vacuum bagged only.

Material	Prepreg plies	Adhesive plies	Length (mm)	Width (mm)	Thickness (mm)
TW USW	2	NA	22.29 ± 0.20	7.43 ± 0.07	3.71 ± 0.03
TW VBO	2	NA	21.85 ± 0.21	7.28 ± 0.07	3.64 ± 0.04
UD USW	4	NA	23.16 ± 0.41	7.72 ± 0.14	3.86 ± 0.07
UD VBO	4	NA	23.34 ± 0.29	7.78 ± 0.10	3.89 ± 0.05
PW USW	2	NA	22.09 ± 0.15	7.36 ± 0.05	3.68 ± 0.02
PW VBO	2	NA	21.76 ± 0.17	7.25 ± 0.06	3.63 ± 0.03
PW USW with FM 300-2M	2	2	23.87 ± 0.27	7.96 ± 0.09	3.98 ± 0.05
PW VBO with FM 300-2M	2	2	22.41 ± 0.24	7.47 ± 0.08	3.73 ± 0.04

3.7.2. Open-Hole Tensile Strength Test

Open-hole tensile strength (OHTS) tests were carried out in accordance to ASTM D5766. Samples with an open-hole will also be referred to as notched samples. Repair of notched samples was performed using ultrasonic welding (USW) and vacuum bagging only (VBO). Welded repair samples were then post-cured in the oven. To compare the strength recovery of repaired samples, notched and unnotched samples were also tested. A schematic of a notched and a repaired sample are shown in Figure 3.10.

Two methods of repair were investigated: soft patch and hard patch repair. As explained in the Literature Review (Chapter 2), a soft patch is a repair method were an adhesive film and uncured plies of prepreg are placed over the damaged region and co-cured (cured together). A hard patch repair is where the prepreg plies have been pre-cured and the adhesive film is used to bond the cured patch over the damaged region. The TW and UD samples were used for the soft patch repair whereas the PW samples were used for hard patch repair illustrated in Figure 3.11.

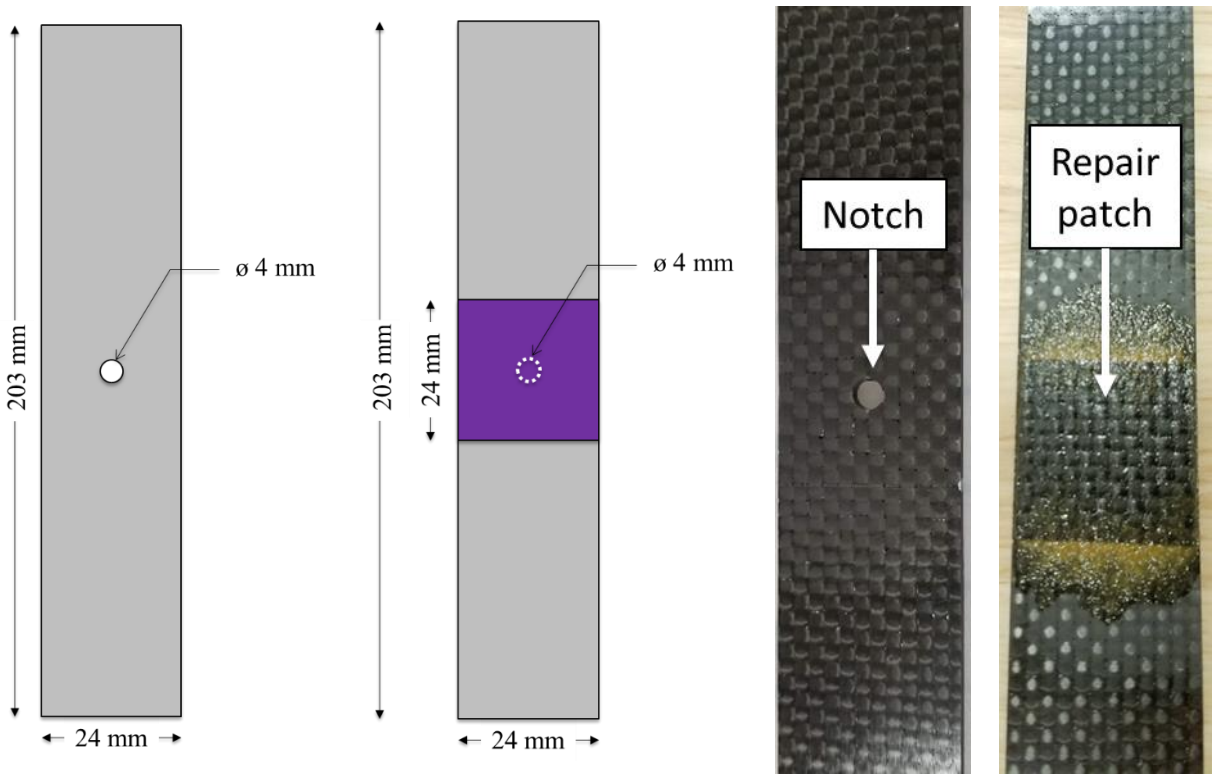

(a) (b) (c) (d)

Figure 3.10. Open-hole tensile strength samples. (a) Notched samples without repair patch, (b) notched samples with repair patch (shaded region), (c) actual PW notched sample, and (d) actual PW vacuum bagged repair sample.

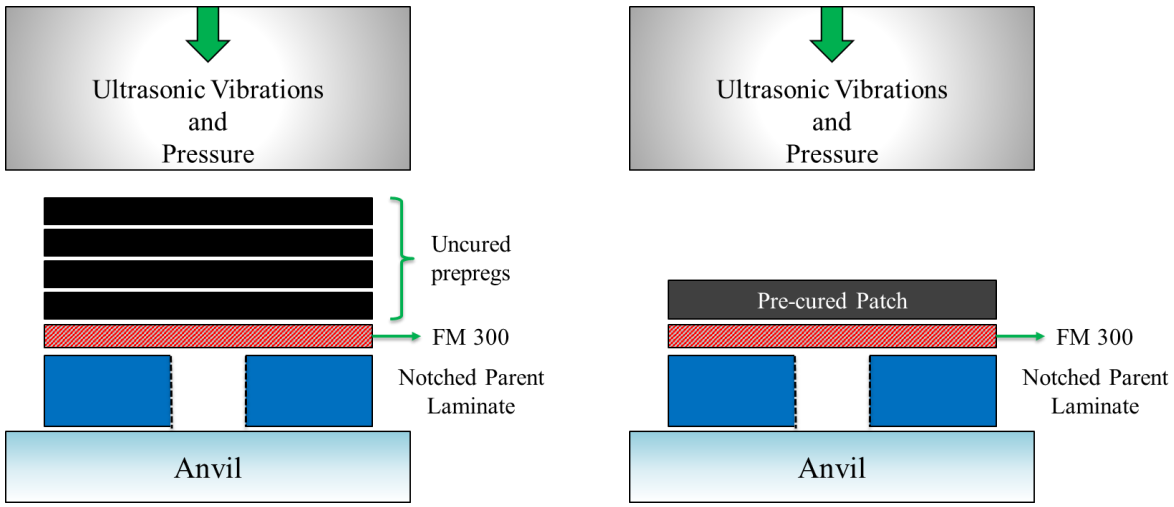

(a) (b)

Figure 3.11. Configuration for welded repair of notched specimens. (a) Soft patch repair consisting of layers of prepreg and 1 layer of adhesive film (FM 300-2M. (b) Hard patch repair consisting of a pre-cured patch (hard patch) and 1 adhesive film.

Ultrasonic welding of repaired patches was done with the fixture shown in Figure 3.12 that prevented the parent laminates from shifting during the welding process. The outer clamps had cut-outs matching the width of the samples while the inner clamps were used for addition support. The center of the specimen with the repair patch was centered below the sonotrode for an optimal weld. All welding parameters were kept constant for all materials except for the travel which depended on the thickness of the repair patch or adhesive film shown in Table 3.9.

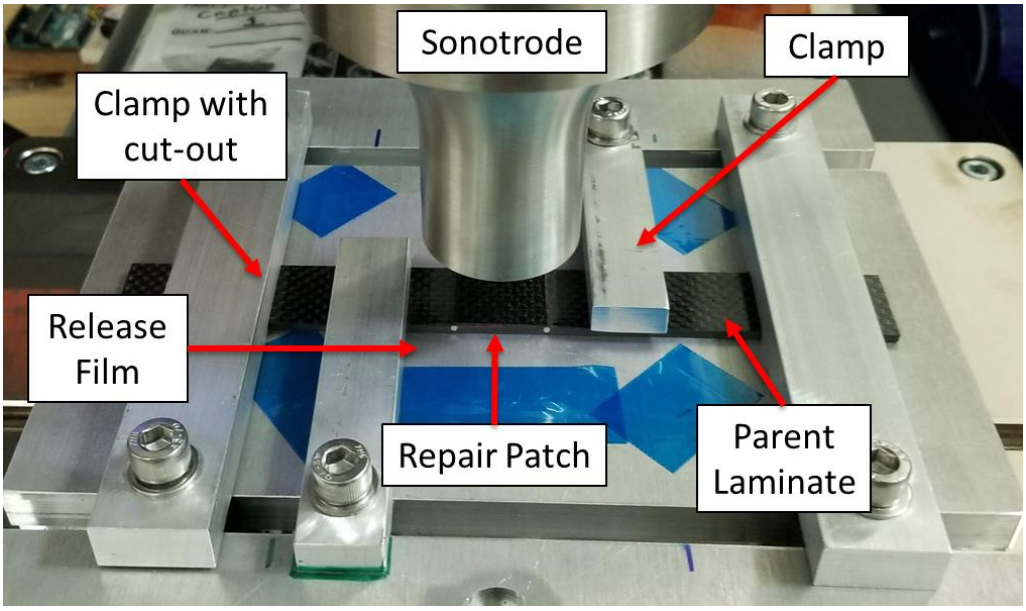

Figure 3.12. Ultrasonic welding fixture used for repair of open-hole samples. Release film was placed below repair region and over the repair patch (not shown) to protect the fixture and sonotrode from flowing resin.

Table 3.9. Description of repair patch constituents and welding parameters.

Material	TW	UD	PW
Repair Method	Soft Patch	Soft Patch	Hard Patch
Prepreg Plies	2 Uncured	4 Uncured	2 Cured
Adhesive Plies	1	1	1
Travel (%)*	25	25	25
Force (N)	100	100	100
Amplitude (μm)	38.1	38.1	38.1

*Regarding the welding travel, for the soft patch repair samples, the travel was set to 25% of the thickness of the prepreg plies and the adhesive film. However, for the hard patch repair, the travel was set to 25% the thickness of the adhesive film.

CHAPTER 4.
RESULTS AND DISCUSSION

This section will follow the order of topics presented in Figure 4.1.This chapter will begin by discussing the effect of welding parameters such as time, travel, force and amplitude on carbon fiber / epoxy prepregs. Next, experimental void content measurements for welded samples will be presented. Temperature measurements for different number of plies and through-thickness will be discussed followed by cure kinetics and viscosity models for Cycom 5320. Lastly, mechanical testing was performed on each prepreg where the interlaminar shear strength and open-hole tensile strength were found.

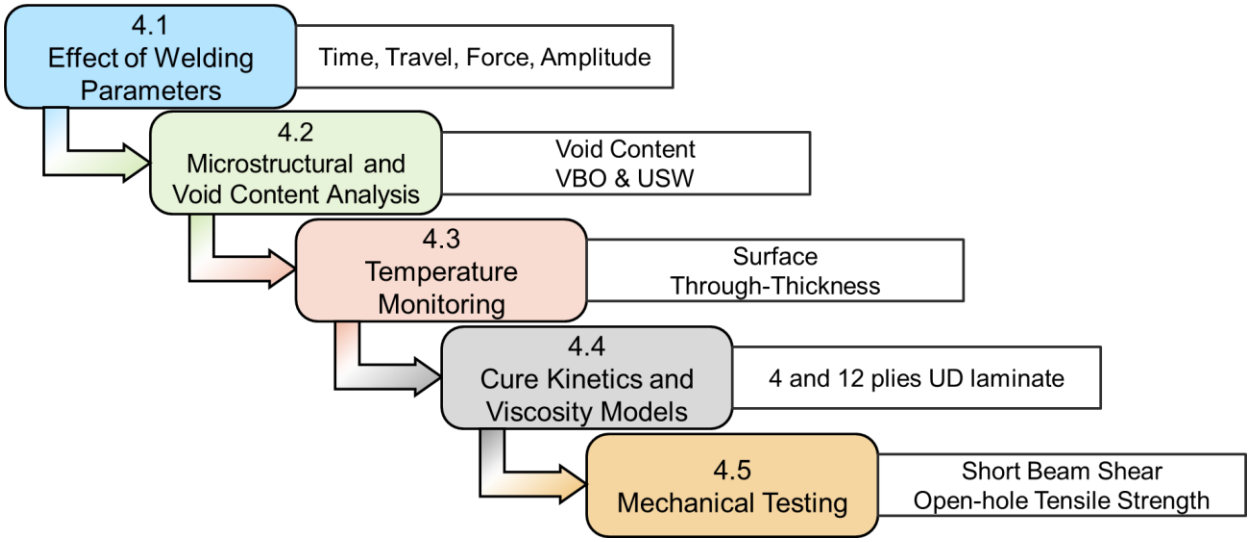

Figure 4.1. Overview of the results presented in this section.

4.1. Effect of Welding Parameters on Prepreg Quality

There is currently a lack of protocol to qualitatively determine the acceptable appearance of welded thermoset composites. Based on a wide range of welding parameters tested, qualitative observations were used to validate the quality of welds. Examining welding parameters must be done one at a time to isolate the effect of individual settings. Due to the large number of possible

combinations, the welding parameters investigated were reduced to the ones that had an evident effect on the quality of the weld shown in Table 3.4. Parameters were tested at the early stages of this project with TW AS4 / Newport 301. Later it was observed that all the conclusions drawn from these tests also applied to the other prepregs.

Before explaining the predominant welding parameters that were tested, it is important to note that some parameters were left constant. For example, force buildup and rise of force were examined individually to understand the effect on the quality of the sample. Force buildup did not actually affect the quality of the sample after testing a range of 0 – 250 N/s (in increments of 50 N/s) because this parameter only controls the rate at which the force is met before the weld. The force buildup was maintained at 50 N/s.

4.1.1. Time

The time setting allowed the user to control the duration of applied vibrations. The in-plane deformation of the square prepreg plies was used as a qualitative criterion to assess the quality of the weld. While it was difficult to tell if a sample had been under-welded, over-welding was more easily observed. Prolonged exposure to ultrasonic vibrations would begin to damage the fiber architecture and disrupt fiber bundles. Weld times over 1.0 s were considered over-welded based on the images of welded samples shown in Figure 4.2.

The change in thickness (Δt) – or the vertical displacement of the sonotrode – was monitored by the welder and measured using a caliper. The change in thickness for each weld time is shown in Figure 4.2. Variations in the thickness were noticed for separate samples welded with the same parameters using the weld by time mode. This could be a result of the materials resistance to the applied force of the sonotrode, position of the plies, and pressure applied during the layup of plies [27].

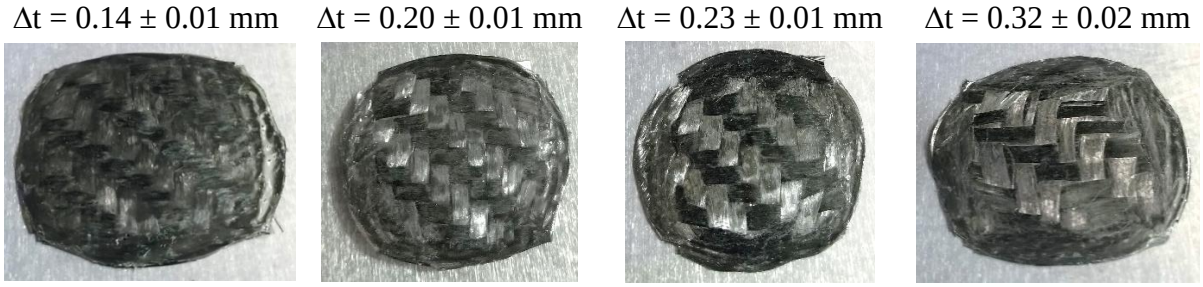

Figure 4.2. Comparison of the effect of vibration time on two plies of twill weave (TW) AS4 / Newport 301. The change in thickness caused by the weld is shown above the image. Force and amplitude were constant at 100 N and 38.1 μm, respectively.

4.1.2. Travel

The travel setting allowed the user to control the vertical displacement of the sonotrode. Using travel to control the duration of the weld offered several advantages. First, the travel programmed into the welder could be directly correlated to the thickness of the welded sample. Second, the travel mode is less sensitive to fluctuations in welding force and vibration amplitude [27]. Lastly, the same displacement can be achieved more quickly using the travel mode versus the time mode. This limits the vibrations applied on the specimen reducing damage over longer weld times. The travel ranged from 12.5% to 50% of the samples thickness. As presented in Figure 4.3, below 12.5%, there was no notable difference to the sample – most likely due to the lack of heat generation, which in turn, does not allow the resin to flow. Above 50% travel, significant damage was observed to the fiber architecture and fibers squeezing out. Therefore, the travel should remain below 50% and be over 12.5% of the samples' thickness.

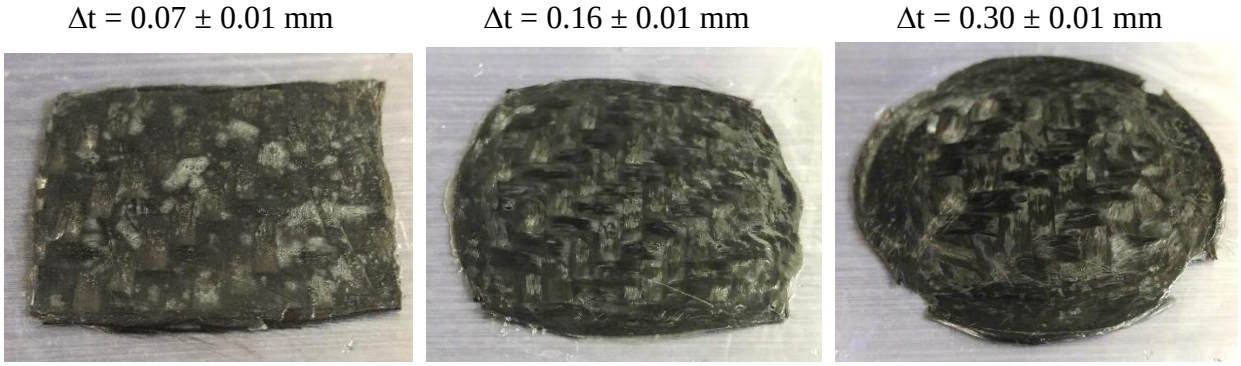

Figure 4.3. Comparing the travel setting for two plies of TW prepreg using displacement values equal to 12.5%, 25%, and 50% of the sample's thickness. Force and amplitude were constant at 100 N and 38.1 μm, respectively.

4.1.3. Force

Rise of force allows the force to increase during the weld. To test whether this parameter was necessary, the force was monitored using a rise of force equal to zero N/s. It was observed that the applied force during a weld decreases over time, which, may occur because the force is controlled pneumatically. A rise of force of 100 N/s was used to keep the force more consistent for longer (>3 s) welds.

The force setting was tested with both welding modes (by travel and by time). Using the weld by travel mode, increasing the force showed no effect on the specimen. The force setting was restricted by the displacement as increasing the force only caused welds to finish sooner. The final thickness of the specimens remained constant upon increasing the force.

Alternatively, the force setting was a significant factor when using the weld by time mode. The force parameters shown in Table 3.4 were examined as illustrated in Figure 4.4. During the vibration phase, increasing the force clearly showed a decrease in the samples thickness (increase in the change in thickness Δt). From Figure 4.4, it was concluded that force should be kept below 300 N to avoid large amount of fiber squeeze out and fiber bundle disruption. For all welds, the

force was left at 100 N as it kept the fiber architecture intact without any excessive fiber or resin squeeze out.

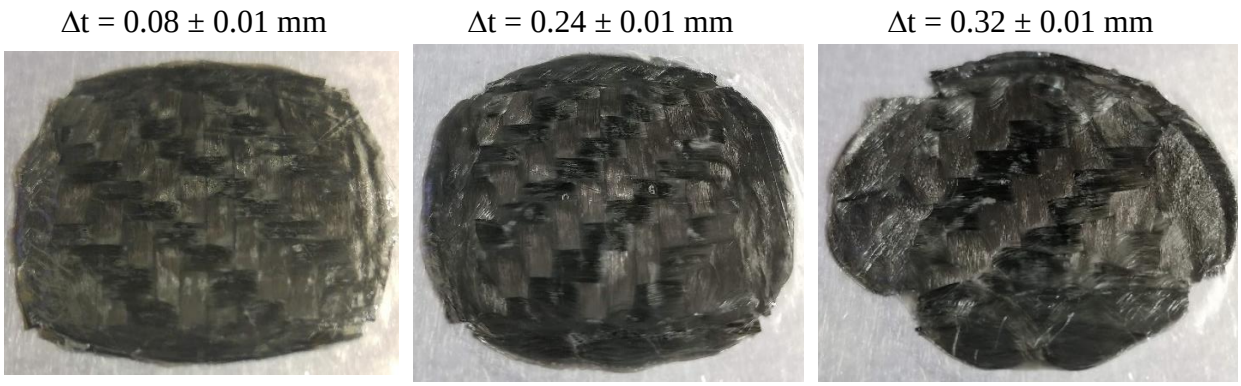

Figure 4.4. Comparing increments in force from 100 – 500 N using a constant weld time of 0.5 s and an amplitude of 38.1 μm for two plies of TW prepreg.

4.1.4. Amplitude

The amplitude setting refers to half the peak-to-peak amplitude of the applied vibrations. Regardless of the weld mode, the amplitude was a significant factor that influenced the resulting quality of the samples. For the booster and sonotrode used in these experiments, the amplitude ranged from 38.1 to 63.5 μm. The welder divides this range into nine settings, allowing the user to make small adjustments to the amplitude in increments of roughly 3.2 μm. It was found that the amplitude should be kept at 38.1 μm since amplitudes greater than 41.3 μm caused damage to the samples. The effects of amplitude on the specimens above 41.3 μm were tested and illustrated in Figure 4.5. The change in thickness is shown above the images in Figure 4.5 where increasing the amplitude will results in a decrease of the samples thickness (or an increase in the change in thickness Δt). Using the weld by time mode, similar qualitative results were obtained when increasing the force or amplitude independently. For all welded samples, the amplitude was left at 38.1 μm.

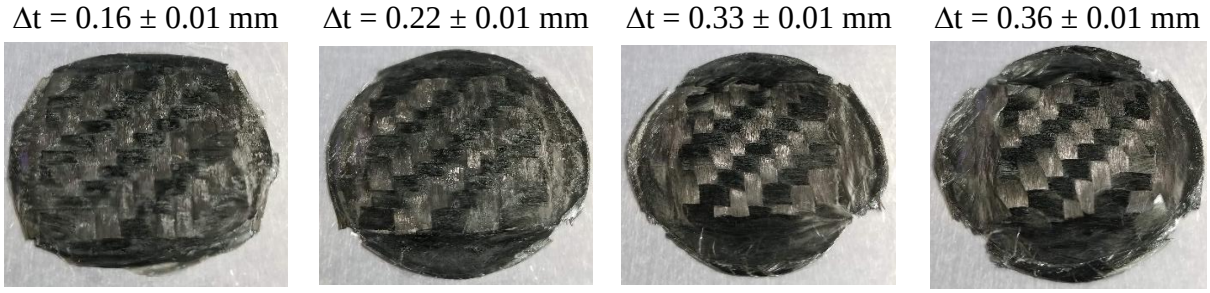

Figure 4.5. Comparing increments in amplitude from 44.5 – 63.5 μm using a constant weld time of 0.5 s and a force of 100 N.

4.2. Microstructural and Void Content Analysis

In addition to a qualitative assessment, the void content of welded samples was measured using ImageJ to identify welding parameters that achieved good consolidation and lowered the void content. The void content for welded samples was compared to vacuum bagged samples with and without a 2-hour debulking cycle. This was done to: (1) get a general sense of the void content range for vacuum bagged samples and (2) because welded samples are only cured in the oven and not debulked.

The void content for twill weave (TW) prepregs was performed on samples with 2 plies and 4 plies shown in Figure 4.6. The void content was measured for samples that were welded using the time and travel mode. For samples welded by travel, the time displayed after the weld was completed was used to plot the void content as a function of weld time.

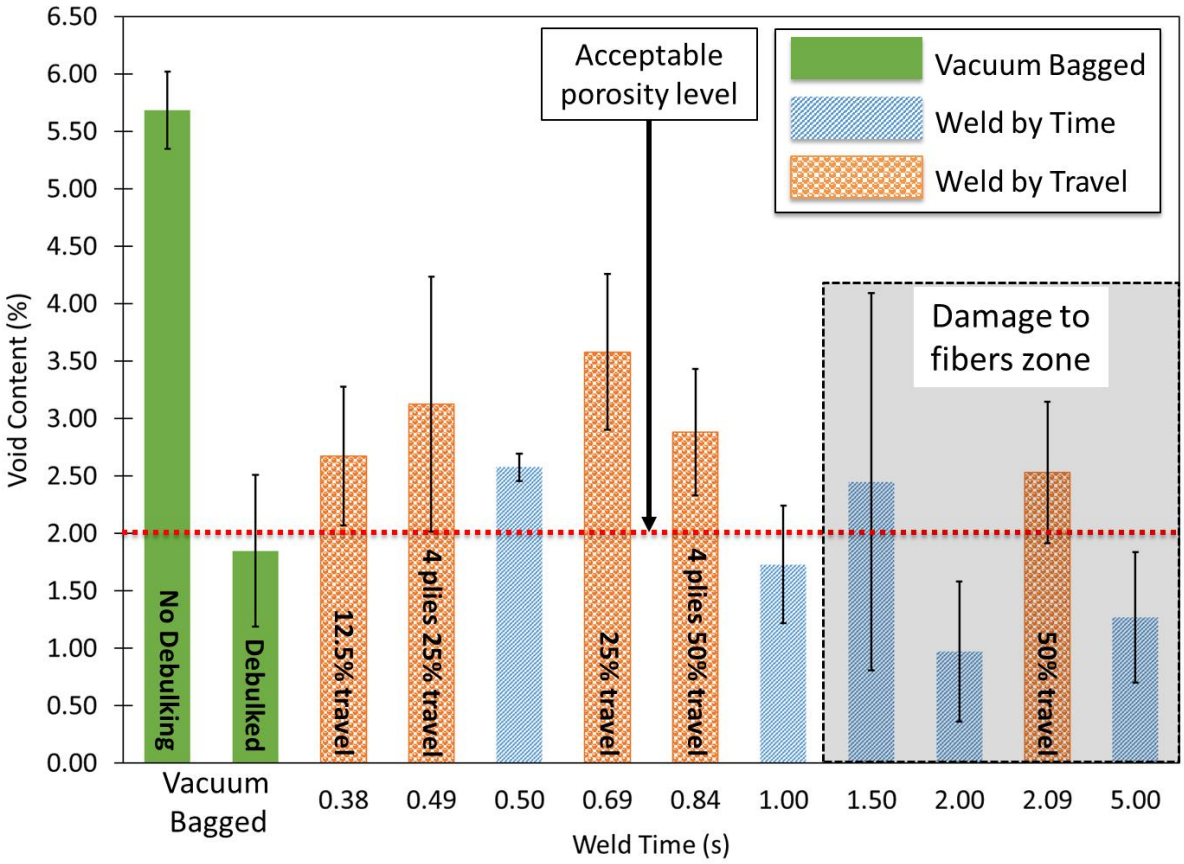

Figure 4.6. Void content for TW AS4 / Newport 301 as a function of weld time. Two plies were used for the welded samples except for the two samples marked with four plies.

As mentioned in Section 4.1, there were certain limitations to the welding parameters that would cause over-welding. While the void content tends to decrease with weld time, the damage to the fiber architecture increases. Samples with a weld time greater than 1.0 s experienced some fiber bundle disruptions while weld times approaching 5.0 s experienced severe damage to the fibers. For this reason, weld times over 1.0 s would not practically be used, but were examined to understand the effect of weld time on the porosity. The accepted void content in the aerospace industry is usually below 2.0%, however, in cases of critical primary structures, the porosity should be below 0.5% [57, 58]. Accepted porosity in aircrafts can range up to 5.0% porosity [59]. Figure 4.6 also indicates that weld by time produces lower void contents, however, the draw back to this

mode is not being able to control the amount of consolidation or the resulting thickness of the welded specimens. Depending on the application, the time mode could be preferred.

Due to the difference in resin, the UD and PW prepregs were compared separately from the TW prepregs. Recall that both the UD and PW prepregs are aerospace-grade out-of-autoclave prepregs, so the void content is expected to be much lower than for the TW prepregs. The void content for welded samples – in this case using the travel mode – was compared to vacuum bagged manufactured samples. For the PW prepregs the void content measurements presented in Figure 4.7 indicate that a welding parameter set to 25% the samples' thickness resulted in the lowest void content. Travel set to 12.5% resulted in poor consolidation of the plies leading to high void content. Travel set to 50% was observed to damage the fiber architecture and cause higher void content compared to 25% travel.

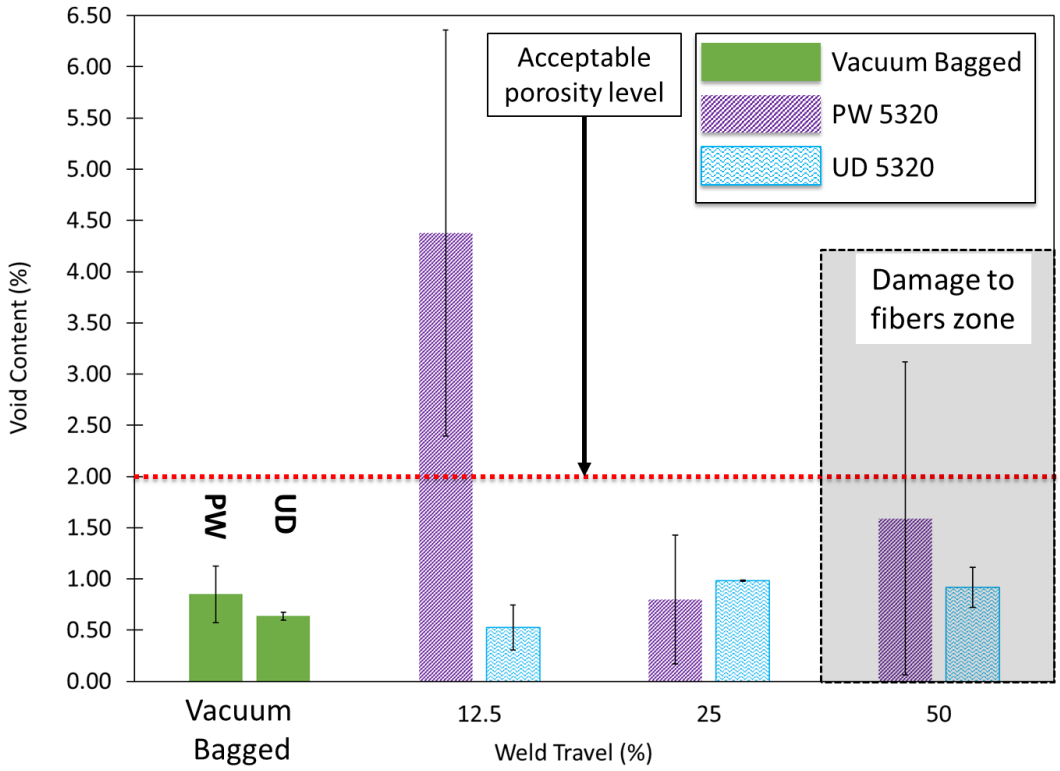

Figure 4.7. Void content as a function of travel for UD IM7 / Cycom 5320 and PW T650 / Cycom 5320. Weld travel corresponds to 12.5%, 25%, and 50% the samples' thickness.

For the UD prepregs, the lowest travel setting of 12.5% the samples' thickness resulted in the lowest void content. Similar to the PW prepregs, damage was observed on UD prepregs for a travel of 50%. The welding parameters for subsequent welds for all three materials was done using 25% travel even though in some cases it did not correspond to the lowest void content. Shorter travel in general, also means shorter weld times, therefore 25% travel was chosen to allow the resin more time to flow during the weld. The flow of resin is specifically important for adhesion and bonding where wetting of the adherend's surface is primordial. This directly applied to welded samples for short beam testing and open-hole repair. The microstructure for each prepreg welded with 25% travel is shown in Figure 4.8 (a),(c), and (e) and compared to vacuum bagged samples (b), (d), and (f).

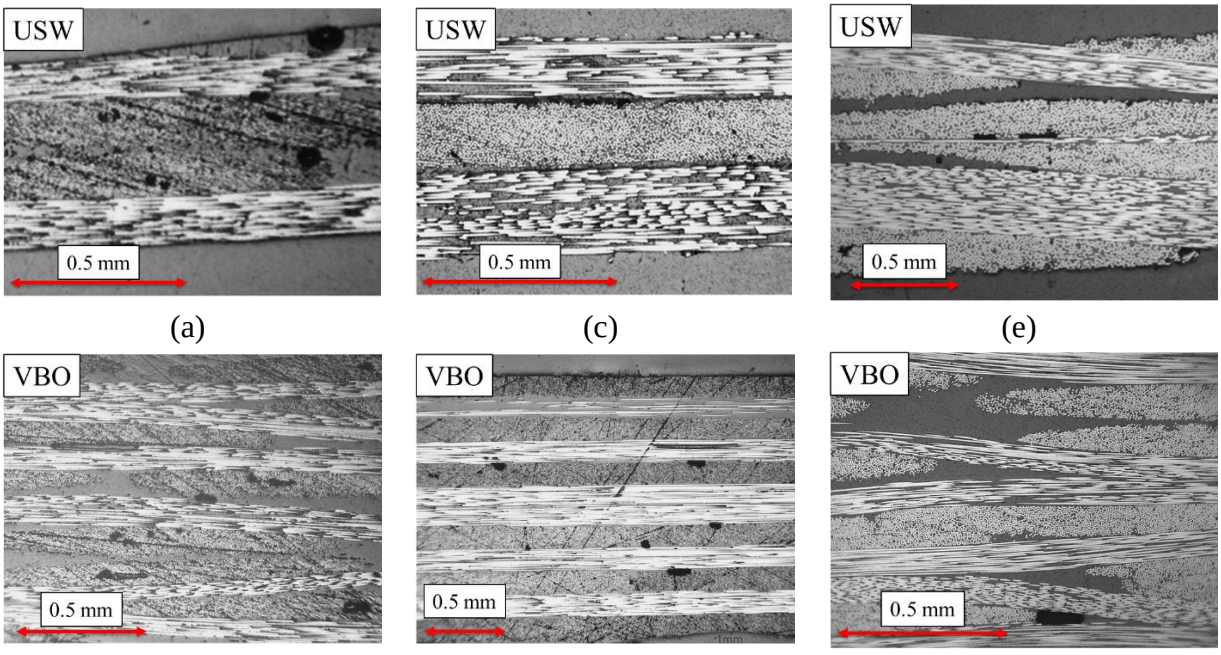

Figure 4.8. Cross-sections for ultrasonic welding (USW) and vacuum bagged only (VBO) samples. Voids can be found as dark spherical or elliptical objects.
(a) TW 2 plies USW 25% travel, (b) TW VBO 6 plies
(c) UD 4 plies USW 25% travel, (d) UD VBO 12 plies
(e) PW 4 plies USW 25 % travel, (f) PW VBO 8 plies

4.3. Temperature Monitoring during Ultrasonic Welding

The temperature measurements were performed using an infrared (IR) camera and type K thermocouples (TCs). As will be shown in Section 4.4, the temperature can be used to understand the behavior of the resin and characterize the viscosity and degree-of-cure. As mentioned in the literature review, it is difficult to capture the temperatures during welding for several reasons: (1) when using thermocouples, the vibrations from the sonotrode may interact with the thermocouple leads causing deviations from the actual temperature and (2) as the sonotrode moves down to apply the vibrations, it covers the top surface of the welded materials blocking the view for the IR camera. This restricts temperature measurements of the surface and only shows heat generation around the perimeter of the sonotrode. Both techniques for temperature measurements were necessary to capture temperatures below the laminate and in between plies as well as surface temperatures.

The temperature during the weld for a 4 ply and 12 ply laminate of UD prepreg are presented in Figure 4.9 and Figure 4.10, respectively using the setup described in Section 3.4. The temperature profiles from the IR camera were exported by capturing temperatures at a single point located at the center of the laminate – a similar position to that of the thermocouples placed above and below the laminate.

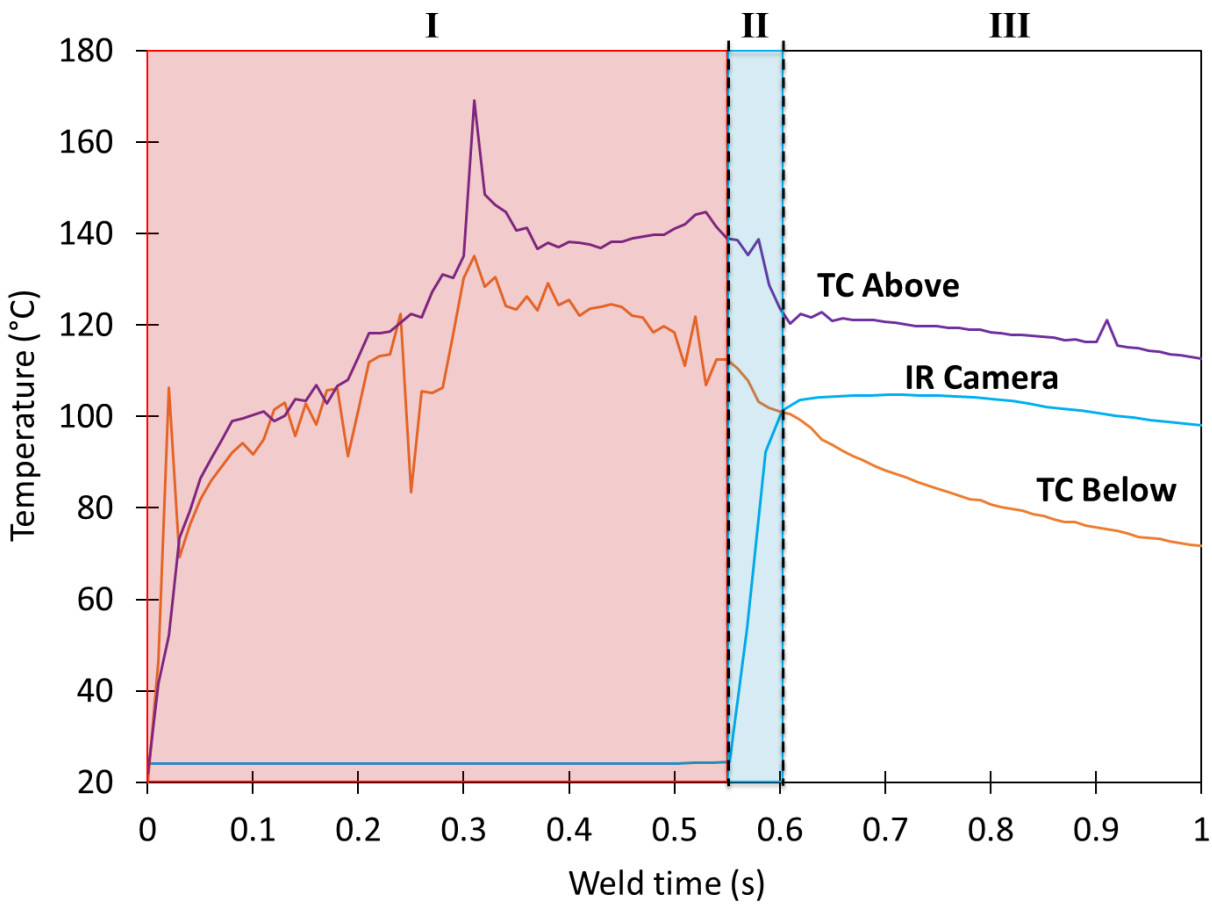

Figure 4.9. Temperature during weld of 4 plies of UD prepreg. Thermocouples (TC) were placed above and below laminate.

As seen in Figure 4.9 and Figure 4.10, three phases were identified during the welding process: (I) the vibration phase; application of vibrations, (II) the transition phase; when the sonotrode returns to its resting position, and (III) the cooling phase; when the sample is allowed to cool down to room temperature. As shown from the thermocouples in Figure 4.9, phase I shows fluctuating temperatures making it difficult to identify a clear temperature. Once the vibrations have ended and phase II begins, the IR camera is able to capture temperature measurements. A temperature gradient between the bottom and the top thermocouples can be observed measuring 22°C at the end of phase II and reaching nearly 40°C by 0.9 s. The temperature profile confirms

heat generation for the thermoset resin and shows the rapid heating rate (roughly 1600 °C/s for the IR camera) caused by ultrasonic vibrations.

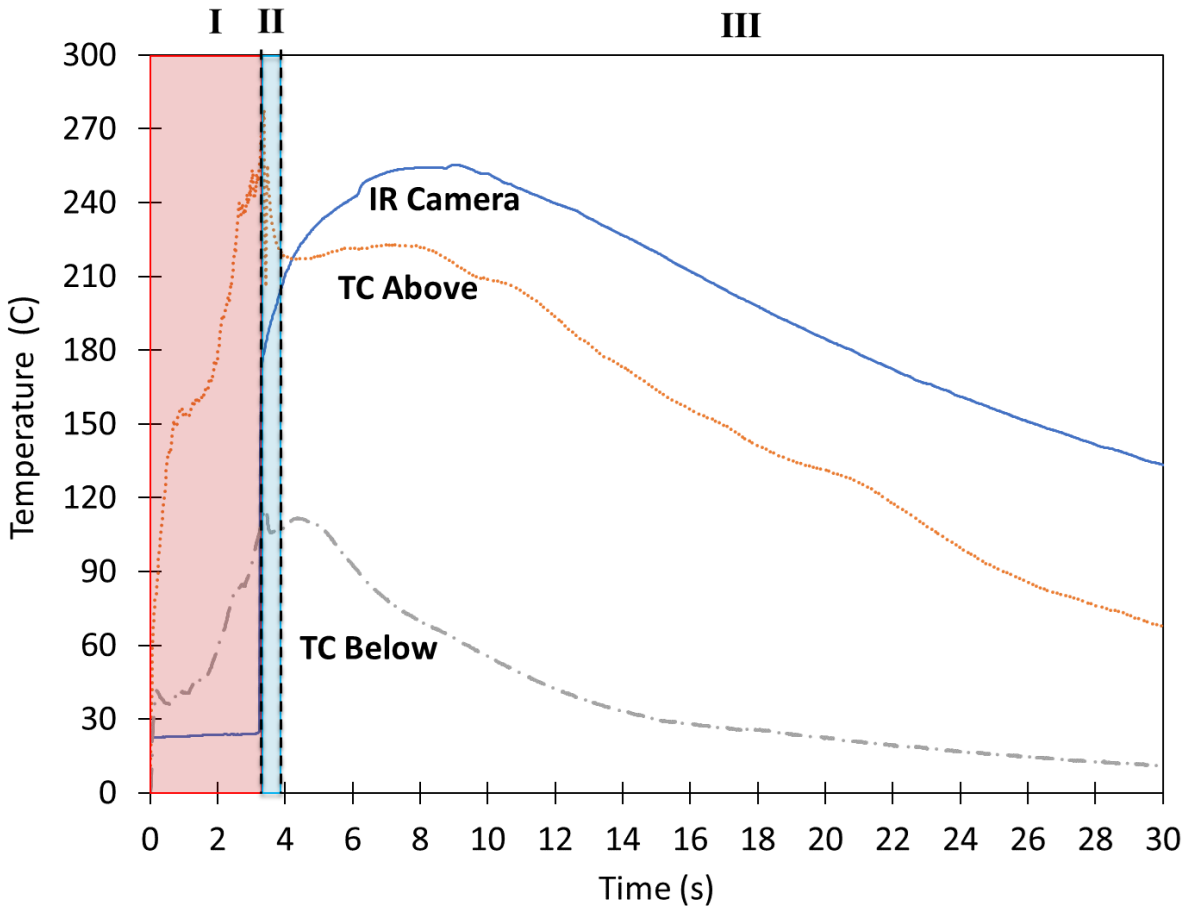

Figure 4.10. Temperature profile during weld for 12 plies of UD prepreg. Thermocouples (TC) were placed above and below laminate.

Although the welding parameters, size of the laminate, and layup were kept constant, Figure 4.10 shows a much different temperature profile. As phase II begins, the IR camera is able to capture the temperature of the surface of the laminate showing a rapid jump to 170°C and reaching a maximum temperature of 261°C. The heating rate measured roughly 3100 °C/s for the IR camera. It can be observed that after phase II has ended, there is a slight increase in temperature on all three curves corresponding to an exotherm caused by the chemical reaction of the epoxy.

Compared to Figure 4.9, there is a much larger temperature gradient between the top and the bottom of the laminate measuring 117.8°C at the end of phase II.

For both welded laminates (4 and 12 plies), heat generation on the surface can be very dependent on the position of the thermocouples and the cursor of the IR camera. This can explain the difference in temperatures for the thermocouple placed above the laminate and the IR camera. By increasing the number of plies, there is an increase in heat generation, heating rate, and in temperature gradient. The temperatures for both the 4- and 12-ply laminates reached and surpassed temperatures within the curing range. In the case of the 12-ply laminate, the surface was partially hardened indicating that some curing took place during the weld.

Regarding the cooling rate, the thermocouple below the laminate has a higher cooling rate because the anvil acts as a heat sink pulling heat away from the laminate. The cooling rate for the top thermocouple is slower because of the heat that is trapped in the bulk of the laminate.

4.3.1. Through-Thickness Temperature

As mentioned at the end of Section 2.4.1, and shown in Figure 4.9 and Figure 4.10, it is challenging to measure the temperature using thermocouples during ultrasonic welding. Due to the uncertainty of thermocouple measurements, the through-thickness temperatures presented in this section should be considered as an approximation.

The configuration shown in Figure 3.8 was used to capture the temperature in between every other ply for a 12-ply UD prepreg laminate. Seven thermocouples were used to measure the through-thickness temperature. Figure 4.11 illustrates what the colormaps obtained look like with the thickness in millimeters for each ply shown on the left axis and the temperature in degrees Celsius shown on the right axis. The thermocouples are located at thicknesses of 0.00, 0.27, 0.53, 0.79, 1.06, 1.33, and 1.59 mm. The colormaps do not consider the lateral position of the

thermocouples and only represent the temperature as a 1D plot of the temperature distributed throughout the thickness of the laminate.

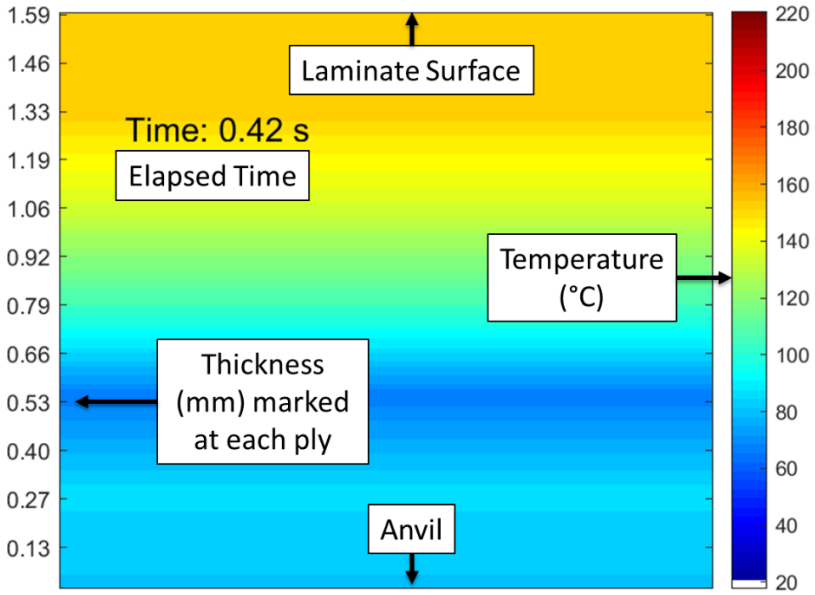

Figure 4.11. Temperature colormap for through-thickness measurements done with 7 thermocouples and linear interpolated values.

To illustrate the change in temperature inside the laminate, the temperatures between the thermocouples were linearly interpolated to obtain 20 calculated values. This allowed the development of higher resolution colormaps to show how the temperature changes during the weld as seen in Figure 4.12. Note that the duration of the weld was 0.772 s.

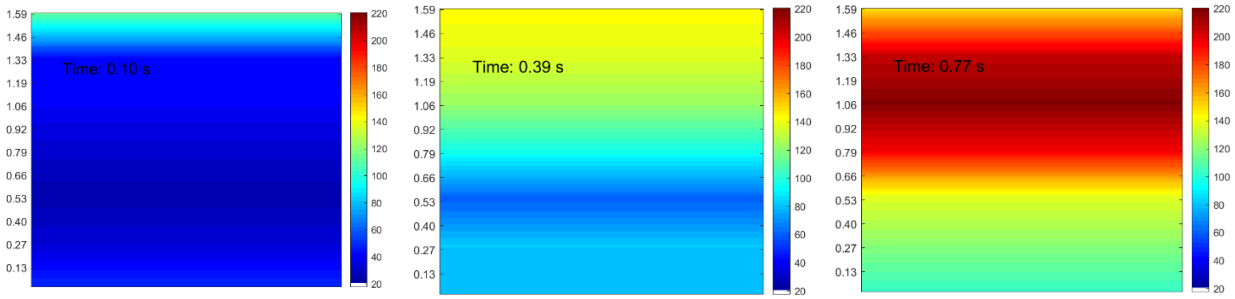

(a) (b) (c)

Figure 4.12. Through-thickness temperatures for 12 plies of UD prepreg using measured and interpolated values from 7 thermocouples. The temperature plots shown correspond to (a) the beginning of the weld at time 0.10 s, (b) the middle of the weld at time 0.39 s, and (c) the end of the weld at time 0.77 s.

These colormaps serve to better understand how heat is generated inside the laminate. From Figure 4.12 (c), the plot indicates higher heat generation located four plies from the surface of the laminate with a temperature of 220°C, versus a maximum surface temperature of 180°C. It is difficult to tell how accurate these temperatures are since temperature measurements with thermocouples were shown to fluctuate during the weld. A non-contact method for through-thickness temperatures would be useful to confirm the accuracy of these results such as a fiber optic sensor. Temperature monitoring is important as uneven heating or temperature gradients may cause uneven curing of epoxy resins. This non-uniformity could lead to inconsistencies in the manufacturing methods and increase void content in the laminates.

4.4. Cure Kinetics and Viscosity Models

The temperatures shown in Figure 4.9 and Figure 4.10 were used with semi-empirical cure kinetics and viscosity models described in Section 3.6. The models were used to obtain the behavior for viscosity and cure kinetics for the laminates with 4 and 12 plies. The temperatures from the bottom thermocouple and the IR camera were used to model these behaviors labeled as “low T” and “high T”, respectively. Figure 4.13 illustrates the viscosity during the welding process for the 4-ply laminate. The three phases of the weld are labeled just like Figure 4.9 to mark the duration of the weld and the cool down. The degree-of-cure is not shown on this graph because there was no significant change to the initial degree-of-cure assumed at 0.01.

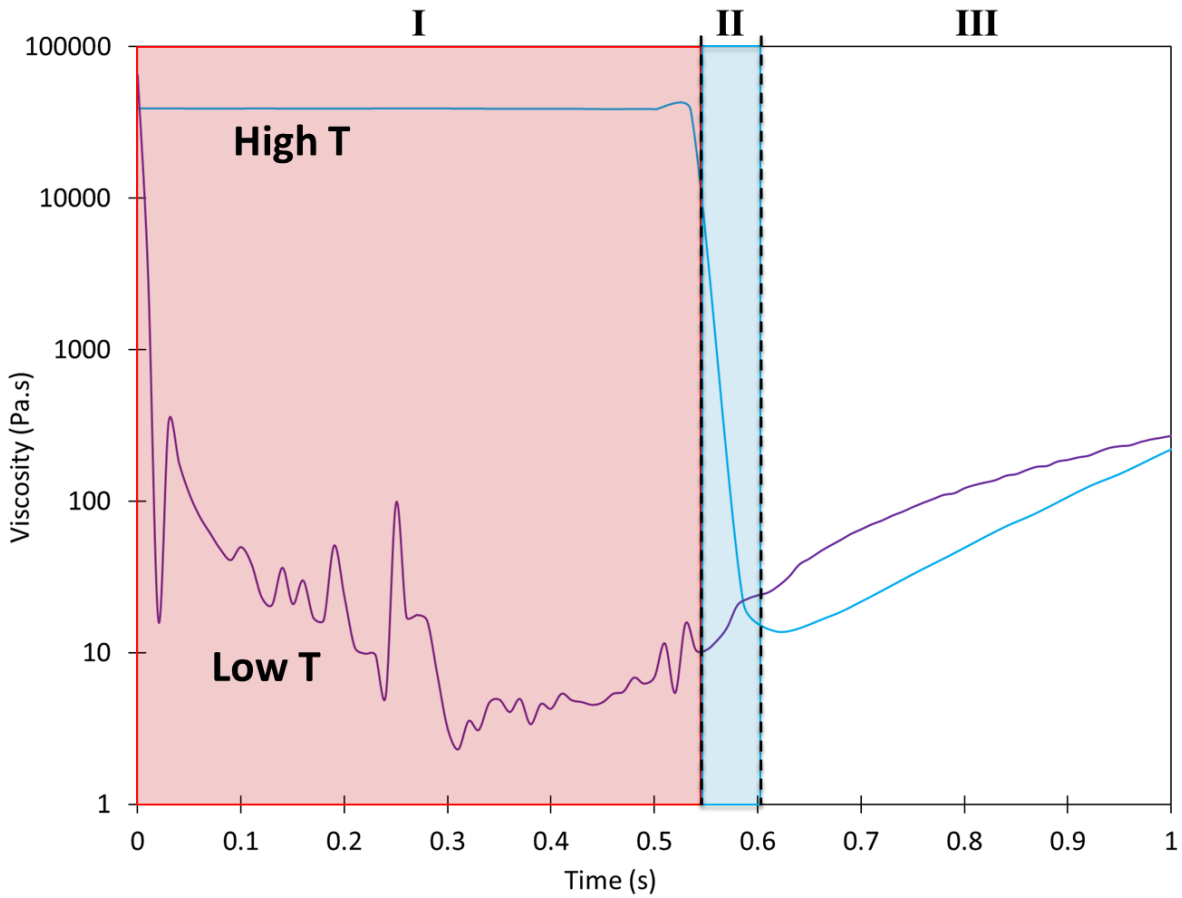

Figure 4.13. Predicted viscosity based on Eq. 3.3 and parameters from Table 3.6 for 4 plies of welded UD prepreg. Welding phases (I-III) included from Figure 4.9.

Figure 4.14 shows the viscosity and degree-of-cure for the 12-ply laminate. As a result of the large temperature gradient observed in Figure 4.10, there is also a gradient in behavior for the viscosity and degree-of-cure. The model indicates that the bottom of the laminate experienced no change in degree-of-cure whereas the top of the laminate reached a degree-of-cure of 0.24.

For Figure 4.13 and Figure 4.14 the flow of resin can be confirmed by observing the viscosity curves. As mentioned by Kratz et al., resin will flow if the viscosity is less than 100 $Pa \cdot s$ which was achieved for the top and bottom plies for both laminates [18]. The duration of flow can also be determined from these figures indicating a very short flow time (< 1.0 s) for the 4-ply laminate and a flow time ranging from 5.0 s to just over 30 s for the 12-ply laminate. With that in

mind, it is important to note that external pressure from the sonotrode will facilitate the flow of resin during the vibration phase.

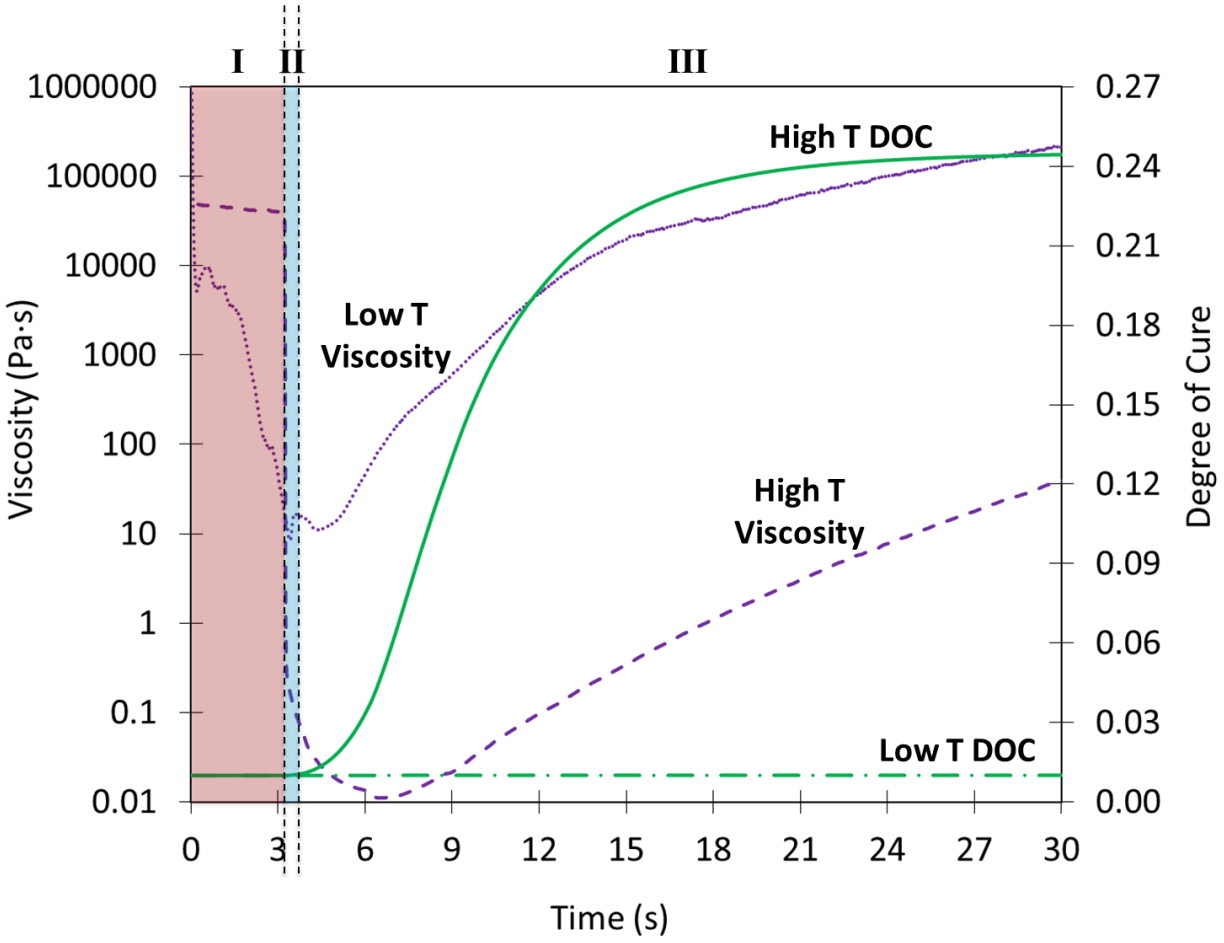

Figure 4.14. Predicted degree-of-cure and viscosity based on Eq. 3.1 and Eq. 3.3 for 12 plies of welded UD prepreg. Welding phases included from Figure 4.10.

From a repair perspective, application of ultrasonic welding would ideally generate enough heat to allow the resin to reach gelation. This would freeze the microstructure avoiding the evolution or introduction of porosity. As a result, the vacuum bagging step would be eliminated since the evacuation of trapped air would not be necessary (or possible) in the gel state. For the case of Cycom 5320, gelation is expected to occur at a degree-of-cure between 0.3 and 0.5 [18]. Vora reported a degree-of-cure of 0.371 at gelation for PW T650 / Cycom 5320 which should be similar to the UD weave [60].

From the temperature profiles to the cure kinetics and viscosity models, several arguments can be made. While increasing the number of plies does increase the degree-of-cure and prolong the flow of resin, this increases the temperature gradient between the top and the bottom of the laminate causing non-homogeneous curing of the resin. Alternatively, while using fewer plies does lower the temperature gradient, it does not generate enough heat to significantly cure the resin and limits the flow time. With this in mind, repair using ultrasonic welding was preferred with fewer plies to achieve more consistent curing of the resin and thus, more consistent mechanical behavior.

4.5. Mechanical Testing

This section will present experimental results on interlaminar shear strength (ILSS) and open-hole tensile strength. Both tests were performed on twill weave (TW) AS4 / Newport 301, unidirectional (UD) IM7 / Cycom 5320, and plain weave (PW) T650 / Cycom 5320. To simplify the discussion, these samples will be referred to by their weave pattern – TW, UD, and PW.

4.5.1. Interlaminar Shear Strength

Short beam shear testing was performed on all three prepregs following the configurations shown in Figure 3.9. The configurations were manufactured by ultrasonic welding (USW) and vacuum bagging only (VBO), then compared to investigate the effects of USW on ILSS shown in Figure 4.15. In addition, the effect of using an adhesive film was tested with the PW short beam samples.

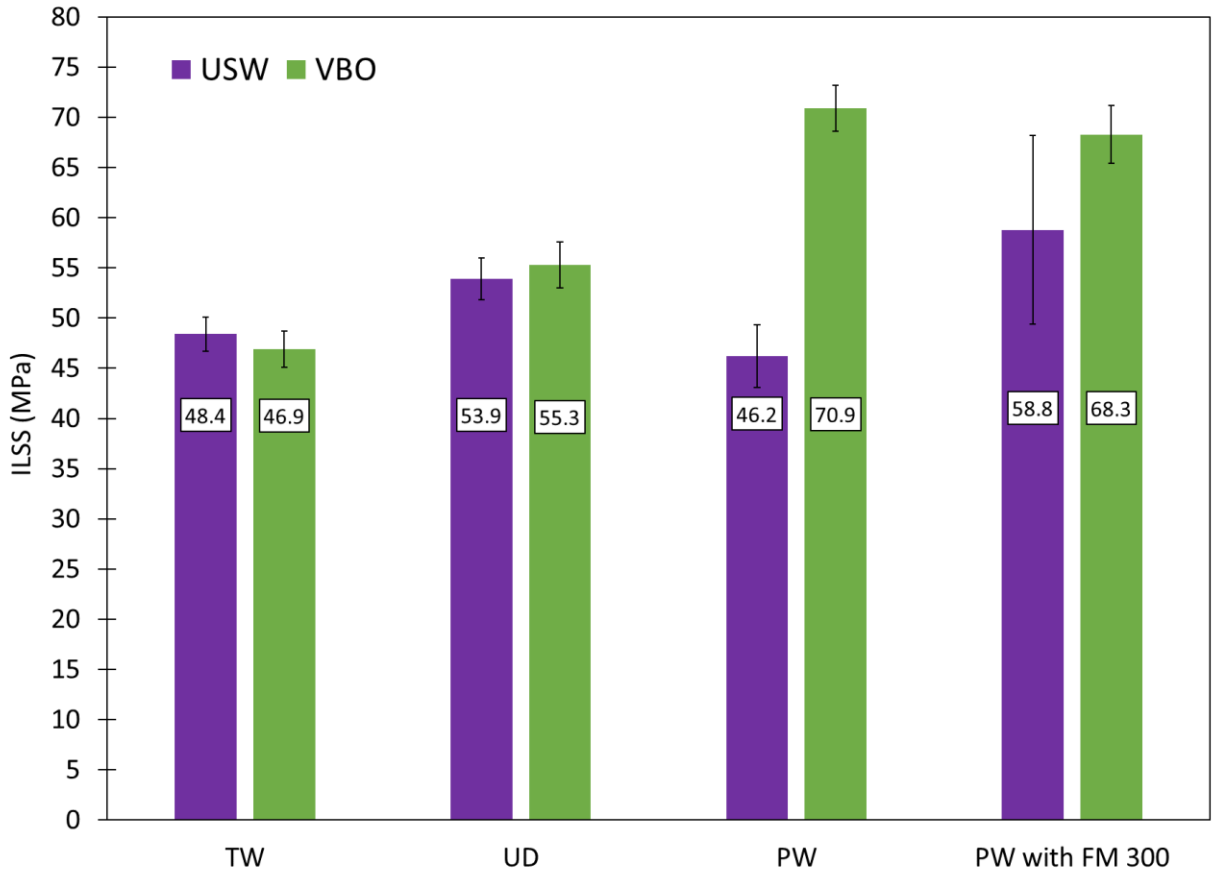

Figure 4.15. ILSS comparison for samples manufactured by ultrasonic welding (USW) and vacuum bagging only (VBO). PW samples were tested with and without the adhesive film, while the TW and UD samples were tested without the adhesive film.

It was expected that vacuum bagging would have superior ILSS compared to USW since the vacuum bagging process includes a 2-hour room temperature debulking cycle followed by a heated cure cycle according to the manufacturer's recommendations. However, the results indicate that for the TW and UD prepregs, USW is a comparable process to vacuum bagging.

For the PW samples without the adhesive film, the ILSS for the USW method is much lower than the VBO samples. Without an adhesive film, the only bonding medium is the resin on the prepregs, which, bonds to the surface of the cured laminates. A low ILSS for the PW samples without the adhesive film indicates poor bonding. This can be attributed to the low resin fraction on the PW prepregs compared to the TW and UD prepregs. The use of an adhesive film for PW

samples clearly demonstrates an increase in ILSS for USW samples. The lower ILSS values for some USW samples could be outweighed by considering the significantly faster manufacturing time.

The most common failures observed for each material are shown in Figure 4.16. For the welded TW prepregs, failure occurred by compression of the top surface of the laminate where the upper support of the testing fixture contacts the sample (Figure 4.16 (a)). Besides the compression failure, small intralaminar cracks were observed throughout the center of the sample on the transverse plies. This was similarly observed for the TW samples manufactured by VBO.

For the UD prepregs, failure occurred by delamination in the transverse plies concentrated around the center of the samples. The failure shown in Figure 4.16 (b) correspond to delamination of the top vacuum bagged laminate eight plies from the top surface near the center of the sample. In the case of VBO manufactured samples, delamination was consistently found at the plies in between the two vacuum bagged laminates (i.e. at the prepregs that were added to bond both laminates together).

For the welded PW prepregs without the adhesive film, failure occurred by compression of the top laminate where the top support of the testing fixture met the specimen, as shown in Figure 4.16 (c). Delamination and intralaminar cracks were also found at the prepreg – laminate interface. In addition to these failure sites, voids were observed throughout the prepreg – laminate interface which, may explain the low ILSS measured in Figure 4.15. The vacuum bagged PW samples without the adhesive film presented delamination and intralaminar cracks in the transverse plies at the prepreg – laminate interface. Similar defects were found just above and below the prepreg – laminate interface near the center of the specimen. Additional cross-sections for welded and

vacuum bagged short beam samples can be found in Appendix A. Characteristic force-displacement curves for short beam shear tests can be found in Appendix B.

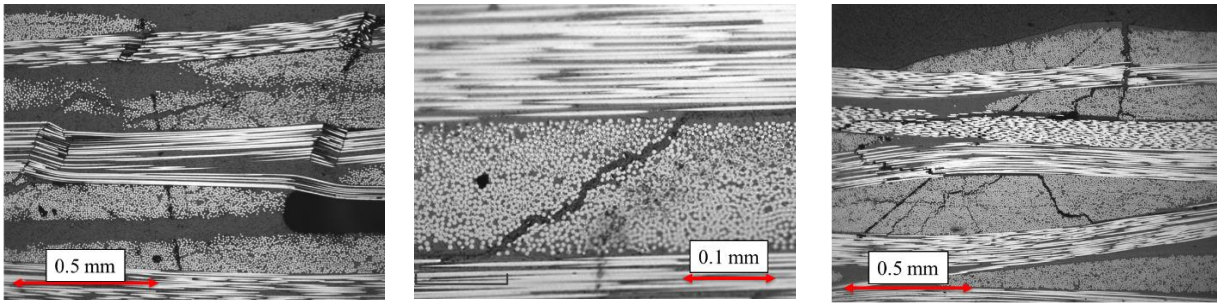

(a) (b) (c)

Figure 4.16. Cross-sectional micrographs for welded short beam shear samples after testing. (a) TW failure at the surface of the top laminate, (b) UD failure eight plies from welded surface, and (c) PW (without adhesive) failure located at the surface of the top laminate.

4.5.2. Open-Hole Tensile Strength

To simulate adhesive repair of composite structures, a circular hole with a diameter of 4 mm – representing damage to the composite – was drilled into the specimens. A square patch was bonded over the drilled hole as shown in Figure 3.10. To evaluate the strength of repair patches over an open-hole, samples were initially prepared following ASTM 5766 – a standard for testing open-hole tensile strength of polymer matrix composite laminates. Repair patches were then applied over the open-hole through vacuum bagging only (VBO) and ultrasonic welding (USW). Soft-patch repair was used for twill weave (TW) and unidirectional (UD) laminates. On the other hand, hard-patch repair was used for plain weave (PW) laminates. Two methods of repair were used to better understand the repair process and to investigate if USW is a viable method for both repair techniques. Characteristic force-displacement curves for repair tests can be found in Appendix B.

The strength recovery of repaired samples was used to compare the quality of the repair patches. To calculate the strength recovery, notched and unnotched samples were also tested. A

comparison between these three conditions better illustrates the strength recovery as shown in Figure 4.17, Figure 4.19, and Figure 4.21.

As shown in Figure 4.17, the open-hole strength for USW repair and VBO repair are very similar. From these results, the strength recovery for repair samples is roughly 50% of the samples unnotched strength. This indicates that repair using USW is a comparable process to VBO. In addition, the standard deviation is smaller for USW repair demonstrating that consistent results can be obtained. The fact that some strength recover was achieved with USW, indicates that proper consolidation of the prepreg plies and bonding at the interface between the adhesive film and the parent laminate was achieved.

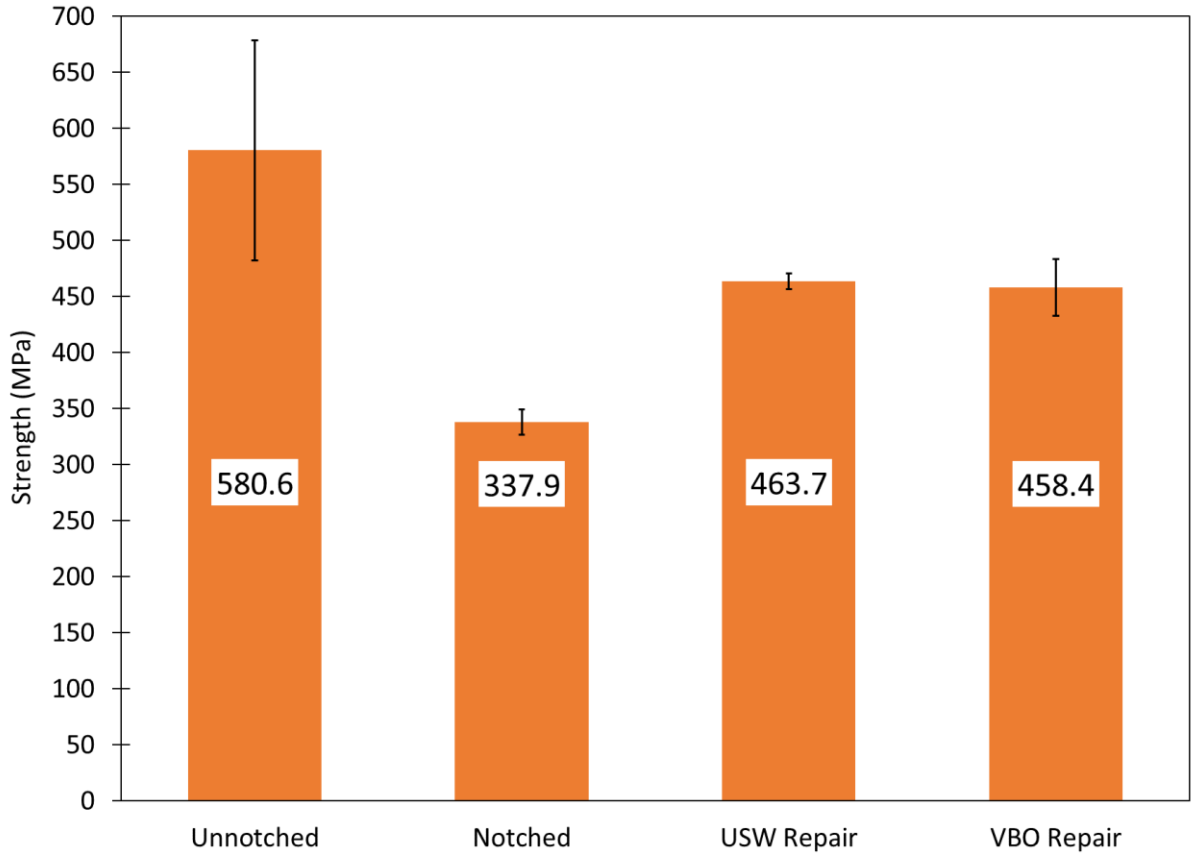

Figure 4.17. Open-hole tensile strength for TW repair. Repair patch manufactured using soft-patch technique illustrated in Figure 3.11 (a). The average strength of each sample is labeled on the respective bars.

Since the notch acts as a stress concentration, net-tension failure occurred as expected, shown in Figure 4.18 for TW repair samples. The repair patch for all tested samples remained bonded to the parent laminate which may be a result of a strong bond between the adhesive and the parent laminate. An alternative reason, could be that the repair patch failed with the parent laminate due to weakness, but the strength recovery shown in Figure 4.17 indicates otherwise. Along the edges of the repair patch there was some delamination indicating a partial cohesive failure along the bondline (through the adhesive film).

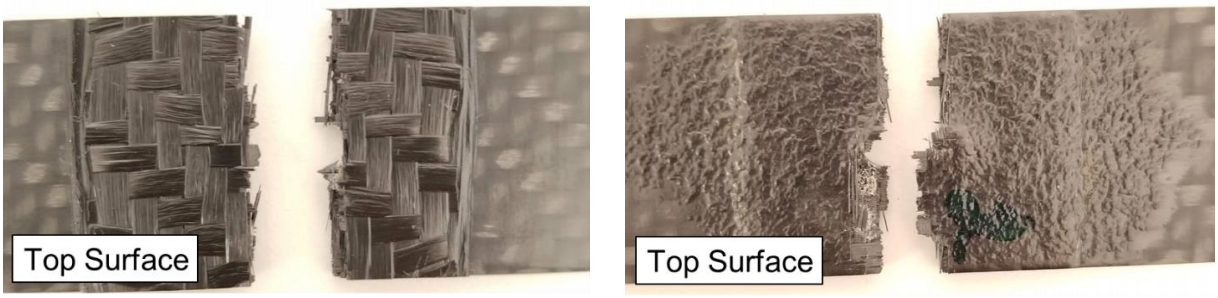

(a) (b)

Figure 4.18. Failure under uniaxial tension for TW repair samples manufactured by (a) USW and (b) VBO. Repair patch consisted of two prepreg plies and one adhesive film.

As shown in Figure 4.19, repair samples show hardly any strength recovery. These are unexpected results especially for the VBO repair samples. The low strength recovery for both USW and VBO samples could be caused by a few reasons: (1) the flat patch repair configuration is inadequate for UD prepregs or (2) possible manufacturing defects which are known to occur. As explain in Section 4.1, prepregs are sensitive to ultrasonic vibrations. For UD prepregs, there is nothing holding adjacent fiber bundles together aside from the resin. This inherently makes UD prepregs more sensitive to the USW process as fiber bundles can be more easily displaced and damaged. TW and PW prepregs are held together by woven fiber bundles resulting in better resistance to being displaced or damaged. The low strength recovery for USW repair in Figure 4.19 can be attributed to the sensitivity to ultrasonic vibrations.

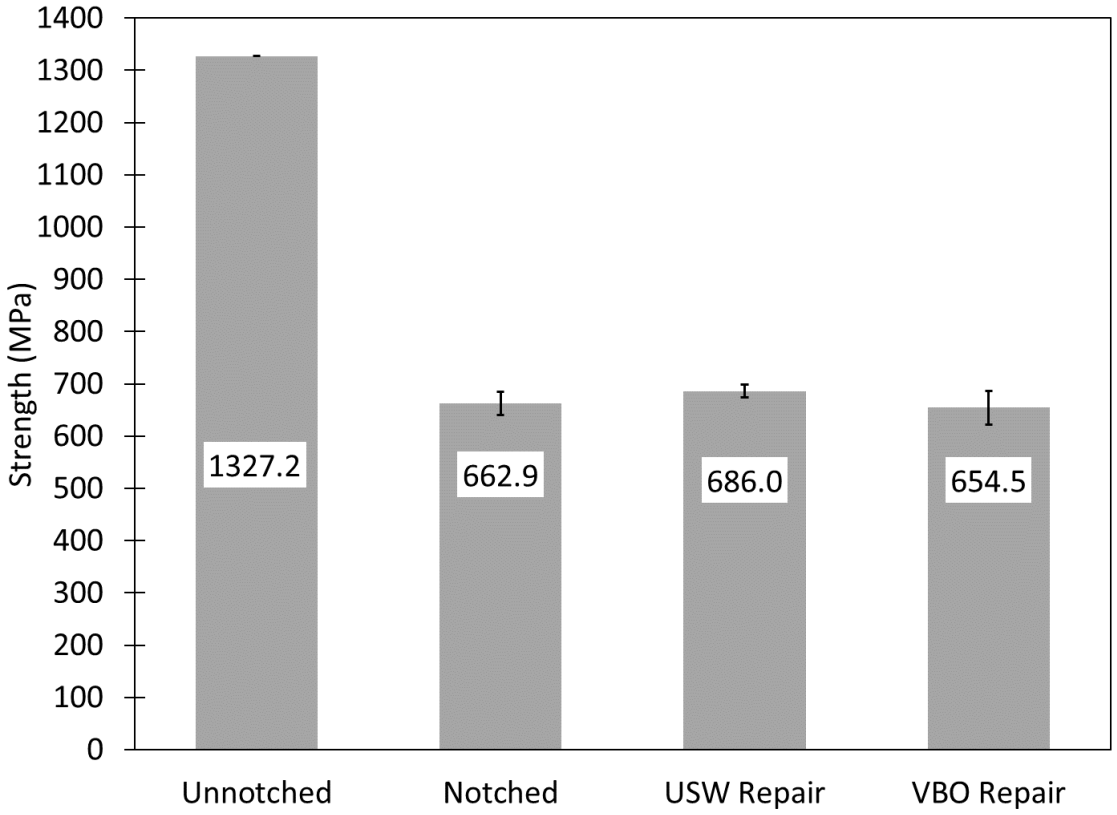

Figure 4.19. Open-hole tensile strength for UD repair. Repair patch manufactured using soft-patch technique. Note that unnotched strength was taken from material specification provided by supplier for 0/90 laminate.

Common failure modes for the UD repair specimens are shown in Figure 4.20. For USW repair patches, mixed-mode failures were observed. Along the center of the open-hole loading axis, a cohesive failure of the patch is shown in Figure 4.20 (a) . On the edges of the open-hole specimens, there is partial adhesive failure. For the VBO repair patches, the failure is primarily cohesive failure of the bondline (through the adhesive film) shown in Figure 4.20 (b).

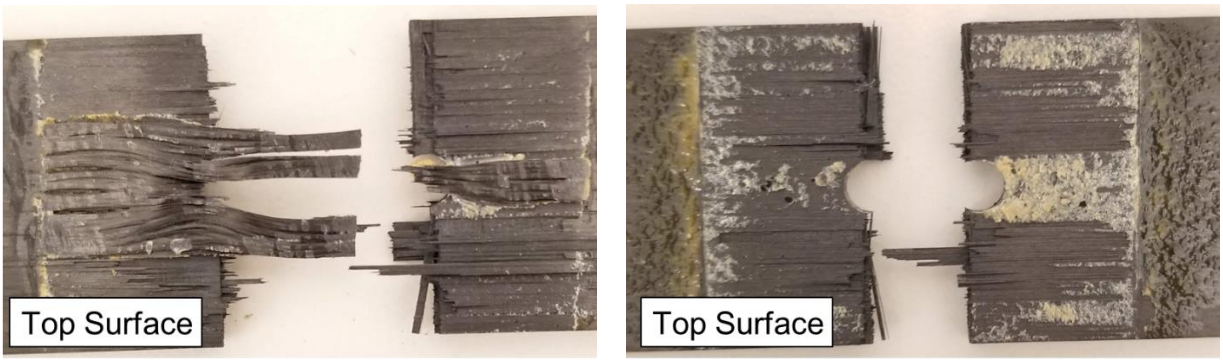

(a) (b)

Figure 4.20. Failure under uniaxial tension for UD repair samples manufactured by (a) USW and (b) VBO. Repair patch consisted of four prepreg plies and one adhesive film.

Figure 4.21 shows the results for the open-hole tensile tests for PW specimens. The strength recovery for USW and VBO repair methods are very similar with a recovery of roughly 20% of the unnotched strength. Similar to the discussion for the TW samples, the USW repair method is comparable to the VBO repair. This confirms that consolidation and bonding of the adhesive film to the parent laminate was achieved. The lower strength recovery compared to the TW samples could be a result of the lower patch thickness compared to the TW repair patch (0.42 mm and 0.60 mm respectively).

The hard-patch repair method was used for PW samples. The repair patch was pre-cured, then bonded to the notched samples using an adhesive film as shown in Figure 3.11 (b). Manufacturing the repair patch by vacuum bagging allows for better control of the fiber volume fraction and porosity. As a result, the hard-patch would ideally have similar properties to the parent laminate. The advantage of using a soft-patch is the availability of resin from the uncured prepregs and the adhesive film. For hard-patch repair there is only resin from the adhesive film to bond the patch to the parent laminate.

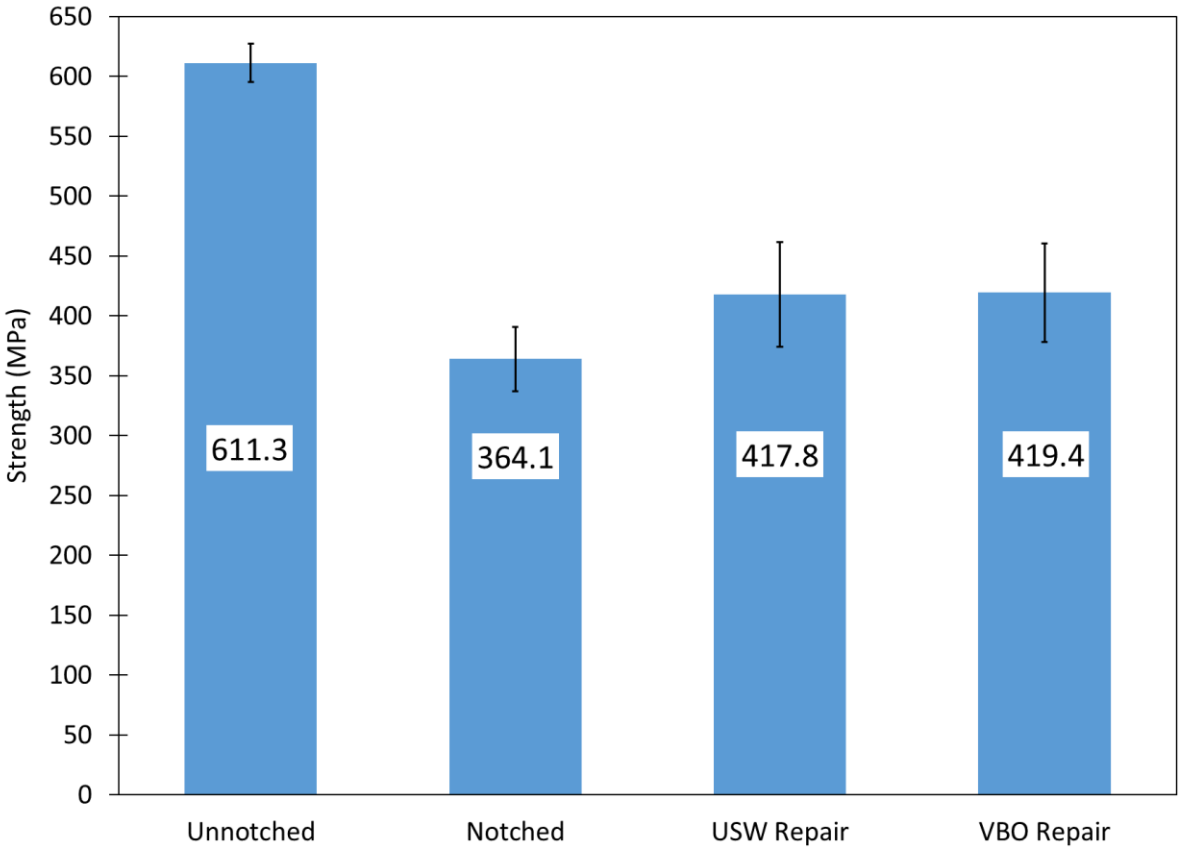

Figure 4.21. Open-hole tensile strength for PW repair. Repair patches manufactured using hard-patch technique illustrated in Figure 3.11 (b).

The failures observed for PW repair samples were different since the repair patch was pre-cured and bonded to the parent laminate with an adhesive film. For USW repair samples, failure of the specimen usually included the complete detachment of the repair patch. As shown in Figure 4.22 (a), a mixed-mode failure occurred where the left half of the specimen experienced an adhesive failure characterized by the smooth and intact surface of the adhesive film. The right side, however, shows a rough surface on the adhesive film indicating a cohesive bondline failure. Damage to the repair patch was also observed as one of the corners would usually be broken off.

In the case of the VBO repair samples, the common failure mode is shown in Figure 4.22 (b) where the patch failed with the parent laminate indicating a net-tension failure. This indicates

that either a good bond between the patch and the parent laminate was formed or the patch failed with the parent laminate due to weakness. Increasing the number of plies for the repair patch would increase the strength recovery for repair samples.

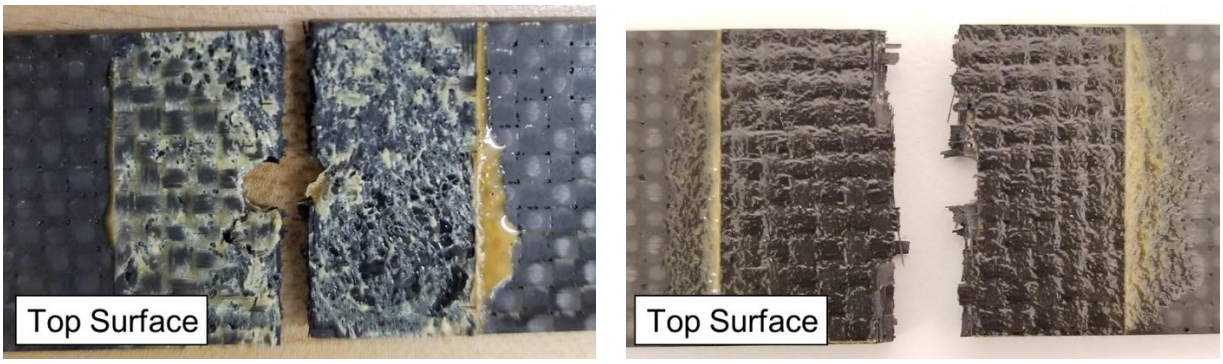

(a) (b)

Figure 4.22. Failure under uniaxial tension for PW repair samples manufactured by (a) USW and (b) VBO. Repair patch consisted of a pre-cured patch with two plies bonded with one adhesive film.

CHAPTER 5.
CONCLUSIONS AND FUTURE WORK

In this study, an in-depth experimental approach was performed to assess the feasibility of using ultrasonic welding as a method of structural repair for carbon fiber / epoxy prepregs. In Chapter 3 the experimental methods used throughout this study were described. Three prepregs were used throughout this study including twill weave AS4 / Newport 301, unidirectional IM7 / Cycom 5320, and plain weave T650 / Cycom 5320. In addition, the adhesive film by Cytec FM 300-2M was used. The manufacturing methods consisted of hand layup followed by vacuum bagging and ultrasonic welding.

The two welding modes used were weld by time and weld by travel. Multiple welding parameters were explored where the most important ones were time, travel, force, and amplitude. The number of plies welded together was also investigated with multiple prepregs. A range of acceptable parameters was identified by qualitatively analyzing the samples and using the void content to verify effective welds. Time should be kept less than 1.0 s, travel should be kept above 12.5% and below 50% of the samples' thickness, force should be kept below 300 N when using the weld by time mode, and amplitude should be kept at 38.1 μm to avoid disrupting the fiber pattern. By increasing the number of welded plies, an increase in heat generation, heating rate, and temperature gradient between the top and the bottom of the laminate was observed.

Using thermocouples and an infrared camera to monitor the temperature, heat generation was observed using ultrasonic vibrations. From the temperature profiles, it was found that heat generated by ultrasonic vibrations can reach and surpass the cure temperature range for both resins investigated (Newport 301 and Cycom 5320). Monitoring the temperature during the weld showed fast heating rates and temperature gradients through the thickness of the samples. Using cure

kinetics and viscosity models for Cycom 5320, it was found that ultrasonic welding generates enough heat to partially cure the resin up to 24% in the case of a 12-ply laminate of unidirectional prepreg. At the same time, the viscosity was reduced enough to allow resin to flow for both a 4-ply and 12-ply laminate of unidirectional prepreg.

The void content for welded samples was analyzed using optical microscopy and measured using ImageJ. These measurements were compared to vacuum bagged samples as a function of weld time for the twill weave prepregs and as a function of weld travel for the unidirectional and plain weave prepregs. For twill weave samples, the void content for some samples was less than 1.0% away from reaching the accepted porosity level. In the case of the unidirectional and plain weave samples, all welded samples were below the 2.0% threshold.

Interlaminar shear strength (ILSS) was found by short beam tests on samples manufactured using ultrasonic welding and vacuum bagging. The twill weave and unidirectional samples were tested without the adhesive film while the plain weave samples were tested with and without the adhesive film. The results were compared for each manufacturing method were the ILSS was found to be comparable for twill weave and unidirectional samples. For plain weave samples, the ILSS was improved by using the adhesive film.

Adhesive repair was simulated by applying a square repair patch to an open-hole tensile specimen. Soft-patch repair was chosen for twill weave and unidirectional specimens while har-patch repair was chosen for the plain weave specimens. Strength recovery for the twill weave and plain weave specimens was achieved by roughly 50% and 20%, respectively, for both manufacturing methods. Repair of unidirectional specimens did not show a noticeable strength recovery due to manufacturing defects of the repair patch and sensitivity to ultrasonic vibrations.

The manufacturing time saved using ultrasonic welding may outweigh the lower mechanical behavior in some cases.

5.1. Future Work

As a preliminary study for structural repair of thermoset composites, ultrasonic welding (USW) showed promising results for consolidation of prepreg plies and as a replacement for the vacuum bagging process. Ultrasonic repair of thermoset composites is a technique that has not been researched. This project was focused on the feasibility of using ultrasonic welding as a repair technique with limited references to any previous work done on the subject. As with most research done for the first time, there is room for improvement and additional areas that can be investigated.

While multiple welding parameters were examined, the solidification time and force were only briefly investigated. An in-depth analysis of the effects of these welding parameters may help to achieve better quality in the welded samples. Regarding the wide range of welding parameters discussed in this study, it would be useful to investigate a narrower range of values for each welding parameter. This way, welding parameters can be adjusted for each material optimizing the heat generation and the conservation of the fiber bundle integrity. In addition, by testing more welding parameters the heat generation could be investigated to better controlled the temperatures reached. This would allow the user to control the degree-of-cure of the resin during the welding process and ideally reach the gel state. Partially curing the resin during the USW process would allow for a supplemental study to quantify how much time can be reduced from the cure cycle and achieve a fully cured composite material.

To produce a more profound understanding of the heat generation during welding, infrared sensors with a high response time could be used alongside the infrared camera. By improving the

collection of temperature data, the cure kinetics and viscosity models could more accurately depict the behavior of the resin during the welding process.

In this study, open-hole repair samples were manufactured to compare the ultrasonic welding method to the vacuum bagged method. There are many characteristics that play an important role in the strength recovery that were not investigated in this study. Future investigations could look at the effect of the shape of the repair patch (i.e. round, square, rectangular) and the scarf angle. In this case, only flat square patches were applied without considering the scarf angle. The effect of the number of plies in the repair patch could also be investigated to maximize the strength recovery. Lastly, as this was more of an issue with the unidirectional prepregs, different ply configurations could be investigated specially for the welded repair procedure.

The future goal for this project is to perform ultrasonic repair on composite structures (or sandwich panels) that were tested by drop-weight impact. The strength recovery could then be found for these structures that are characteristically used in the aerospace industry. Ultrasonic repair on such structures would provide a good comparison to other adhesive repair techniques that are commonly found in the literature.

APPENDIX A.
OPTICAL MICROGRAPHS

Additional micrographs are shown in the order they were discussed: TW, UD, and PW samples.

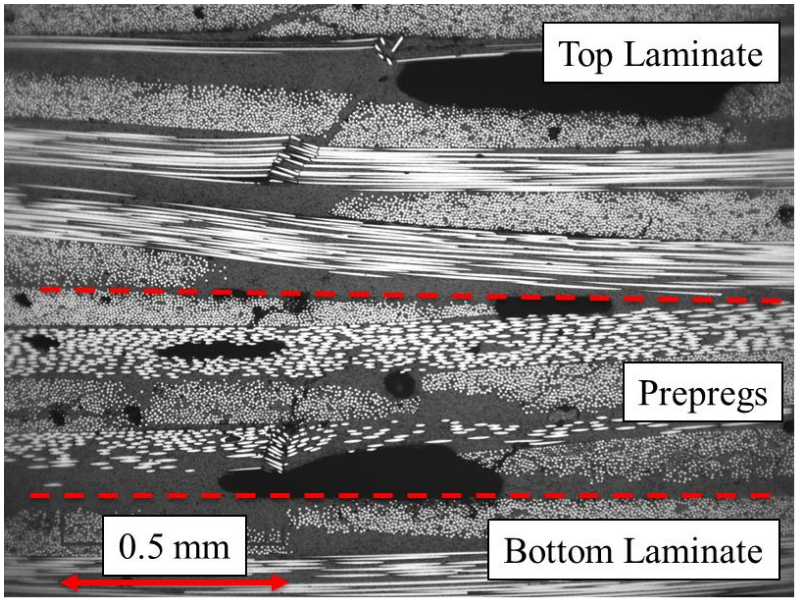

Figure A.1. Cross-section micrograph for tested TW short beam shear sample manufactured by USW. Dotted lines indicate prepreg – laminate interfaces.

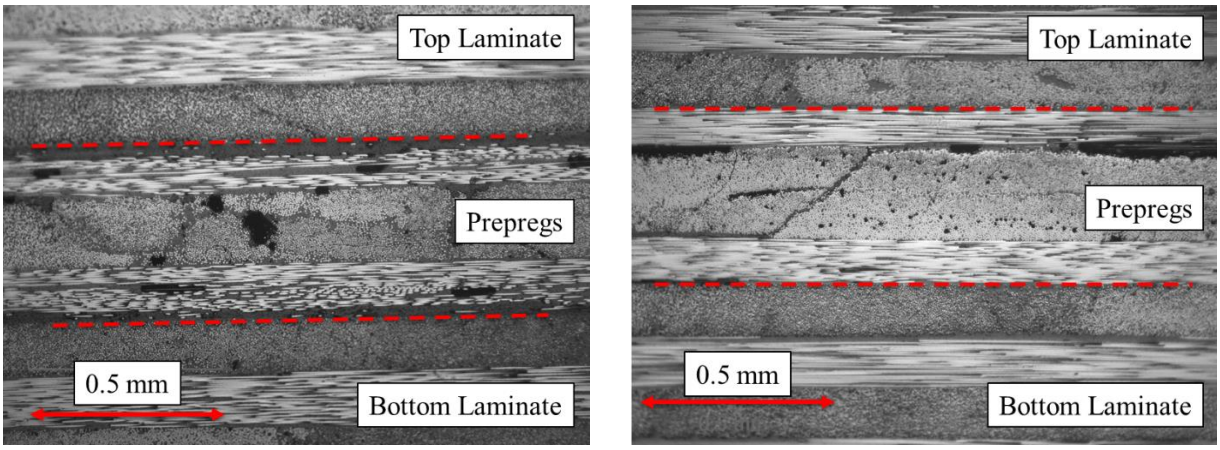

(a) (b)

Figure A.2. Cross-section micrograph for tested UD short beam shear sample. Dotted lines indicate prepreg – laminate interfaces. (a) Manufactured by USW and (b) manufactured by VBO.

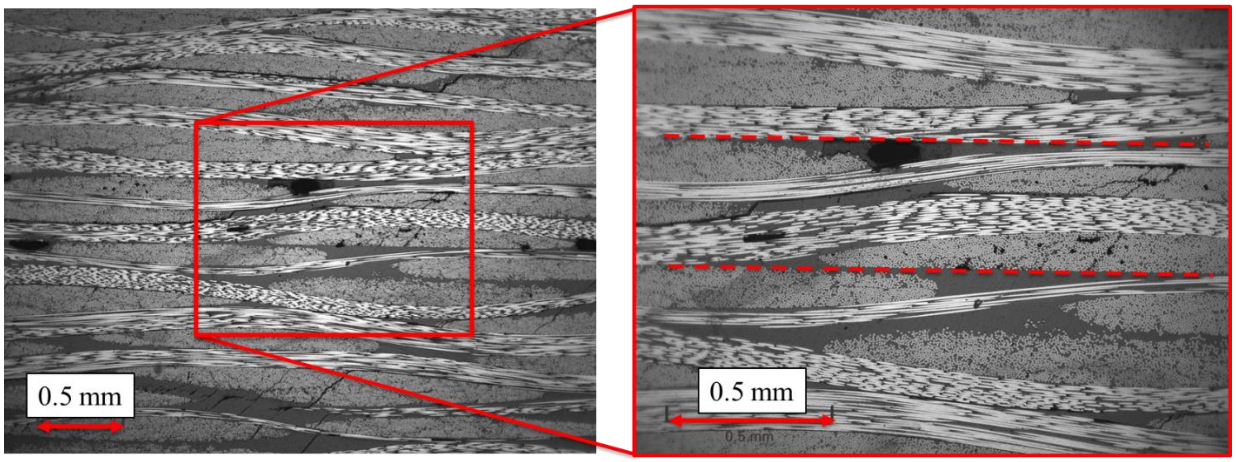

(a) (b)

Figure A.3. Cross-section micrograph for VBO short beam shear samples after testing. Both images correspond to PW sample without adhesive film. (a) Image of the center of the short beam sample. (b) Magnified micrograph from (a) showing dotted lines representing the prepreg – laminate interfaces.

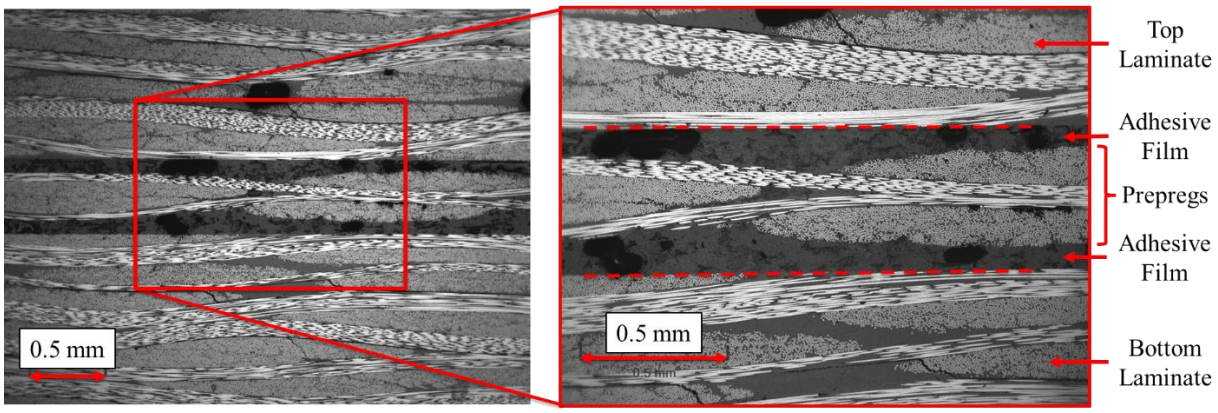

(a) (b)

Figure A.4. Cross-section micrograph for VBO short beam shear samples after testing. Both images correspond to PW sample with adhesive film. (a) Image to the right of the center of the sample. (b) Magnified micrograph from (a) with constituents labeled on the right. Dotted lines represent adhesive film – laminate interfaces.

APPENDIX B.
FORCE – DISPLACEMENT CURVES

Force – Displacement Curves Short Beam Samples

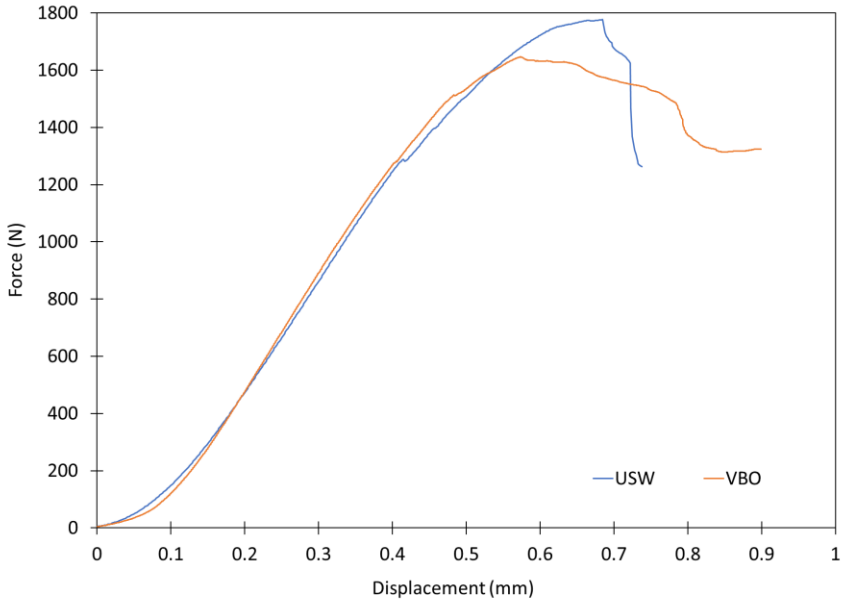

Figure B.1. Characteristic force-displacement curves for TW short beam shear samples manufactured by ultrasonic welding (USW) and vacuum bagged only (VBO).

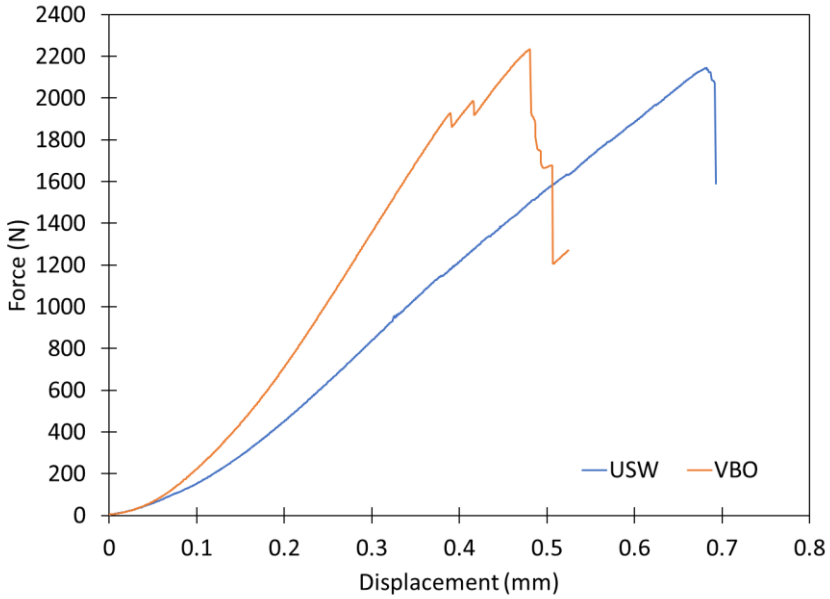

Figure B.2. Characteristic force-displacement curves for UD short beam shear samples manufactured by ultrasonic welding (USW) and vacuum bagged only (VBO).

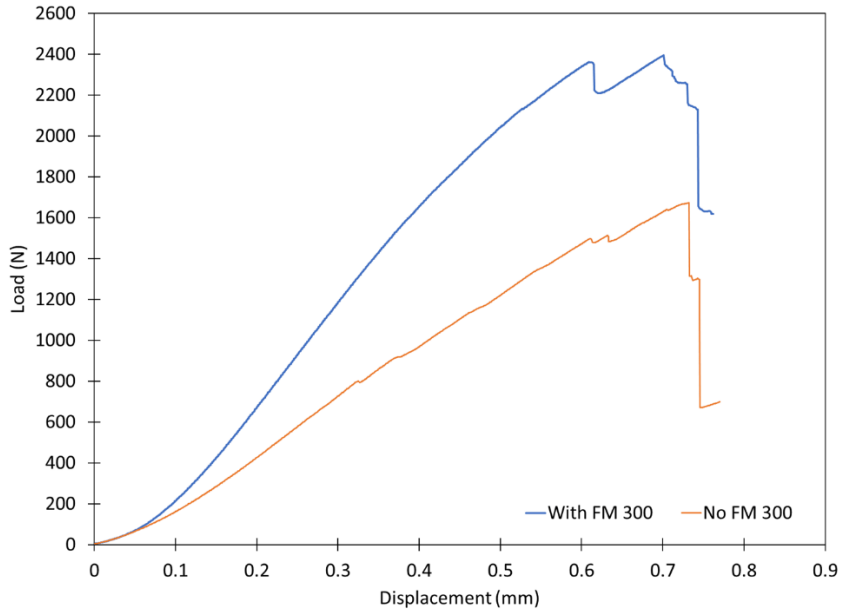

Figure B.3. Characteristic force-displacement curves for PW short beam shear samples manufactured by USW. Blue curve corresponds to samples with adhesive film (FM 300) and orange curve corresponds to sample without adhesive film.

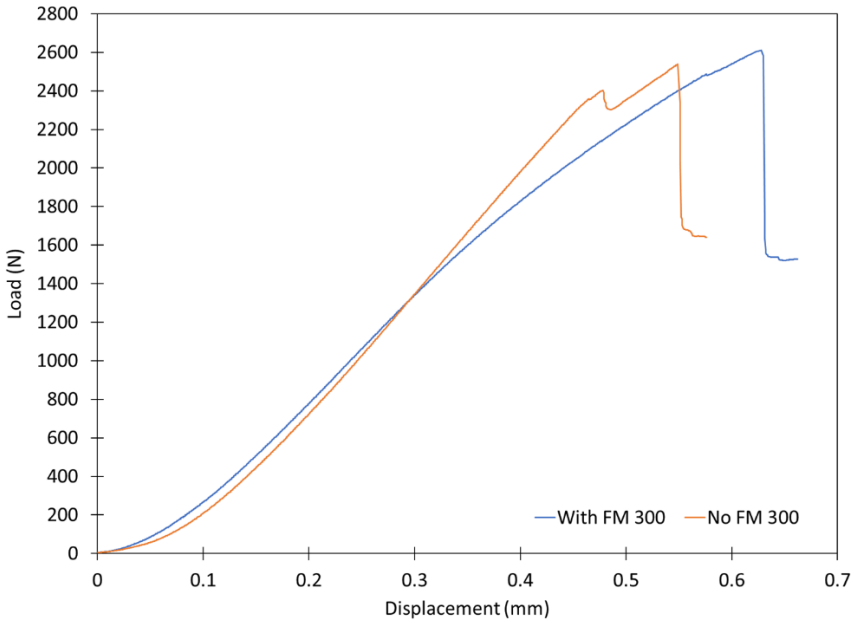

Figure B.4. Characteristic force-displacement curves for PW short beam shear samples manufactured by VBO. Blue curve corresponds to samples with adhesive film (FM 300) and the orange curve corresponds to samples without adhesive film.

Force – Displacement Curves for Open-Hole Samples

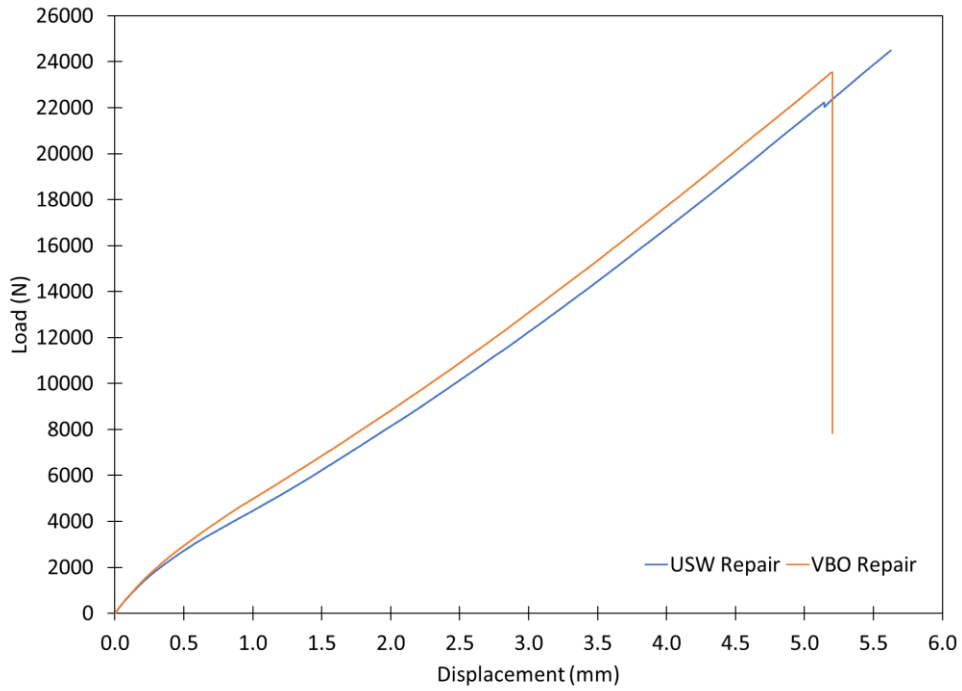

Figure B.5. Characteristic force-displacement curves for TW open-hole repair by ultrasonic welding (USW) and vacuum bagged only (VBO).

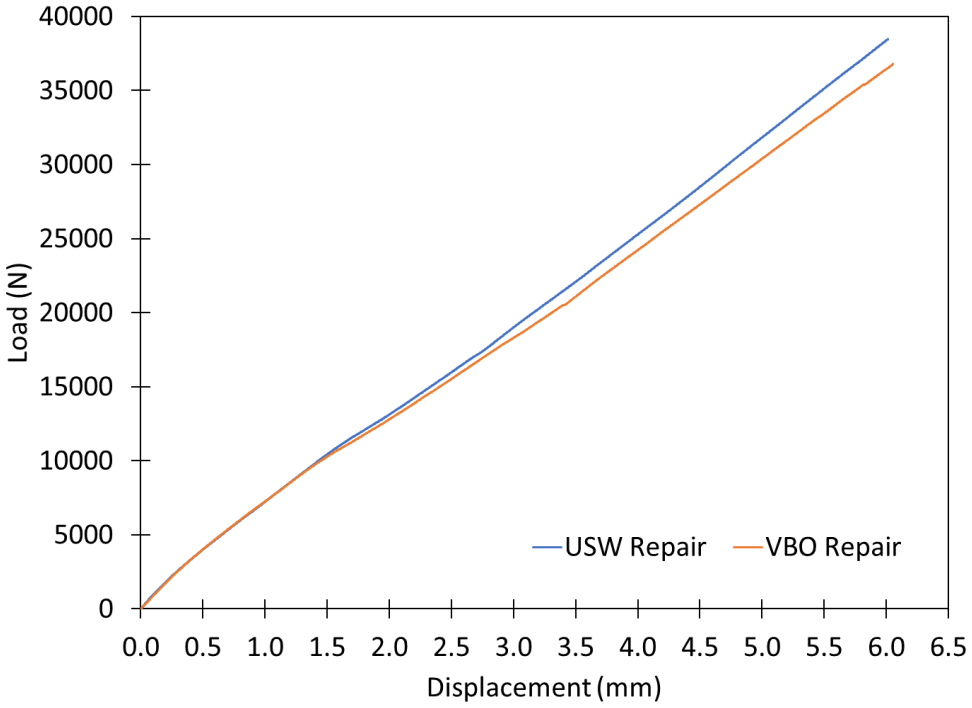

Figure B.6. Characteristic force-displacement curves for UD open-hole repair by ultrasonic welding (USW) and vacuum bagging only (VBO).

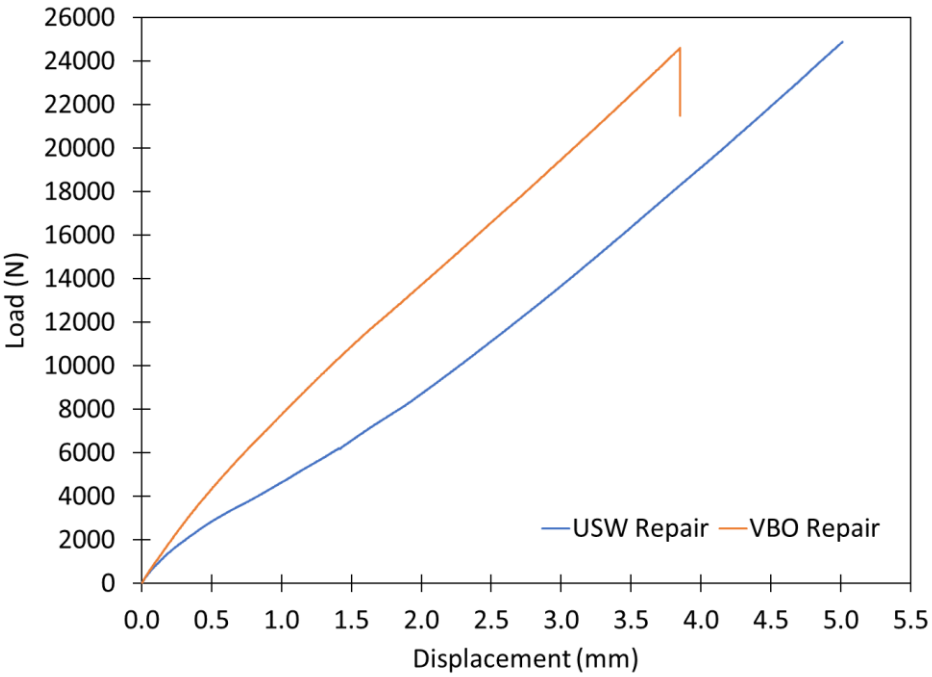

Figure B.7. Characteristic force-displacement curves for PW open-hole repair by ultrasonic welding (USW) and vacuum bagging only (VBO).

REFERENCES

1. Esp, B., *Practical Analysis of Aircraft Composites* 1st ed. 2017: Grand Oak Publishing.

2. Katnam, K.B., L.F.M. Da Silva, and T.M. Young, *Bonded repair of composite aircraft structures: A review of scientific challenges and opportunities.* Progress in Aerospace Sciences, 2013. **61**: p. 26-42.

3. Préau, M. and P. Hubert, *Processing of co-bonded scarf repairs: Void reduction strategies and influence on strength recovery.* Composites Part A: Applied Science and Manufacturing, 2016. **84**: p. 236-245.

4. Hogerbrug, M., K. Koc, and C. Zandvliet. *Repair of Composites Fact Sheet*. 2016.

5. Lionetto, F., et al., *Ultrasonic assisted consolidation of commingled thermoplastic/glass fiber rovings.* Frontiers in Materials, 2015: p. 9.

6. Rizzolo, R.H. and D.F. Walczyk, *Ultrasonic consolidation of thermoplastic composite prepreg for automated fiber placement.* Journal of Thermoplastic Composite Materials, 2016. **29**(11): p. 1480-1497.

7. Ageorges, C., L. Ye, and M. Hou, *Advances in fusion bonding techniques for joining thermoplastic matrix composites: a review.* Composites Part A: Applied Science and Manufacturing, 2001. **32**(6): p. 839-857.

8. Roylance, M., et al., *Modeling of ultrasonic processing.* Journal of Applied Polymer Science, 2004. **93**(4): p. 1609-1615.

9. Grewell, D., et al., *Development of an ultrasonic debulking technique for composite laminates.* Annual forum proceedings, 2005. **2**: p. 2085-2095.

10. Y. Zhao, e.a., *Ultrasonic Processing of Epoxy/CNT Nanopaper Composites.* 2017.

11. Agarwal, B.D., L.J. Broutman, and K. Chandrashekhara, *Analysis and Performance of Fiber Composites* 4ed. 2018: John Wiley & Sons, Inc.

12. Carbon.ee. *Carbon Fiber - All Patterns Explained*. 2015 [cited 2019.

13. Centea, T., L.K. Grunenfelder, and S.R. Nutt, *A review of out-of-autoclave prepregs – Material properties, process phenomena, and manufacturing considerations.* Composites Part A: Applied Science and Manufacturing, 2015. **70**: p. 132-154.

14. Goren, A. and C. Atas, *Manufacturing of polymer matrix composites using vacuum assisted resin infusion molding.* Archives of Materials Science and Engineering, 2008. **34**(2): p. 117-120.

15. Gardiner, G. *HP-RTM on the rise*. 2015.

16. Hardis, R., et al., *Cure kinetics characterization and monitoring of an epoxy resin using DSC, Raman spectroscopy, and DEA.* Composites Part A: Applied Science and Manufacturing, 2013. **49**: p. 100-108.

17. Sourour, S. and M.R. Kamal, *Differential scanning calorimetry of epoxy cure: isothermal cure kinetics.* Thermochimica Acta, 1976. **14**(1): p. 41-59.

18. Kratz, J., et al., *Thermal models for MTM45-1 and Cycom 5320 out-of-autoclave prepreg resins.* Journal of Composite Materials, 2013. **47**(3): p. 341-352.

19. Centea, T. and P. Hubert, *Measuring the impregnation of an out-of-autoclave prepreg by micro-CT.* Composites Science and Technology, 2011. **71**(5): p. 593-599.

20. Vora, K., *Mechanical Properties Evolution During Cure for Out-of-Autoclave Carbon-Epoxy Prepregs*, in *Mechanical Engineering*. 2012, Wichita State University.

21. Cole, K.C., J. Hechler, -J., and D. Noel, *A New Approach to Modeling the Cure Kinetics of Epoxy Amine Thermosetting Resins. 2. Application to a Typical System Based on Bis [4-(diglycidylamino)phenyl] methane and Bis(4-aminophenyl) Sulfone.* Macromolecules, 1991. **24**(11): p. 3098-3110.

22. Mahdavi, S., *Thermal Cycling of Out-Of-Autoclave Thermosetting Composite Materials*, in *Mechanical and Industrial Engineering*. 2017, Concordia: Montreal, Quebec, Canada.

23. Bilyeu, B., W. Brostow, and K.p. Menar, *Epoxy Thermosets and Their Applications III. Kinetic Equations and Models.* Journal of Materials Education 2001. **23**(4): p. 189-204.

24. Karkanas, P.I. and I.K. Partridge, *Cure modeling and monitoring of epoxy/amine resin systems. II. Network formation and chemoviscosity modeling.* Journal of Applied Polymer Science, 2000. **77**(10): p. 2178-2188.

25. Broek, C.A., *Optimizing of Ultrasonic Welding of Carbon Fiber PEKK Composites Literature Review*. 2015, Delft University of Technology

26. Benatar, A. and T.G. Gutowski, *Ultrasonic welding of PEEK graphite APC-2 composites.* Polymer Engineering and Science, 1989. **29**(23): p. 1705-1721.

27. Villegas, I., *Strength development versus process data in ultrasonic welding of thermoplastic composites with flat energy directors and its application to the definition of optimum processing parameters.* Composites Part a-Applied Science and Manufacturing, 2014. **65**: p. 27-37.

28. Tolunay, M.N. and P.R.W. Dawson, K. K., *Heating and Bonding Mechanisms in Ultrasonic Welding of Thermoplastics.* Polymer Engineering & Science, 1983. **23**(13).

29. Levy, A., S. Le Corre, and I.F. Villegas, *Modeling of the heating phenomena in ultrasonic welding of thermoplastic composites with flat energy directors.* Journal of Materials Processing Technology, 2014. **214**(7): p. 1361-1371.

30. Zhang, Z.B., et al., *Study on Heating Process of Ultrasonic Welding for Thermoplastics.* Journal of Thermoplastic Composite Materials, 2010. **23**(5): p. 647-664.

31. Palardy, G. and I.F. Villegas, *On the effect of flat energy directors thickness on heat generation during ultrasonic welding of thermoplastic composites.* Composite Interfaces, 2017. **24**(2): p. 203-214.

32. Justo, J., et al., *Study of the ultrasonic compaction process of composite laminates - part I: process modeling.* International Journal of Material Forming, 2014. **8**: p. 613-623.

33. Justo, J., et al., *Study of the ultrasonic compaction process of composite laminates—part II: advanced numerical simulation.* International Journal of Material Forming, 2015. **8**(4): p. 625-637.

34. Lee, E.W., A. Benatar, and D. Grewell, *Apparatus and Method for Ultrasonic Processing of Laminates*. 2006, Textron Innovations Inc.: United States.

35. Levy, A., et al., *A level set based approach for the finite element simulation of a forming process involving multiphysics coupling: Ultrasonic welding of thermoplastic composites.* European Journal of Mechanics - A/Solids, 2011. **30**(4): p. 501-509.

36. Levy, A., et al., *Ultrasonic Welding of Thermoplastic Composites, Modeling of the Process.* International Journal of Material Forming, 2008. **1**(1): p. 887-890.

37. Wang, X., et al., *FEM Investigation of the Temperature Field of Energy Director During Ultrasonic Welding of PEEK Composites*. Journal of Thermoplastic Composite Materials, 2006. **19**(5): p. 593-607.

38. Yan, J.C., et al., *The Effects of Energy Director Shape on Temperature Field during Ultrasonic Welding of Thermoplastic Composites.* Key Engineering Materials, 2007. **353-358**: p. 2007-2010.

39. Levy, A., S. Le Corre, and A. Poitou, *Ultrasonic welding of thermoplastic composites: A numerical analysis at the mesoscopic scale relating processing parameters, flow of polymer and quality of adhesion.* International Journal of Material Forming, 2014. **7**: p. 39-51.

40. Villegas, I. and G. Palardy, *Ultrasonic welding of CF/PPS composites with integrated triangular energy directors: melting, flow and weld strength development.* Composite Interfaces, 2016. **24**: p. 1-14.

41. Tateishi, N., T.H. North, and R.T. Woodhams, *Ultrasonic welding using tie-layer materials. part I: Analysis of process operation.* Polymer Engineering & Science, 1992. **32**(9): p. 600-611.

42. Justo, J., *Modeling the compaction of composite materials with ultrasonic vibrations*, in *Grupo de elasticidad y resistencia de materiales*. 2014, Universidad de Sevilla: Sevilla.

43. Gotro, J. *Practical Tips for Curing Thermosets Part One: Review of Gelation and Vitrification*. 2016.

44. Centea, T. and P. Hubert, *Out-of-autoclave prepreg consolidation under deficient pressure conditions.* Journal of Composite Materials, 2014. **48**(16): p. 2033-2045.

45. Bowles, K.J. and S. Frimpong, *Relationship Between Voids and Interlaminar Shear Strength of Polymer Matrix Composites*, N.L.R. Center, Editor. 1991, NASA: SAMPE.

46. Koushyar, H., et al., *Effects of variation in autoclave pressure, temperature, and vacuum-application time on porosity and mechanical properties of a carbon fiber/epoxy composite.* Journal of Composite Materials, 2012. **46**(16): p. 1985-2004.

47. Costa, M.L., S.F.M.d. Almeida, and M.C. Rezende, *The influence of porosity on the interlaminar shear strength of carbon/epoxy and carbon/bismaleimide fabric laminates.* Composites Science and Technology, 2001. **61**(14): p. 2101-2108.

48. Cox, A., et al., *Repair Development for a Composite Cryotank*. 2014, ASM International; Materials Park: AeroMat 25 Conference and Expo.

49. Whittingham, B., et al., *Micrographic studies on adhesively bonded scarf repairs to thick composite aircraft structure.* Composites Part A: Applied Science and Manufacturing, 2009. **40**(9): p. 1419-1432.

50. Caminero, M.A., et al., *Damage monitoring and analysis of composite laminates with an open hole and adhesively bonded repairs using digital image correlation.* Composites Part B: Engineering, 2013. **53**: p. 76-91.

51. de Morais, A.B., *Open-hole tensile strength of quasi-isotropic laminates.* Composites Science and Technology, 2000. **60**(10): p. 1997-2004.

52. S Balakrishnan, V., H. Seidlitz, and S. Weiss, *Layup Configuration Effect on Notch Residual Strength in Composite Laminates.* Materials, 2018. **11**.

53. Topolo, *UD Tape*. 2017: Topolo.

54. Composites, A. *Plain Weave Carbon Fiber*. 2019.

55. Composites, R.W. *Twill Weave Carbon Fiber*.

56. Rinco, *Operating Instructions Dynamics 3000*, R. Ultrasonics, Editor. 2008: Switzerland.

57. Hillger, W. and S.E. Brauschweig, *Determination of Porosity in Aerospace Structures by Ultrasonic Pulse Echo Technique*, in *ECNDT*. 2002, ECNDT: Barcelona.

58. Mortimer, S., M.J. Smith, and E. Olk, *Product Development for Out-of-Autoclave (OOA) Manufacture Aerospace Structures*, Hexcel, Editor. 2017, Hexcel.

59. Kastner, J., et al., *Defect and Porosity Determination of Fibre Reinforced Polymers by X-ray Computed Tomography*, in *2nd International Symposium on NDT in Aerospace*. 2010, NDT in Aerospace: Hamburg, Germany.

60. Vora, K., et al., *Evolution of Mechanical Properties During Cure for Out-of-Autoclave Carbon-Epoxy Prepregs.* Journal of Applied Polymer Science, 2014.

VITA

David Hoskins was born and raised in La Paz, Bolivia. After graduating High School from the American Cooperative School, he moved to Ames, Iowa where he completed his Bachelor of Science degree in Materials Engineering in May 2017. Upon graduating, he moved to Baton Rouge, Louisiana to pursue a Master of Science degree in Mechanical Engineering. He plans to pursue a career in research and development in composite materials after the completion of his degree.